# CODE DESIGN FOR VISIBLE LIGHT COMMUNICATIONS UNDER ILLUMINATION CONSTRAINTS

A Dissertation

by

CARLOS EDUARDO MEJIA MEJIA

Submitted to the Office of Graduate and Professional Studies of
Texas A&M University
in partial fulfillment of the requirements for the degree of

DOCTOR OF PHILOSOPHY

| | |
|---|---|
| Chair of Committee, | Costas N. Georghiades |
| Committee Members, | Scott L. Miller |
| | Sebastian Hoyos |
| | Anxiao Jiang |
| Head of Department, | Miroslav M. Begovic |

December 2018

Major Subject: Electrical Engineering

# ABSTRACT

Visible light communication (VLC) uses the same LEDs which are an efficient source of illumination to transmit information concurrently using optical direct-detection. As a result of modulating the LED to convey information, there may be a perceived change in the light perception which besides being annoying, may produce physiological consequences under prolonged exposure. The aim of this research is to propose code design methodologies for controlling the effects of light intensity flickering, brightness control, and color shifts due to the modulation, encoding information bits in organized optical symbol sequences, and improving the coding gain by the use of the Viterbi algorithm.

In order to mitigate the effect of intensity flickering presented in On-Off Keying modulation, five codes are designed with two proposed algorithms using finite-state machines (FSMs) for constraining the runs of zeros or ones. The codes are compared with the codes proposed in the IEEE 802.15.7 standard on VLC (Manchester code, 4B6B code, and the 8B10B code) in terms of flicker mitigation using the perceived flicker index (PFI) (a mathematical measure of flicker introduced in this study) and error-rate performance. The designed codes show asymptotic coding gains between $1.25$ and $6$ dB with a low sacrifice in PFI.

To avoid color shifts in color-shift keying (CSK) modulation, four codes were designed from optimally CSK constellations and two classes of codes where one class is based on FSMs and the other on trellis-coded modulation (TCM) according to the desired color perception constraint. The designed codes show asymptotic coding gains between $1.5$ to $3.5$ dB with respect to uncoded transmission.

For brightness control, variable-weight multipulse pulse-position modulation (VW-MPPM) is introduced as an alternative for increasing the spectral efficiency by the selection of multipulse pulse-position modulation symbols of diverse weight to attain the desired dimming level. Combining VM-MPPM symbols with Huffman codes and TCM, two designed codes are compared with MPPM codes for dimming level of $0.67$ and $0.40$ showing an asymptotic coding gain of $0.94$ and

1.29 dB, respectively.

Finally, we show the trade-offs between coding gain improvement and their effects on light perception.

# DEDICATION

To my wife Tatiana

and my children Carlos and Victoria.

# ACKNOWLEDGMENTS

I would like to express my sincere gratitude to my advisor Dr. Costas Georghiades for accepting me into his research group. He dedicated his time, effort, and support while encouraging me to be successful in my Ph.D study at Texas A&M University. I feel privileged to work with him because he strengthened in me the values and skills it takes to prosper as a researcher through his exemplary guidance and advice. This work would not have been possible without him.

My sincere gratitude to the dissertation committee members, Dr. Scott L. Miller, Dr. Sebastian Hoyos, and Dr. Anxiao Jiang for their remarkable comments and insightful suggestions that aided in the improvement of this work. I would also like to thank Dr. Chao Tian for his insightful observations during the thesis presentation and Dr. Sam Mannan who was a crucial part of this committee during the early stages and is now in the grace of God.

I wish to thank Dr. Mohammed Abdallah for his invaluable comments and suggestions that contributed to the improvement of my research skills during the early years.

Special thanks also to my undergraduate advisor, Dr. Rodrigo Correa for nurturing in me the curiosity and the motivation to be successful as a researcher.

Thank you to Ms. Anni Brunker, Ms. Katherine Cates, Ms. Tammy Carda, Ms. Katie Bryan, Ms. Melissa Sheldon, and Ms. Shelly Martin for their patience and kindness towards me as I familiarized myself with all the requirements of the Ph.D. program.

Thank you to Dr. Krishna Narayanan, Dr. Scott L. Miller, Dr. Sebastian Hoyos, Dr. Henry Pfister, Dr. Jean-Francois Chamberland, Dr. Sunil Khatri, and Dr. Sam Villareal for being available for discussions every time I saw their door open. Also, I want to thank my colleagues Dr. Avinash Vem, Dr. Lucia Sui, and Dr. Yazan Al-badarneh for their cooperative efforts and suggestions during my Ph.D. studies.

Thank you to Juan Moreno, Mike Evans, Bobby Fair, Sam Hogue, and the research group for believing in my professional skills, and for giving me the opportunity to complete two internships at ST Genetics. These internships opened doors professionally and allowed me to continue doing

high impact research. I also want to extend thanks to all the ST Genetics family.

Thank you to my school Gimnasio Saucara and Industrial University of Santander for my personal, professional, and academic foundation. Also, thank you to my Sensei Saul Suarez, my martial art friends, and my rugby family team "Toros" for teaching me that I have to be persistent and disciplined to fulfill my goals. To the Colombian Navy, my superiors, friends, and "cursos", thank you for being part of my military formation.

Thank you to Dan and Rhonda Miller and their beautiful family for their prayers, advice, and support given during these years of adjustment for my family. Through your love, we had experienced family, community, and true American culture. We feel at peace and as if our problems are solved every time we go to their home in Wheelock. Also, I want to thank our little sister Rachel for being our unconditional friend and supporter. She is an angel of God living here on the earth.

Thank you to my "parceros" Dr. Elvis Dominguez, Dr. Sanjay Nair, and Dr. Marco Roquesol and their families for sharing their friendship and support with my family. Also, I want to thank Jeremy and Laura, Javier and Marianela, Julio and Maricarmen, Gabriel and Ingrid, Alex and Cristina, Anibal and Viviana, Carlos and Yuliana, Elvis and Pilar, Lucho and Stephany and many other friends for sharing unforgetable moments with my family. I consider myself fortunate to have so many great friends in College Station.

Thank you to my parents Julio and Olga for providing me with the highest quality love, values, and education. Also to my siblings Andres and Olga, my sister-in-law Diana, and my brother-in-law Stephan for their support and encouraging words. I thank God for this family.

Many thanks to my children Carlos and Victoria because you are the energy and fuel that I needed in my life. I want you to always remember this experience. I want you to be encouraged to chase your dreams. You can do anything you wish with your life.

Last but not least, an endless amount of thanks must go to my wife Tatiana. The support and love you have given me these past nine years, from the day we committed our lives to each other before God, has been essential to my success. We have been through many journeys together and you have always been there. I feel blessed to have such a great wife, sometimes I think that this

is a dream. Thank you for everything you sacrifice for our family and for always giving me the correct advice at the correct time.

# CONTRIBUTORS AND FUNDING SOURCES

## Contributors

This work was supported by a dissertation committee consisting of Professors Dr. Costas Georghiades, Dr. Scott Miller, and Dr. Sebastian Hoyos of the Department of Electrical and Computer Engineering and Dr. Sam Mannan of the Department of Chemical Engineering. All work for the dissertation was completed independently by the student.

Chapter 3 was developed in collaboration with Professor Dr. Mohammed Abdallah from the College of Science and Engineering, Hamad Bin Khalifa University, Doha, Qatar.

## Funding Sources

This graduate study was sponsored by a graduate assistantship from Texas A&M University and supported by NPRP award under grant No. 8-648-2-273 from Qatar National Research Fund (a member of Qatar Fundation).

# NOMENCLATURE

| | |
|---|---|
| VLC | Visible light Communications |
| OWC | Optical Wireless Communications |
| LED | Light-emitted diode |
| RGB-LED | Red, green, and blue Light-emitted diode |
| PD | Photodetector |
| OOK | On-off keying |
| 2PPM | Binary pulse-position modulation |
| VPPM | Variable pulse-position modulation |
| OPPM | Overlap pulse-position modulation |
| MPPM | Multipulse pulse-position modulation |
| CSK | Color-shift keying |
| PFI | Perceived Flicker Index |
| RDS | Running digital sum |
| FSM | Finite-state machine |
| TCM | Trellis-coded modulation |
| VW-MPPM | Variable-weight multipulse pulse-position modulation |
| AWGN | Additive white Gaussian noise |
| FOV | Field-of-view |
| LOS | Line-of-sight |
| ISI | Intersymbol interference |
| OCR | Optical clock rate |
| CER | Codeword error rate |

| | |
|---|---|
| SER | Symbol error rate |
| $d_{\min}$ | Minimum Euclidean distance |
| $d_{\min,\mathrm{c}}$ | Minimum Euclidean distance of the code |
| $d_H$ | Minimum Hamming distance |
| $\bar{E}$ | Average energy per symbol |
| $\bar{E}_b$ | Average energy per bit |
| $\mathbb{E}[\cdot]$ | Expected value |
| $\mathrm{Var}(\cdot)$ | Variance |

TABLE OF CONTENTS

Page

LIST OF FIGURES

FIGURE Page

LIST OF TABLES

TABLE Page

# 1. INTRODUCTION*

The 5th generation in wireless systems promises to fulfill the current requirements of higher data rates, quality of service, mobility, low latency, and low energy/cost consumption. These improvements introduce innovative technologies that contribute to develop and modify the current telecommunication systems to meet the user demands in spectral availability [1]. Thus, new wireless communication alternatives suggest dealing with new challenges in signal modulation, channel coding, and optimal reception.

The increasing demand for additional bandwidth to transmit data turns the attention on using the visible light spectrum known as optical wireless communications (OWC) which uses the wide and unregulated color spectrum from 380 to 780 nm as an alternative to decrease the spectral load on radio frequency systems. The short-range field in OWC is known as Visible Light Communications (VLC) which uses light-emitted diodes (LEDs) to provide simultaneously the illumination and data transmission with minimum RF interference, high spacial reuse, security, and high energy efficiency [2].

The solid-state lighting has evolved in the use of LEDs as an attractive way to fulfill the illumination requirements due to its energy/illumination efficiency, longer lifetime, lower power consumption, and reduced heat generation compared for instance with incandescent light sources. Also, LEDs allow fast switching to modulate the visible light waves in a wireless optical environment to transmit at high data rates [3] [4]. However, the uncontrolled sequences of optical symbols produce perceptible and imperceptible changes in the illumination that are potentially harmful in humans [5].

The IEEE 802.15.7 standard in VLC [6] proposes three physical layer operation modes: PHY I which operates at rates from 11.67 to 266.66 Kb/s, PHY II which operates at rates from 1.25 to

*Parts of this chapter are reprinted with permission from "Code design for flicker mitigation in visible light communications using finite state machines" by Mejia CE, Georghiades CN, Abdallah MM, Al-Badarneh YH, 2017. *IEEE Transactions on Communications*, 65(5) pp.2091-2100, and "Code design for flicker mitigation in visible light communications using finite state machines" by Mejia CE, Georghiades CN, Abdallah MM, Al-Badarneh YH, 2017. *IEEE Transactions on Communications*, 65(5) pp.2091-2100, Copyright © 2011 IEEE

96 Mb/s, and PHY III which operates from 12 to 96 Mb/s. These modes are classified according to their modulation schemes, forward-error correcting codes, inner codes for reducing undesired light perception effects, and optical clock rate (OCR) to mitigate the illumination perception problems during transmission [7].

For error correction, the standard proposes Reed-Solomon codes where coding requirements are less rigorous at short distances. These codes belong to a polynomial forward-error correcting code family which adds data redundancy to the message so a receiver can better recover a bit sequence affected by errors caused by the communication channel. These codes are designed to provide reliability with some efficiency regarding energy per bit in data transmission. However, Reed-Solomon codes are not designed to avoid light perception issues during transmission and they are required to be concatenated with an inner code in the physical layer which mitigates the undesired illumination perception effects caused by the uncontrolled sequence modulation of optical signals through the LED.

The modulation schemes suggested by the standard are on-off Keying (OOK), variable pulse position modulation (VPPM), and Color-Shift Keying (CSK). OOK modulation is proposed for the PHY I and PHY II modes and simply in turning ON or OFF an LED if the transmitted data bit is one or zero, respectively. However, the transmission of unbalanced and unconstrained long sequences of like symbols bits produce undesired effects in the intensity perception denoted as *intensity flicker*. To mitigate the perception problem, the standard proposed the use of run-limited length (RLL) codes whose codewords are balanced for mitigating changes in the illumination. The codes proposed are the Manchester code in PHY I and 8B10B code [8] for PHY II.

VPPM modulation is suggested also in PHY I and PHY II modes to control the light brightness. VPPM transmit binary 2-PPM symbols to represent logical zeros and ones, but with variable pulse-width for controlling the average perceived illumination intensity. This modulation does not present problems of flicker because the illumination power is constant, but has a higher bit error probability and lower spectral efficiency the duty-cycle is above or below $50\%$ compared with OOK. The code proposed for this modulation is the 4B6B code in PHY I and PHY II modes

for synchronization. Due to the low spectral efficiency and error-rate performance of VPPM, new modulations schemes as variable on-off Keying (VOOK) and multipulse pulse-position modulation (MPPM) are proposed in the literature.

CSK modulation is proposed in PHY III mode as a solution to increase the data rate by transmitting colors using the proportional combination of the red, green and blue LEDs and keeping each color with fix luminous flux to eliminate the intensity flicker. The color generation depends on the instantaneous current driving and the physical characteristics of the RGB-LED allowing a large possibility of color combinations for encoding the information bits for increasing the data throughput. Each transmitted color modulated at high frequencies can be detected by current photodectors, but the human eye only perceives the average of the color sequence in a perceived time window. However, the uncontrolled color sequence could generate color-shifts around the desired color. Thus, this mode propose 4-CSK, 8-CSK, and 16-CSK whose design consists in allocate symbols in a balanced manner around the desired color and the scrambler which encodes the information bit in a pseudo-random sequence to transmit each symbol with equal probability.

Based on the VLC standard, Sarbazi and Uysal in [9] present the first evaluation of the error rate performance of PHY I, PHY II, and PHY III operation modes using Monte Carlo simulations. Even though the proposed modes of the VLC standard are effective in the light perception control, researchers are looking for alternatives to enhance the performance of these modes finding new modulation and coding alternatives under the physical constraints of the optical channel and the human vision. For reducing the light perception effects during transmission, the authors in [10] propose overlapping pulse-position modulation (OPPM) as an alternative for controlling the light dimming level and reducing the flicker effects during transmission. They compare OPPM with OOK and VPPM showing the trade-offs in terms of cut-off rate, power efficiency, and bandwidth requirements for different values of duty cycle. An important contribution in brightness control was reported in [11] where the authors present multiple pulse-position modulation (MPPM) as an alternative for increasing the spectral efficiency and attain the desired intensity level in each transmitted symbol. In [12] the authors present an alternative pulse shape to transmit a logical

zero and one for mitigating the intensity flicker by reducing the drastic transitions between zeros and ones. In [13], the authors propose a modulation based on the symbol duty cycle variability to increase the data rate and improve the bandwidth efficiency and present some experimental results for calculating the symbol error rate in terms of rate and distance. In [14], the authors use Miller codes for PHY I applications and compare their performance in terms of bandwidth and channel coexistence with the Manchester code. In [15], the author proposes an inverse source code for dimming level control based on the Huffman code for increasing the spectral efficiency. In [16] and [17] the authors propose a guided scrambling (GS) approach with Reed-Muller codes and turbo codes, respectively. In [18], the authors present a soft-decision decoding unary variable-length code that results on high improvement in data rate and error-rate performance compared with other modulations for limited dimming levels. In [19], the author shows a symbol encoder and decoder methodology using multiple level MPPM symbols by using multiple LEDs showing an improvement in spectral efficiency. In [20], the authors propose an algorithm to design the encoder and decoder for constant weight codes that do not require look-up tables.

To avoid color shifts during transmission in CSK, the authors in [21]. evaluate the performance of the PHY III layer for different color band combinations. To maximize the minimum Euclidean distance among symbols, $d_{\min}$, Drost [22] and Monteiro [23] propose the use of the billiards and interior points algorithms, respectively. In [24] the authors present constellation design in CSK and amplitude-shift-keying (ASK) with a single or multiple RGB-LEDs with channel precompensation. Singh *et. al.* [25] propose the use of four LEDs to increase the color plane, and therefore $d_{\min}$, and [26] analyzes the performance of Reed-Solomon codes using CSK.

Based on these previous works, the motivation of this dissertation is to propose code design methodologies which simultaneously control the light perception and improve the coding gain by modeling the desired sequence using finite-state machines (FSMs) and fundamental concepts of trellis-coded modulation (TCM) according to the illuminations constraints. An advantage of using these code structures is that they allow soft-decision decoding by using the Viterbi algorithm which is an optimal decoder.

The contributions of this dissertation are divided into five chapters. Chapter 2 presents a theoretical background related to the optical system model for monochromatic and tri-chromatic channels, explains the illumination constraints used in this dissertation to design codes for OOK modulation and CSK modulation, explains the dimming level constraints, summarizes the current dimming control methodologies, and presents a brief overview of the directed graphs methodologies (FSM and TCM) used for modeling the desired sequence.

Chapter 3 presents the perceived flicker index (PFI) as the first flicker measure that considers the coding effect, the pulse-shape, and the modulation format as a function of the optical clock rate (OCR). Also, it introduces two algorithms for designing codes which simultaneously mitigate flicker and provide a coding gain using FSMs limiting the number of consecutive zeros and ones in the transmitted sequence to reduce light flicker. These methodologies show the trade-off between data rates and the perceived flicker mitigation. In addition, the PFI and the codeword-error rate (CER) are used for comparing the designed codes with the Manchester code, the 4B6B code, and the 8B10B code proposed in the standard.

Chapter 4 presents triangle partition as a methodology to design CSK constellations by partitioning each side of the intensity plane triangle uniformly and compare with other constellations designs in terms of their minimum Euclidean distance per average information bit energy versus their achieved rate. Based on these constellations, two code design methodologies denoted as CSK-FSM and CSK-TCM codes are introduced for preserving the average perceived color. As a result, four codes using these methodologies are compared with optimal uncoded 4-CSK and 8-CSK constellations.

Chapter 5 introduces variable-weight multipulse pulse-position modulation (VW-MPPM) as a scheme consisting in selecting MPPM symbols of multiple weights to increase the spectral efficiency and compared with VOOK, MPPM, ISC, and unary-codes for different dimming levels. Also, a methodology to design VW-MPPM-TCM codes based on Huffman codes and TCM is presented for keeping the spectral efficiency of uncoded VW-MPPM while improving the modulation coding gain.

Finally, Chapter 6 concludes the dissertation and discusses future work and extensions.

# 2. THEORETICAL BACKGROUND*

## 2.1 Communication System Model

### 2.1.1 Monochromatic System Model

The block diagram in Figure 2.1 presents the VLC system studied. The encoder is a look-up table where the transmitted symbol depends on the input bits and the current state of the encoder. This trellis encoder is designed based on a state transition diagram obtained from a directed graph modeling the desired sequence according to the illumination perception constraint.


Figure 2.1: VLC block diagram system [Reprinted with permission from "Code design for flicker mitigation in visible light communications using finite state machines" by Mejia CE, Georghiades CN, Abdallah MM, Al-Badarneh YH, 2017. *IEEE Transactions on Communications*, 65(5) pp.2091-2100, Copyright © 2011 IEEE].

The encoded sequence is amplified according to the desired illumination level and modulated by the LED (usually white). The LED conveys the signal according to the bit sequence through the optical channel which is modeled as additive white Gaussian noise (AWGN) coming from the ambient light, the shot noise, and the electrical pre-amplifier noise. Because this study focuses on the code design to mitigate illumination perception, this research assumes the receiver is within the field-of-view (FOV) and in line-of-sight (LOS) of the transmitting LED. Parameters like distance, angle of incidence, angle of irradiance, and physical characteristic of the devices are fixed, i.e.

*Parts of this chapter are reprinted with permission from "Code design for flicker mitigation in visible light communications using finite state machines" by Mejia CE, Georghiades CN, Abdallah MM, Al-Badarneh YH, 2017. *IEEE Transactions on Communications*, 65(5) pp.2091-2100, Copyright © 2011 IEEE

each channel attenuates by a constant factor the optical signal transmitted by the LED. Intersymbol interference (ISI), cross-talk, dispersion, and light reflections are not considered in this thesis.

Accordingly, the received signal in the equivalent discrete time baseband is represented as

$$y_i = hx_i + n_i, \tag{2.1}$$

where $h$ is the channel attenuation, $x_i$ is the amplified transmitted symbol at time $i$ and $n_i$ is the AWGN noise. Finally, the received optical signal is transformed to an electrical signal by the photodetector and used to estimate by soft-decision decoding transmitted symbols assuming that the receiver has perfect knowledge of the channel.

### 2.1.2 Tri-chromatic System Model

The block diagram in Figure 2.2 presents the VLC system studied. In this study, an CSK constellation composed of $N$ symbols, where each symbol represents the instantaneous current driving at the RGB-LED

$$\mathcal{S} = \{s_1, s_2, s_3, \ldots, s_N\} \tag{2.2}$$

where the $j^{th}$ symbol

$$s_j = [i_{r,j}\, i_{g,j}\, i_{b,j}]^T \tag{2.3}$$

is a triplet whose elements are the electrical current in amperes for the red, green, and blue LED, respectively. Each element of the symbol is positive and the sum of its elements is constant; i.e.

$$I(s_j) = i_{r,j} + i_{g,j} + i_{b,j} \tag{2.4}$$

for $\forall j$. An alternative representation of the $s_j$ is the following

$$s_j = \mathcal{I}\sigma_j \tag{2.5}$$

where $\mathcal{I}$ denotes the peak current for each color LED in [A] represented as a 3x3 diagonal matrix whose elements are positive and $\sigma_j$ is the relative *intensity symbol* represented as a 3x1 vector whose elements are the proportional amount of electrical current in the range $[0, 1]$, and based on (2.4) they sum to one.

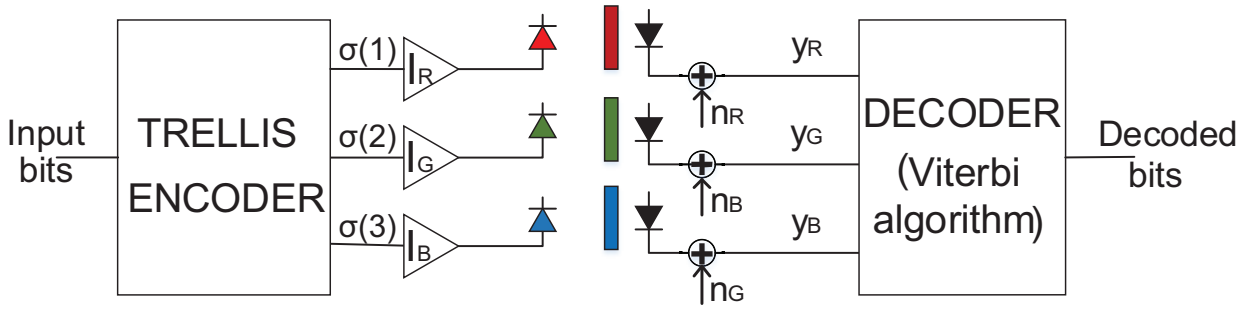


Figure 2.2: CSK block diagram system.

Once the RGB-LEDs do the electrical-to-optical conversion, the signal is transmitted through the optical channel represented with the 3x3 matrix

$$H = \begin{bmatrix} h_{r,r} & h_{r,g} & h_{r,b} \\ h_{g,r} & h_{g,g} & h_{g,b} \\ h_{b,i} & h_{b,g} & h_{b,b} \end{bmatrix}, \tag{2.6}$$

where each element represents the channel gain. In addition to the assumptions presented in the monochromatic channel, the color channels are modeled as independent with constant attenuation and additive white Gaussian noise. The optical signal detected by the three photo-detectors is represented in the equivalent discrete time baseband as

$$y_i = \mathcal{A}\sigma_i + n_i, \tag{2.7}$$

where $\mathcal{A} = H\mathcal{I}$ is a 3x3 diagonal matrix, $\sigma_i$ is the intensity symbol transmitted at time $i$, and $n_i$ is a

3x1 vector that represents the AWGN noise vector. Finally, each component of the received optical signal is converted to electrical signals, which are estimated by soft-decision decoding, assuming that the receiver has perfect knowledge of the channel.

## 2.2 Perceived Illuminations Constraints

### 2.2.1 Intensity Flicker Constraint in OOK

In OOK, the intensity flicker effect is produced by the transmission of unbalanced and unconstrained sequences of zeros and ones. In the baseband power spectral density domain representation of the transmitted sequence, the unbalanced effect is reflected in the energy at the zero frequency, while the perceived energy of the unconstrained effect is at the low frequencies. For any code, the total power spectral density is a function that accounts for the randomness of the code as a function of the autocorrelation coefficients, the pulse-shape, and modulation format of the symbols [27].

Therefore, this thesis introduces a flicker measure denoted as perceived flicker index to quantify the effects of the communication system in the optical perception as a function of the optical clock rate. Based on this measurement, this study can compare the trade-offs between the coding rate and the flicker mitigation of the designed codes with the codes proposed in the standard.

### 2.2.2 Luminous Flux Constraint for CSK

The optical gain of red, green, and blue LED are represented with the matrix

$$\mathcal{P} = \begin{bmatrix} \rho_r & 0 & 0 \\ 0 & \rho_g & 0 \\ 0 & 0 & \rho_b \end{bmatrix} \tag{2.8}$$

where each element in the diagonal denotes the lumen per ampere [lm/A]. Then, the luminous flux of each LED due to the transmission of the symbol $s_j$ is represented by the $3x1$ vector

$$\mathcal{L}(\sigma_j) = \mathcal{P}\mathcal{I}\sigma_j. \tag{2.9}$$

where the average luminous flux is equal to

$$L = \mathbb{E}[\mathbb{1}^T \mathcal{L}(\chi)] \text{ [lm]}, \tag{2.10}$$

where $\chi$ is a random vector from relative intensity symbol from the constellation $S = \{\sigma_1, \sigma_2, ..., \sigma_N\}$, $\mathbb{E}[\cdot]$ denotes expectation, and $\mathbb{1}$ is the $3x1$ all one vector.

### 2.2.3 Chromaticity Constraint in CSK

The *chromaticity diagram* presented in Fig. 2.3 represents the gamut of colors perceived by the human eye where the $x$ and $y$ coordinates represent the normalized two of the three stimuli of the color. The curve shape that encloses the color gamut represents the spectral wavelength of the monochromatic colors in nanometers ($nm$).

According to [28], the desired color with coordinates ($x_s$,$y_s$) is obtained by the mixture of the relative luminous flux of the red, green, and blue LEDs with respectively chromaticity coordinates ($x_i$,$y_i$), ($x_j$,$y_j$), and ($x_k$,$y_k$)from the following expression

$$\begin{bmatrix} \frac{x_i}{y_i} & \frac{x_j}{y_j} & \frac{x_k}{y_k} \\ 1 & 1 & 1 \\ \frac{1-x_i-y_i}{y_i} & \frac{1-x_j-y_j}{y_j} & \frac{1-x_k-y_k}{y_k} \end{bmatrix} \eta = \begin{bmatrix} \frac{x_s}{y_s} \\ 1 \\ \frac{1-x_s-y_s}{y_s} \end{bmatrix} \tag{2.11}$$

where $\eta$ is a $3x1$ vector representing the relative flux of each LED. By definition, the elements of $\eta$ sum to one. Under the assumptions that the LED color in not a function of $L$ and the visible light power spectral density of the LED scales linearly over the current range, the perceived chromaticity of the RGB-LED is equal

$$\mathbb{E}[\mathcal{L}(\chi)] = L\eta. \tag{2.12}$$

Replacing (2.10) in the previous expression, the perceived chromaticity of the RGB-LED could be rewritten as

$$\mathcal{PIE}[\chi] = L\eta \tag{2.13}$$

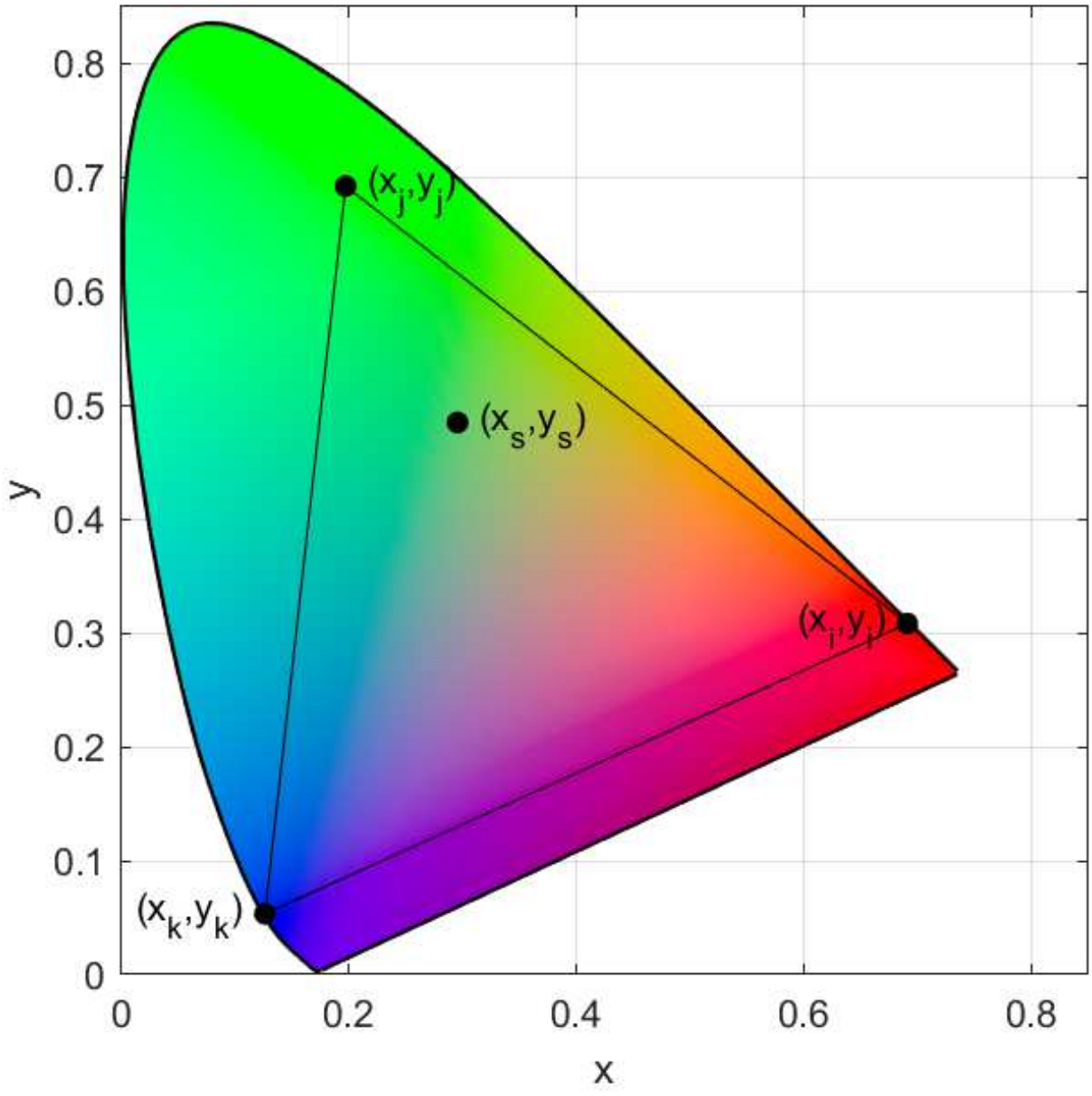


Figure 2.3: Chromaticity diagram.

where $\chi$ is a random vector from relative intensity symbol from the constellation $S = \{\sigma_1, \sigma_2, ..., \sigma_N\}$. The optical gains of the RGB-LEDs and the physical characteristics of the photodetectors are considered as part of the channel gain $H$.

In the literature, constellations are designed assuming that the information bits are independent and transmitted with equal probability, and the selected symbols are selected such that there is a balance in the designed constellations. However, the statistical mean of the transmitted symbols is an appropriate measurement to quantify the tolerated shifts from the desired color. Because the human eye acts like a low-pass filter and perceives an average of the transmitted color sequence and based on expressions (2.12) and (2.10), the chromaticity perception is defined in a discrete time model as

$$\Omega_n = \frac{1}{n}\sum_{l=0}^{n-1}\mathcal{L}(\chi_l) \tag{2.14}$$

$$= \frac{\mathcal{PI}}{n}\sum_{l=0}^{n-1}\chi_l \tag{2.15}$$

where $n$ is the number of transmitted symbols during a perceived time window, $T_p = nT_b$, where $T_b$ is the CSK symbol duration. Note that an uncontrolled and potentially unbalanced transmitted sequence may produce undesired effects in the color perception if $\Omega_n$ varies significantly over $T_p$. It is thus desirable to make the short-term average in (2.15) as small as possible relative to the human eye color perception response time through appropriate code design.

### 2.2.4 Dimming Level Constraint for Brightness Control

For mitigating the light brightness changes during transmission, the transmitted symbol sequence should fulfill conditions related to the desired average intensity level in the room by modifying the duty-cycle of the intensity symbol. Therefore, the illumination constraint for a maximum optical flux, $L$, is given by

$$\mathbb{E}[x] = \gamma L, \tag{2.16}$$

where $x$ is a discrete random variable from the $n$ dimensional symbol constellation and $0 \leq \gamma \leq 1$ denotes the desired dimming level.

### 2.3 Trellis Coded Modulation (TCM)

Trellis coded modulation is a coding technique used commonly with convolutional codes to improve the bandwidth efficiency and error rate performance through the adequate selection of symbols and transitions. The trellis structure of the code is composed of states connected with unidirectional edges labeled with symbols from a constellation to improve the error-rate probability. In the process, a symbol set is partitioned in symbol subsets and distributed such that the transition between states increases the minimum Euclidean distance among sequences assuming that the received sequence is decoded using the maximum-likelihood soft-decision Viterbi decoding [29, Chapter 12].

In this case, given a transmitted sequence $\bar{y}$ is encoded from a trellis code, the union upper bound on the event error probability is given by

$$P_e(\bar{y}) \leq \sum_{\bar{y}' \neq \bar{y}} Q\left(\sqrt{\frac{d_E^2(\bar{y}, \bar{y}')}{2N_0}}\right) \tag{2.17}$$

where $N_0$ is the one side AWGN noise power spectral density, and

$$d_E^2(\bar{y}, \bar{y}') = \sum_l d_E^2(y_l, y') = \sum_l \|y_l - y_l'\|^2 . \tag{2.18}$$

Now defining $d_{\min,\mathrm{c}}$ as the minimum squared Euclidean distance between $\bar{y}$ and other sequence $\bar{y}'$, and $K_s$ the number of nearest neighboring sequences, the event error probability is equal to

$$P_e(\bar{y}) \leq K_s Q\left(\sqrt{\frac{d_{\min,\mathrm{c}}^2}{2N_0}}\right) \tag{2.19}$$

$$\approx \frac{K_s}{2} e^{-\frac{d_{\min,\mathrm{c}}^2}{4N_0}} . \tag{2.20}$$

Similarly, the approximate symbol-error probability of a constellation is given by

$$P_s \approx \frac{K}{2} e^{-\frac{d^2_{\min}}{4N_0}}. \tag{2.21}$$

where $d^2_{\min}$ is the minimum Euclidean distance between symbols in a constellation, and $K$ is the number of nearest neighboring symbols. Because of the exponential behavior of expressions (2.20) and (2.21), the asymptotic coding gain of the TCM code and the uncoded modulation can be expressed as follows:

$$\gamma = \frac{\frac{d_{\min,c^2}}{E_b}}{\frac{d^2_{\min}}{E_b}} \tag{2.22}$$

where $E_b$ is the average energy per bit.

In order to improve the error rate performance, the trellis structure should be manipulated such that the $d^2_{\min,c}$ of TCM codes are greater than $d^2_{\min}$. The $d^2_{\min,c}$ is calculated by

$$d^2_{\min,c} = \min\{d^2_{\text{mcw}}, d^2_{\text{scw}}\}, \tag{2.23}$$

where $d^2_{\text{mcw}}$ and $d^2_{\text{scw}}$ are minimum squared Euclidean distances of parallel transition and paths longer than one codeword transition in length, respectively.

In addition to the previous design considerations, the trellis codes designed in this study should consider the optical constraints presented in the previous sections.

## 2.4 Code Design Using FSMs

FSM is a well studied topic and has been widely used in communication and mass digital store systems. These structures could accurately represent the physical constraints in VLC and a potential achieved coding capacity.

A FSM is a directed graph providing a graphical representation of a system composed of a discrete and finite set of states connected with edges with labels from a finite alphabet. Each edge represents an allowable, directed, transition among states. An FSM is represented by a set of states

(nodes) connected with labeled edges representing the allowable transitions amongst states.

The *adjacency matrix*, $D$ is a square matrix with elements $D(i,j)$ representing the number of directed transitions from state $i$ to state $j$. An element of the adjacency matrix, $D_{i,j}$, is either 0 or 1 with $D_{i,j} = 1$ and $D_{i,j} = 0$ indicating an allowable transition from the current state $i$ to the next state $j$ and no transition, respectively (note that transitions are directional).

Let the number of distinct transitions of length $q$ in the FSM be $Q(q)$, represented by $\log_2(Q(q))$ bits. The average number of bits per transition then, $G(q)$, is:

$$G(q) = \frac{\log_2(Q(q))}{q}. \tag{2.24}$$

Shannon [30] defined the FSM *capacity* as

$$C = \lim_{q \to \infty} G(q) \tag{2.25}$$

and showed that it is given by

$$C = \log_2(\lambda_{max}), \tag{2.26}$$

where $\lambda_{max}$ is the largest positive eigenvalue of the FSM adjacency matrix $D$.

For fix-length codes, the *$q$-th power of the adjacency matrix*, $D^q$, represents the transitions of length $q$. Each element of $D^q$ represents the number of unidirectional transitions (codewords in a coding context) of length $q$. The sum of the elements in a row represents the total number of possible transitions from that state to other states. In general, this number is not a power of two and varies from state to state. To produce a code, the FSM must be manipulated through splitting and merging of states and possible elimination of transitions at some states ( [31] is an excellent exposition to this process) to ensure there are exactly $2^p$ transitions at each state. After manipulating elements of the FSM and assigning $p$ information bits to each of the $2^p$ transitions (codewords), the code rate is defined as

$$R = \frac{p}{q}. \tag{2.27}$$

Shannon [30] showed that codes can be designed for any rate $R \leq C$ and the designed codes naturally inherit the constraints on symbol sequences imposed by the FSM.

To improve the coding properties, the trellis structure of the FSM is manipulated through different methodologies to obtain some desired characteristics in performance like state splitting and merging [31] and mapping by set partitioning [32] without affecting the constrained properties of the trellis diagram.

# 3. CODE DESIGN FOR INTENSITY FLICKER MITIGATION IN VISIBLE LIGHT COMMUNICATIONS USING FINITE STATE MACHINES*

The IEEE 802.15.7 standard for visible light communications (VLC) includes the use of run-length-limited (RLL) codes to mitigate modulation-induced flickering and the further use of coding to improve bit error rate performance. In this chapter, two algorithms to design codes using FSMs are introduced for providing simultaneously a coding gain while also mitigating flicker. The codes have the additional advantage of being optimally soft-decision decodable using the Viterbi algorithm. Trade-offs between flicker mitigation, code rate and coding gain, are discussed by designing several codes and compare their error rate and flicker mitigation performance with codes proposed in the VLC standard.

## 3.1 Perceived Flicker Index (PFI)

The Illumination Engineering Association (IES) describes two widely used light flicker measures: the *flicker index* and the *flicker percent*. In [33], the authors define the *low-frequency flicker index*, the *low-frequency percent flicker*, and the *low-frequency flicker distortion* based on the Fourier series decomposition of the received luminous power to measure the energy produced at frequencies below 200 Hz. These measures are inadequate in this study because they describe the flicker of illumination of deterministic optical signals and do not quantify the effect of the parameters of communication systems. Thus, this study proposes a flicker measure as a function of the optical clock rate (OCR), the coding effect, the modulation format, and the pulse-shape of the transmitted signals.

Letting $\omega = 2\pi F/F_b$ be the normalized angular frequency, where $F$ is the optical frequency, $F_b = 1/T_b$ is the bit-rate, and $T_b$ is the bit period, the proposed flicker measurement referred as

*Reprinted with permission from "Code design for flicker mitigation in visible light communications using finite state machines" by Mejia CE, Georghiades CN, Abdallah MM, Al-Badarneh YH, 2017. *IEEE Transactions on Communications*, 65(5) pp.2091-2100, Copyright © 2011 IEEE

*perceived flicker index* (PFI) is defined as

$$\mathrm{PFI} = \frac{E_c(\omega_0)}{E_u(\omega_0)}, \tag{3.1}$$

where $E(\omega_0)$ is the *perceived flicker energy*, $\omega_0$ is the normalized angular frequency corresponding to the maximum perceived flicker frequency ($F = F_0$) and the subindices $c$ and $u$ denote coded and uncoded systems, respectively.

To understand the nature of $E(\omega_0)$, the *total power spectral density* is defined as the product of the *power spectral density* function, $P(\omega)$, and the *energy spectrum*, $Q(\omega)$ [27]. While $P(\omega)$ accounts for the optical power introduced by the randomness of the code as a function of the *autocorrelation coefficients* [27, Chapter 3], $Q(\omega)$ represents the optical power related to both the pulse-shape and modulation format. Finally, $E(\omega_0)$ is defined as

$$E(\omega_0) = \frac{1}{2\pi} \int_{-\omega_0}^{\omega_0} P(\omega) Q(\omega) d\omega. \tag{3.2}$$

A physical meaning of $E(\omega_0)$ is the total amount of optical energy located in the frequency range where the human eye perceives light flickering.

To evaluate $E_c(\omega)$, $P(\omega)$ is calculated using the expression presented in Appendix A.1 by obtaining the *autocorrelation coefficients*, $R_x(k)$, of each code assuming the encoding process is stationary with independent and equiprobable input bits. Examples to calculate $R_x(k)$ of codes are presented in [27, Chapter 3]. Expressions of $Q(\omega)$ for OOK and VPPM with rectangular pulses are presented in Appendix A.2. In Chapter 3, VPPM of 50% duty-cycle is used for computing PFI and evaluating error rate, and referred as binary PPM (2PPM) in there.

Finally, Appendix A.3 presents an expression for $E_u(\omega_0)$ assuming both zeros and ones are transmitted with equal probability, OOK modulation and rectangular pulses.

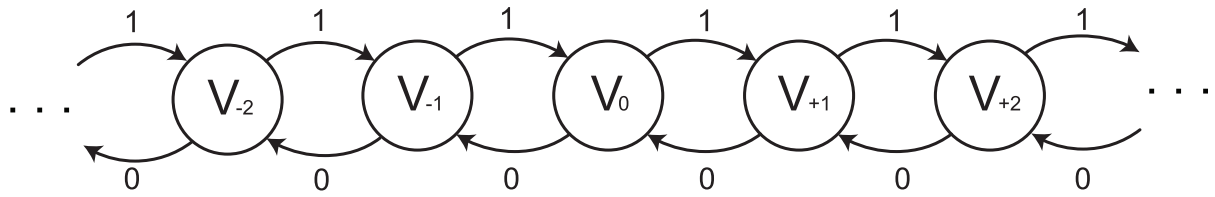


Figure 3.1: DC-balanced code finite-state machine [Reprinted with permission from "Code design for flicker mitigation in visible light communications using finite state machines" by Mejia CE, Georghiades CN, Abdallah MM, Al-Badarneh YH, 2017. *IEEE Transactions on Communications*, 65(5) pp.2091-2100, Copyright © 2011 IEEE].

### 3.2 Code Design for Intensity Flicker Mitigation

The FSM in Fig. 3.1 constrains the number of consecutive zeros or ones to a finite number. For example, with 3 states, $V_{-1}, V_0, V_{+1}$, the longest string of zeros or ones is limited to 2. With the initial state being $V_0$ (perfect balance) and logic bit one mapped into $x = 1$ and logic bit zero mapped into $x = -1$, each state represents the *running digital sum* (RDS) (sum of transmitted 1s or -1s) in the transmitted sequence and each branch represents a unidirectional transition due to either zero or one being transmitted. In this Chapter, $V_{+i}$ denotes the state where RDS=$i$.

As shown in [27], the low-frequency components of the *Power Spectral Density* (PSD) and the number of allowable sequences generated from the FSM in Fig. 3.1 increase with the *number of states*, $N$. The increase of the low-frequency components of the PSD leads to a higher flicker energy while the increase in the number of allowable sequences implies a higher FSM capacity and therefore the possibility of designing higher rate codes. Thus, the value of $N$ involves a trade-off between perceived flicker and code rate.

In particular, the adjacency matrix of the FSM in Fig. 3.1 is an $N \times N$ symmetric Toeplitz matrix. For the FSM in Fig. 3.1 with $N$ states, the capacity is shown in [34] (see also [27, Chapter 8]) to be $C(N) = \log_2 \left[2 \cos\left(\frac{\pi}{N+1}\right)\right]$ bits for $N \geq 3$, which as expected is an increasing function of $N$.

For $p$ in the code design, one simple option is to choose $p = \lfloor \log_2 \left( \min_{i \in RDS} |CW(V_{+i})| \right) \rfloor$ and then eliminate all codewords in excess of $2^p$ emanating from each state. However, this in general

results in a low code rate. An alternative option to design higher rate codes is to eliminate states to achieve a larger $p$. In order to increase the code rate, the algorithms are based on the following three observations:

1. Rates closer to the capacity can potentially be achieved by increasing $q$.

2. Higher capacities are obtained by increasing the number of states; however, the larger the number of states, the higher the perceived flicker energy and potentially complexity.

3. For even $q$, the minimum Hamming distance, $d_H$, between codewords of the sets $CW(V_{+i})$ and $CW(V_{+j})$ is equal to $\frac{(i-j)}{2}$. The $d_H$ between codewords of the same disparity is equal to 2.

As a result, and as pointed out above, there is a trade-off between high rate, perceived light flicker, and coding gain where $N$ is the control variable. Therefore, two algorithms are proposed to design high rate codes with low perceived flicker and soft-decision decoding by the Viterbi algorithm. The first algorithm designs codes for small $N$ in the FSM, while the second algorithm design codes relaxing $N$ to obtain higher $d_H$ between sequences.

In the following sections, the notation used for the algorithms is: the state $V_{+i}^{j}$ denotes a split state $j$ with RDS $i$. If $j$ is omitted, the state is not split (a state is split if the state is partitioned in two or more states with the same RDS). For the codeword notation, a *codeword subset* is denoted by $CW_{+k}^{y}$ where the superscript $y$ is to identify the subset. Finally, $CW(V_{+i})$ denotes the set of all possible codewords in state $V_{+i}$ and $|CW(V_{+i})|$ is its cardinality.

### 3.3 Algorithm 1: High Rate Codes with Low PFI Based on Small Number of States

The main idea of Algorithm 1 is to obtain high code rates with a reduced number of states to mitigate flickering. The algorithm begins with $D^q$ and the set of edges (codewords of length $q$) emanating from each state. Based on the FSM capacity $C$, $p$ is selected such that $p/q \leq C$ and check the number of codewords per state. If any of the states has a total of codewords less than $2^p$, states with a larger number of codewords are split and repeated as needed until the minimum

number of codewords out of each state is $2^p$ eliminating codewords in excess until obtaining $2^p$ per state. If the number of codewords at all states is larger or equal to $2^p$, proceed directly with the elimination of codewords. Finally, the codewords are tagged with information bits. In eliminating codewords, look for ways to increase minimum distance if possible. There is no unique way to split states or to eliminate codewords and part of the process to design the best possible code relies on the intuition of the designer. To illustrate Algorithm 1, an example composed of two alternatives is presented. The first alternative is used when the number of codewords per state is greater or equal to $2^p$ while the second is a hypothetical example when the number of codewords per state is lower than $2^p$.

**Algorithm 1** Constraining the Number of States

From $D^q$, select states $\left(\overline{V}\right)$ and their codeword sets $CW$
Select $p$ such that $C \geq \frac{p}{q}$
**if** $|CW(V_{+i})| < 2^p$ for any $i$ **then**
    **repeat**
        **for** $V_{+i} \in \overline{V}$ **do**
            **if** $|CW(V_{+i})| > 2^p$ **then**
                Split $V_{+i}$ in $m$ states
                Partition $CW(V_{+i})$ in $m$ subsets
                Ensure $\bigcap_{all\, w} CW(V_{+i}^w) = \emptyset$ for $w = 1, ..m$
                **for** $V_{+i}^k$ for k=1,..m **do**
                    **if** $|CW(V_{+i}^k)| < 2^p$ **then**
                        Replicate $m$ times $CW(V_{+i}^k)$ and connect to the states depending of the disparity
                    **else**
                        Connect to the states depending of the disparity
                    **end if**
                **end for**
            **else**
                Partition codewords in $CW(V_{+i})$ in subsets
                Replicate codewords in $CW(V_{+i}^k)$ and connect to the next state according disparity
            **end if**
            Ensure repeated codewords are uniquely decoded using future codewords
            Eliminate codewords until there are $2^p$ codewords in all states
        **end for**
    **until** $|CW(V_{+i}^k)| = 2^p \; \forall i, j$
**end if**
Ensure $|CW(V_{+i}^k)| = 2^p \; \forall i, j$ and do the mapping between information bits and codewords

For the first alternative, Fig. 3.2(a) presents an FSM composed of four states. By selecting $q = 2$, the possible codeword sets are $CW(V_{-1}) = \{01, 11\}$, $CW(V_0) = \{01, 10, 11\}$ , $CW(V_{+1}) = \{01, 10, 00\}$, and $CW(V_{+2}) = \{10, 00\}$ shown in Fig. 3.2(b). Then, states $V_0$ and $V_{+2}$ are eliminated keeping an FSM composed from states $V_{-1}$ and $V_{+1}$. Interestingly, this does not reduce the capacity as the two pairs of states are not connected. Choosing $p = 1$, the codeword $01$ is eliminated from $CW(V_{+1})$ obtaining a code with rate $1/2$ presented in Fig. 3.2(c).

For the second alternative, an FSM composed of four states with $q = 2$ is used obtaining the FSM in Fig. 3.3(b). Eliminating states $V_0$ and $V_{+2}$ and codeword $01$ from $CW(V_{-1})$, the FSM presented in Fig. 3.3(b) is obtained where $CW(V_{-1}) = \{11\}$ and $CW(V_{+1}) = \{00, 01, 10\}$. This is a hypothetical example to explain the case where a state has a low number of codewords. Because of $|CW(V_{-1})| < 2$, state $V_{+1}$ are split in two states ($V_{+1}^1$ and $V_{+1}^2$) and the set $CW(V_{+1})$ is partitioned in two subsets $CW(V_{+1}^1) = \{01\}$ and $CW(V_{+1}^2) = \{00, 10\}$. In state $V_{+1}^1$, codeword $01$ is repeated twice; one codeword is connected to $V_{+1}^1$ and the other to $V_{+1}^2$. In $V_{+1}^2$, codeword $10$ is repeated twice, and similarly to codeword $01$ in $V_{+1}^1$, one codeword is connected to $V_{+1}^2$ and the other to $V_{+1}^1$. In addition, codeword $00$ is connected to state $V_{-1}$.

In state $V_{-1}$, codeword $11$ is repeated and connected to state $V_{+1}^1$ and $V_{+1}^2$ as presented in Fig. 3.3(c) ensuring the set of codewords in both states are different. Then,the excess of codewords at each state is eliminated and each codeword is tagged to an information bit. The final FSM is presented in Fig. 3.3(d).

During the process, the codewords $01$, $10$ and $11$ are ensured to be uniquely decoded by observing future codewords. For example, if codeword $11$ is received and the next codeword is $\{01\}$ the decoded information bit is $0$ while if the next codeword is either $\{10\}$ or $\{00\}$ the decoded bit is $1$. The codeword $00$ could be decoded without looking ahead.

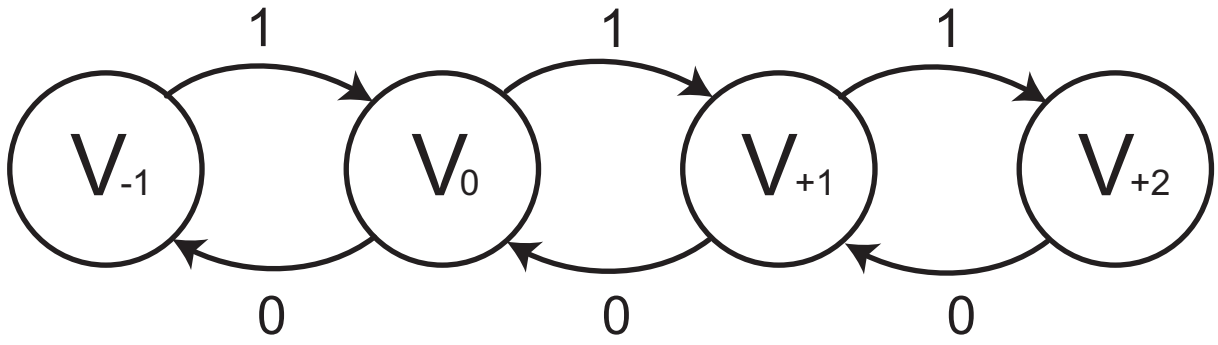


(a)

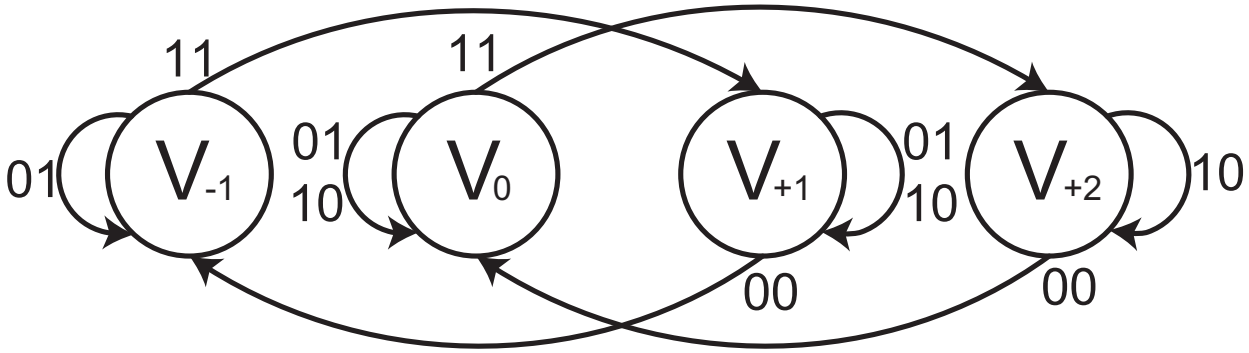


(b)

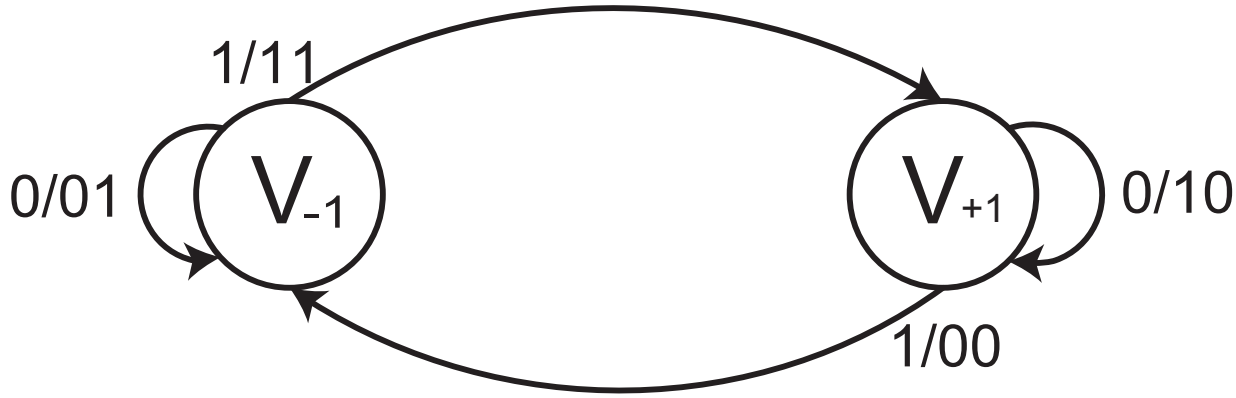


(c)

Figure 3.2: Example of Algorithm 1 - Alternative 1 [Reprinted with permission from "Code design for flicker mitigation in visible light communications using finite state machines" by Mejia CE, Georghiades CN, Abdallah MM, Al-Badarneh YH, 2017. *IEEE Transactions on Communications*, 65(5) pp.2091-2100, Copyright © 2011 IEEE].

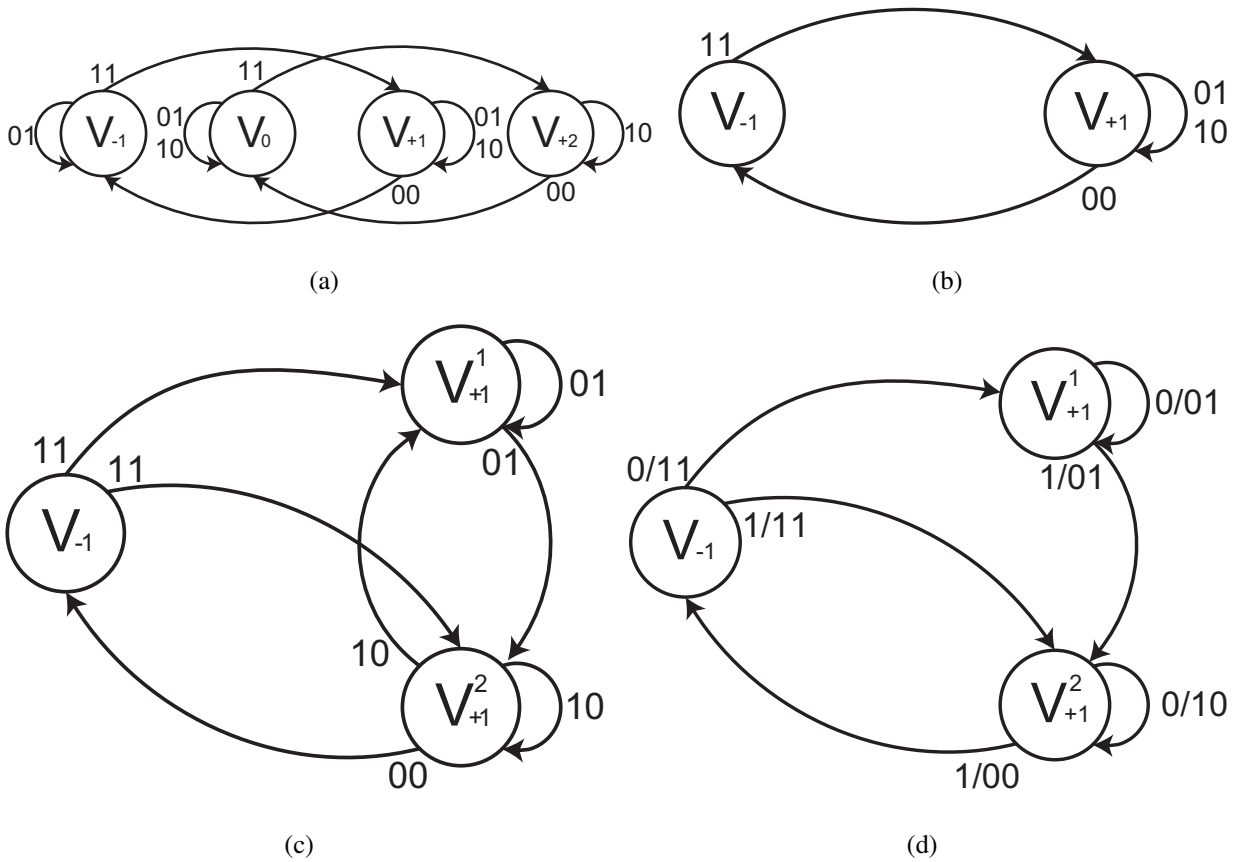


Figure 3.3: Example of Algorithm 1 - Alternative 2 [Reprinted with permission from "Code design for flicker mitigation in visible light communications using finite state machines" by Mejia CE, Georghiades CN, Abdallah MM, Al-Badarneh YH, 2017. *IEEE Transactions on Communications*, 65(5) pp.2091-2100, Copyright © 2011 IEEE].

The (4,6,3) and (3,4,4) codes are developed using this algorithm where the triplet $(p, q, d)$ is a code with rate $p/q$ and sequences of at most $d$ equal consecutive bits. We choose these parameters for labeling our codes because they describe the code in terms of rate and flicker attenuation. Both codes are presented in Appendices B.2 and B.3, respectively.

### 3.4 Algorithm 2: High Rate Codes with Low PFI and $d_H = 4$.

Algorithm 2 is based on the partitioning of a codeword set in subsets of high $d_H$, splitting of the states, and distributing the codeword subsets such that all possible sequences in the FSM have a $d_H = 4$. The algorithm begins by choosing states $V_{-2}$ and $V_{+2}$ and selects all possi-

ble codewords of length $q$ with disparity $+4$, $-4$ and $0$ and chooses $p$ such that $|CW(V_{+2})|$ and $|CW(V_{-2})|$ are less than $2^p$. Then, it partitions the codewords in subsets where $d_H = 4$ and splits both states avoiding that codewords of the same subset arrive to a common state. Finally, it eliminates codewords until the number of codewords is equal to $2^p$ and tags with the information bits. To illustrate the algorithm, Fig. 3.4(a) presents a FSM with two states $V_{-2}$ and $V_{+2}$, codewords $CW(V_{-2}) = \{1100, 0011, 0101, 1010, 1001, 0110, 1111\}$, and $CW(V_{+2}) = \{1100, 0011, 0101, 1010, 1001, 0110, 0000\}$ as a result from a FSM with 9 states ($V_{-4}$, $V_{-3}$, $V_{-2}$, $V_{-1}$, $V_0$, $V_{+1}$, $V_{+2}$, $V_{+3}$, and $V_{+4}$). As a result, the FSM in Fig. 3.4(a) has a $d_H = 2$.

**Algorithm 2** Improving the CER Performance for $d_H = 4$

**Input:** $V_{+2}$, $V_{-2}$ and $q$
1: Obtain $CW_{-4}$ and $CW_0$ at $V_{+2}$
2: Obtain $CW_{+4}$ and $CW_0$ at $V_{-2}$
3: $CW(V_{+2}) = CW_{-4} \cup CW_0$
4: $CW(V_{-2}) = CW_{+4} \cup CW_0$
5: Choose $p$ s.t. both $|CW(V_{+2})|$ and $|CW(V_{-2})| \geq 2^p$
6: **repeat**
7: Create $CW_{+x}^y \subset CW_{+x}$ s.t. the $d_H = 4$ for $x = 0, \pm 4$
8: Split both $V_{+2}$ and $V_{-2}$
9: Connect the codeword subsets
10: Ensure no codeword is connected twice to a state
11: **until** all FSM sequences have $d_H = 4$
12: Eliminate codewords until $|CW(V_{+i}^j)| = 2^p$ for $i = \pm 2$
**Output:**
$|CW(V_{+i}^j)| = 2^p,\ i, j$ and map codewords to information bits

In $V_{-2}$ and $V_{+2}$, the codewords are partitioned in subsets with $d_H = 4$: $CW_{+4} = \{1111\}$, $CW_{-4} = \{0000\}$, $CW_0^1 = \{0101, 1010\}$, $CW_0^2 = \{1100, 0011\}$, and $CW_0^3 = \{1001, 0110\}$. Then, $V_{-2}$ is split in two states $V_{-2}^1$ and $V_{-2}^2$; the split states are connected by the codeword subsets with zero-disparity. The same process is repeated for state $V_{+2}$. Now, the split states are connected by the codeword subset with disparity different than zero ensuring $d_H = 4$ is preserved in the sequence as shown in Fig. 3.4(b). Finally, the excess codewords are eliminated and the codewords

are tagged to be uniquely decodable using all the codewords in subsets $CW_0^1$, $CW_0^2$, and $CW_0^3$ to increase the diversity during the decoding process. The resulting FSM is presented in Fig. 3.4(c).

The (4,6,7), (6,8,9), and (8,10,11) codes are designed with Algorithm 2. The codes are presented in Appendices B.4, B.5, and B.6, respectively.

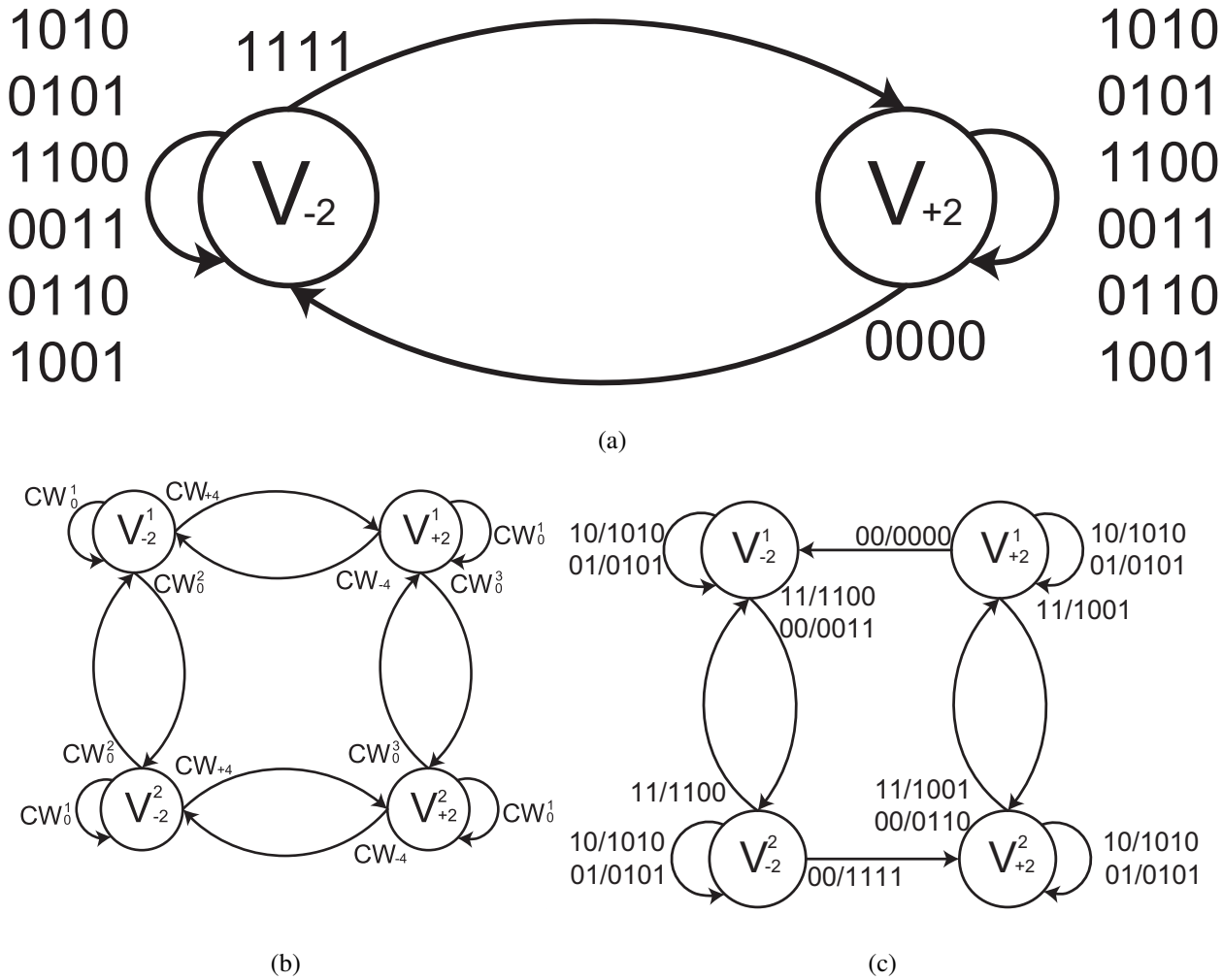


Figure 3.4: Example of Algorithm 2 [Reprinted with permission from "Code design for flicker mitigation in visible light communications using finite state machines" by Mejia CE, Georghiades CN, Abdallah MM, Al-Badarneh YH, 2017. *IEEE Transactions on Communications*, 65(5) pp.2091-2100, Copyright © 2011 IEEE].

## 3.5 Performance Analysis

### 3.5.1 Perceived Flicker Index

In [7], the authors report that flicker frequencies above 200Hz are not perceived by the human eye. Even though, there are certainly variations in visual perception from human to human, this frequency value was used to produce some numerical results for relative comparison of the different coding schemes. Similar comparisons can be easily made for other reference frequencies. Based on this, the PFI in (3.1) is calculated with parameter $F_0 = 200$Hz for an optical signal with a clock rate $F_b$ between 200 bps and 120 Mbps. To calculate $E_c(\omega_0)$, the modulation is OOK except in the 4B6B standard code which uses 2PPM; the energy per symbol is normalized to one. The PFI for each studied code is presented in Fig. 3.5.

### 3.5.2 Codeword Error Rate

The simulations are conducted by encoding equiprobable information bits. The Manchester, 4B6B and 8B10B codes are decoded by brute force, optimal soft-decision decoding, while the developed codes are optimally soft-decision decoded using the Viterbi algorithm with a sliding window of $200$ codewords. For the simulations of our codes, the initial state is the positive state closest to $V_0$ and is known by the receiver.

Table 3.1 presents the analytical parameters of each studied codes and Fig. 3.6 shows the simulation results.

### 3.5.3 Discussion

Based on the code PFI and CER performance at $10^{-5}$, the simulation results present the following behavior:

- Comparing the PFI between the studied codes, the 4B6B standard code with 2PPM is the best with respect to flicker mitigation. This is not surprising since 2PPM is an equal energy signaling scheme, albeit requiring twice the clock rate compared to OOK. Similarly, the Manchester code is better than other OOK modulated codes, which is again not surprising

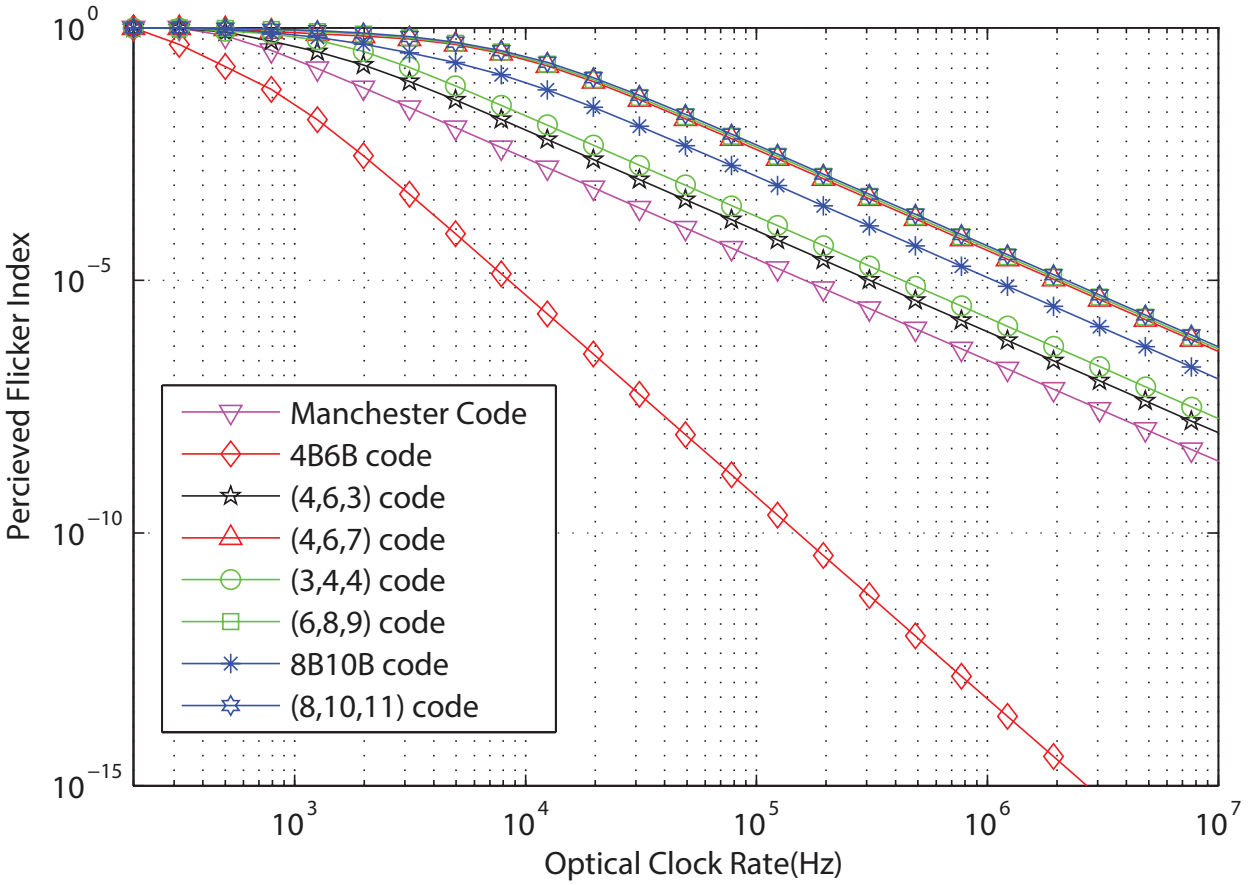


Figure 3.5: The Perceived Flicker Index of the studied codes [Reprinted with permission from "Code design for flicker mitigation in visible light communications using finite state machines" by Mejia CE, Georghiades CN, Abdallah MM, Al-Badarneh YH, 2017. *IEEE Transactions on Communications*, 65(5) pp.2091-2100, Copyright © 2011 IEEE].

Table 3.1: Parameters for Code Simulation [Reprinted with permission from "Code design for flicker mitigation in visible light communications using finite state machines" by Mejia CE, Georghiades CN, Abdallah MM, Al-Badarneh YH, 2017. *IEEE Transactions on Communications*, 65(5) pp.2091-2100, Copyright © 2011 IEEE]

| Code | Parameters | | | |
|---|---|---|---|---|
| | Modulation | $R$ | $K_c$ | $d^2_{\min}$ |
| Manchester Code (MC) | OOK | 1/2 | 1 | $4E_s$ |
| 4B6B | 2PPM | 2/3 | 7 | $4E_s$ |
| 8B10B | OOK | 4/5 | 7.62 | $2E_s$ |
| (4,6,3) | OOK | 2/3 | 11.43 | $4E_s$ |
| (3,4,4) | OOK | 3/4 | 12.25 | $4E_s$ |
| (4,6,7) | OOK | 2/3 | 40.64 | $8E_s$ |
| (6,8,9) | OOK | 3/4 | 128.1 | $8E_s$ |
| (8,10,11) | OOK | 4/5 | 305.6 | $8E_s$ |

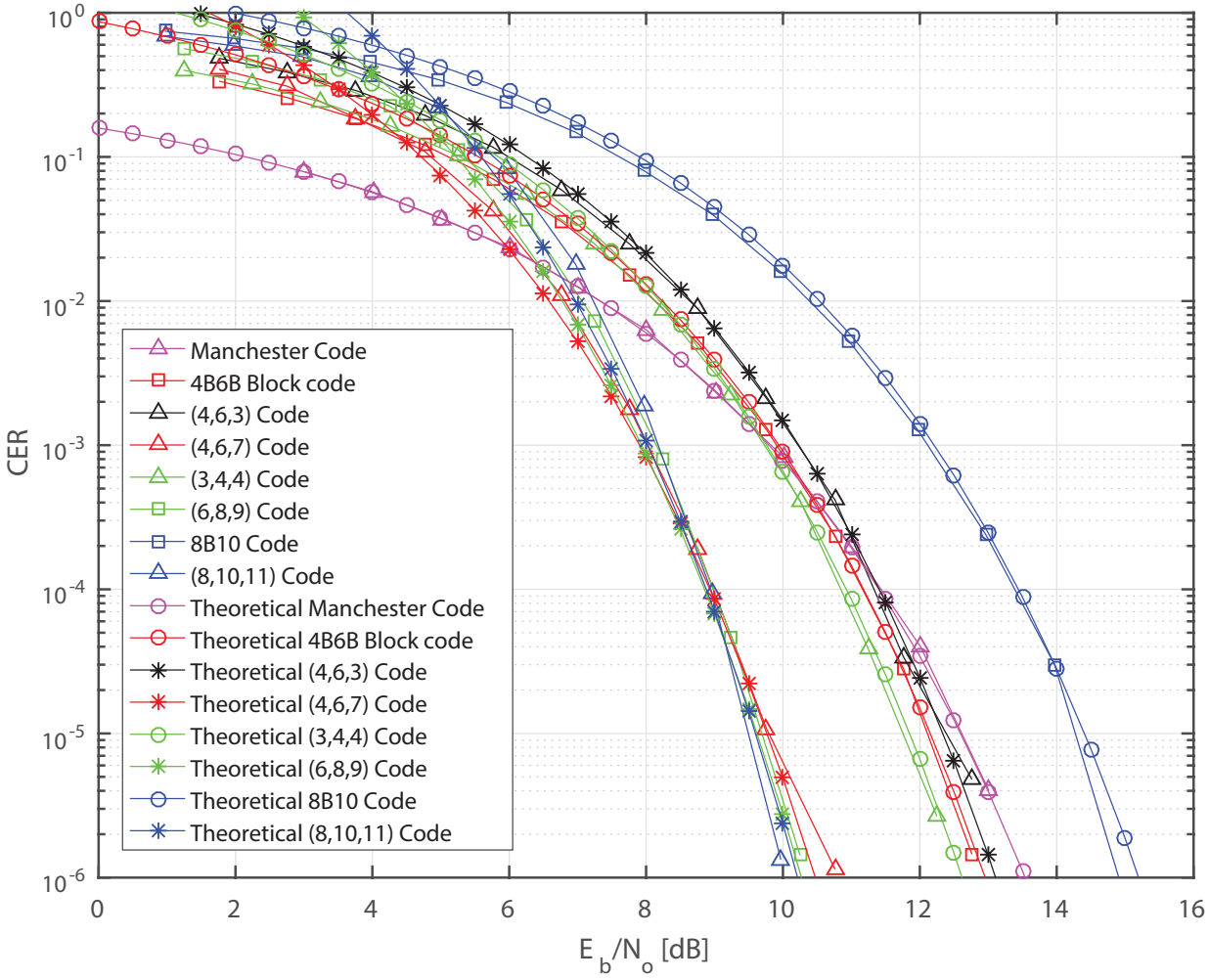


Figure 3.6: Codeword error-rate probability of the studied codes [Reprinted with permission from "Code design for flicker mitigation in visible light communications using finite state machines" by Mejia CE, Georghiades CN, Abdallah MM, Al-Badarneh YH, 2017. *IEEE Transactions on Communications*, 65(5) pp.2091-2100, Copyright © 2011 IEEE].

since each information bit is mapped into an equal energy pair of transmitted bits (01 and 10). In terms of coding gain, the 4B6B standard code is about 0.5 dB better than the Manchester code at an error rate of $10^{-5}$ (and asymptotically at high SNRs about 1.25dB better).

- To obtain a PFI similar to the Manchester code, the $(4, 6, 3)$ code must transmit at approximately twice the optical clock rate (OCR). In coding gain, the $(4, 6, 3)$ code is approximately 0.2 dB better than the Manchester code (which has a lower rate), but approximately 0.2 dB worse than the 4B6B code. Theoretically and for large SNR of course the $(4, 6, 3)$ code and the 4B6B code have similar performance which is about 1.25dB (asymptotically) better than the Manchester code. It would seem then the main benefit of the $(4, 6, 3)$ code is in its trellis structure which allows efficient optimal soft-decision decoding using the Viterbi algorithm and which can make it easier to combine an inner code with an outer code for better performance.

- The $(3, 4, 4)$ code requires approximately three times the Manchester code OCR to obtain the same PFI and has a coding gain about 0.7dB and 0.3dB compared to the Manchester and 4B6B codes, respectively, while also having a higher rate (3/4 vs 1/2 and 2/3).

- The $(4, 6, 7)$ code needs to transmit at an OCR of about 2 and 10 times greater to obtain the same PFI as the 8B10B code and the Manchester code, respectively. Its coding gain at a CER of $10^{-5}$ is about 2.7, 2.2 and 4.5dB greater than the Manchester code, the 4B6B code, and the 8B10B code, respectively. Asymptotically for high SNRs these gains are about 4.0, 3.0 and 5.0 dB, respectively. Similarly, the $(6, 8, 9)$ code requires about twice and twelve times greater OCR than the 8B10B code and Manchester code for the same PFI, respectively. Therefore, the $(4, 6, 7)$ and $(6, 8, 9)$ codes are good candidates for high rate and high reliability applications in PHY II.

- For the same code rate, the $(8, 10, 11)$ code has almost a 4.5dB gain at a CER of $10^{-5}$ compared to the 8B10B standard code (and asymptotically a 6dB gain). Since the $(8, 10, 11)$

code requires more than 2 times the 8B10B code OCR and about 13 times the Manchester code OCR, it may be more suitable for the higher OCR in PHY II.

# 4. CODE DESIGN WITH COLOR-SHIFT-KEYING CONSTELLATIONS

Color-shift-keying (CSK) is a modulation scheme used in visible light communication (VLC) to transmit data by varying the intensity of red, green and blue LEDs. This chapter proposes channel coding for VLC using CSK under constraints of no color-shift and no intensity flicker (explained in Chapter 2) during transmission and design codes over newly introduced CSK constellations using triangle partition. Two classes of codes are proposed: one class of codes is based on FSMs which impose the no intensity and no color shift constraints and the other class of codes is based on the concept of TCM referred to as CSK-FSM and CSK-TCM, respectively.

## 4.1 Constellation Design by Triangle Partition (TP)

The constellation design presented in this paper consists of grouping symbols such that the mean of their coordinates is equal to the $T_c$, chosen here to be at the intensity plane centroid. Also, the constellation sizes are not constrained to be in powers of two as we carefully map information bits to symbol sequences instead of single symbols in the encoding process.

This study assumes ideal conditions at the receiver denoting $\mathrm{diag}(\mathcal{A}) = \sqrt{\frac{E}{T_b}}[1\ 1\ 1]^T$, where $E$ is the received energy and $T_b$ is the CSK symbol duration. Fig. 4.1(b) presents an example of the transformation from the chromaticity diagram to the intensity plane whose vertices are orthogonal. However, this section presents analytical results for non-orthogonal intensity planes.

In this constellation design methodology, the symbols are selected in three steps:

- Allocate intensity symbols $\sigma_1$, $\sigma_2$, and $\sigma_3$ in the vertices of the intensity plane.
- Divide the intensity plane triangle presented in Fig. 4.1(b) into $K^2,\ K = 1, 2, \cdots$, equal triangles similar to the intensity plane such that their angles are congruent to the intensity plane angles.
- Designate symbols to be at the vertices of each triangle resulting in $N = (K+1)(K+2)/2$ constellation symbols.

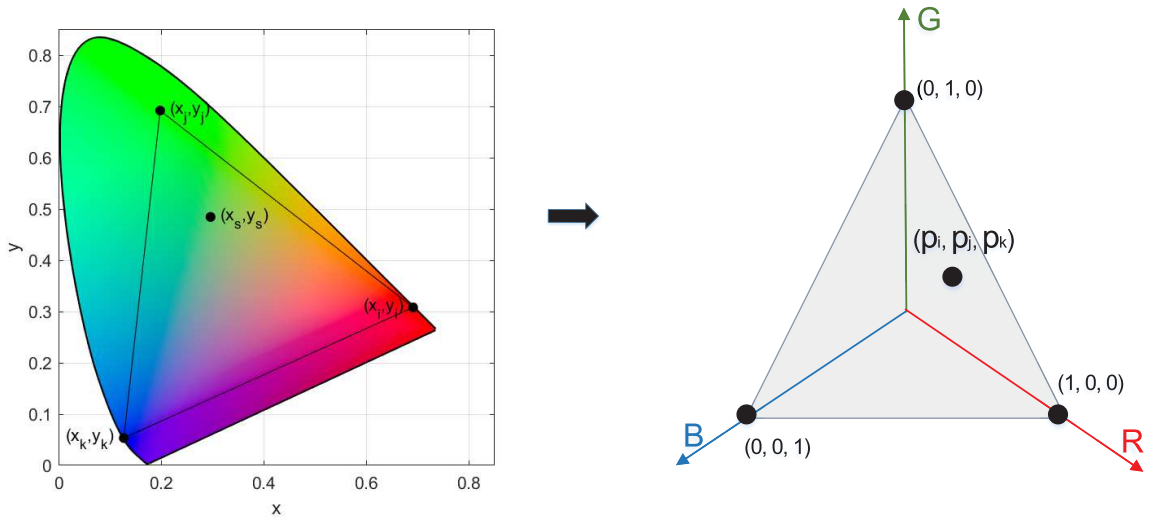


(a) Chromaticity diagram.

(b) Intensity plane.

Figure 4.1: Mapping from the chromaticity diagram to the intensity plane.

Fig. 4.2 presents four constellations for $K = 1, 2, 3, 4$. We refer to this methodology for constellation design as *triangle partition* (TP).

In TP, the designed constellations are composed of the symbol set $S = \{\sigma_1, \sigma_2, ...\sigma_N\}$ with cardinality

$$N = \frac{(K+1)(K+2)}{2}, \tag{4.1}$$

where each symbol is at coordinates

$$\sigma_x = \frac{K-i}{K}\sigma_1 + \frac{i-j}{K}\sigma_2 + \frac{j}{K}\sigma_3 \quad for \quad 0 \leq j \leq i \leq K \tag{4.2}$$

in the intensity triangle plane with vertices $\sigma_1$, $\sigma_2$, and $\sigma_3$, all three of which are part of each triangle partition constellation; $x \in \{4, 5, \cdots, N\}$ is the constellation symbol index.

Next, we analyze the performance of the triangle partition constellations by determining their minimum Euclidean distance normalized by the average energy per information bit. The three

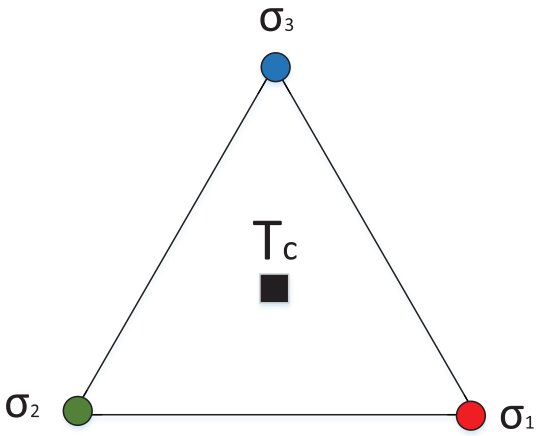


(a) 3-CSK constellation.

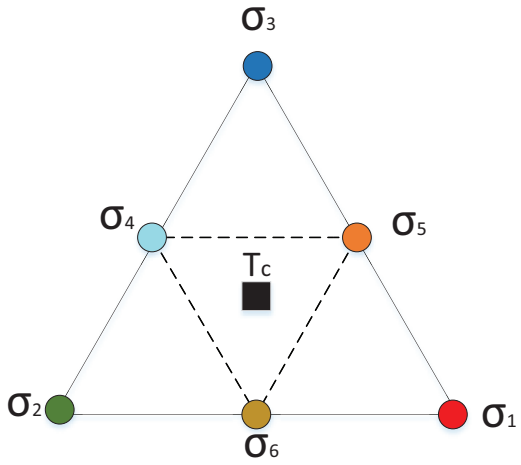


(b) 6-CSK constellation.

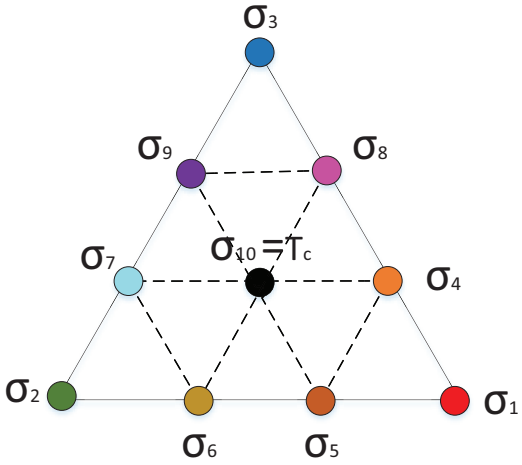


(c) 10-CSK constellation.

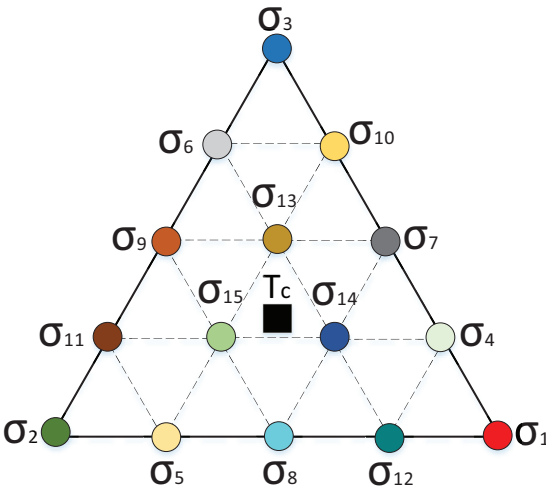


(d) 15-CSK constellation.

Figure 4.2: CSK constellations using TP for a) $K = 1$, b) $K = 2$, c) $K = 3$, and d) $K = 4$.

constellation symbols at the vertices of the triangle intensity plane in general are scaled by $\sqrt{E}$ according to the ideal conditions presented above, i.e., $\sigma_1\sqrt{E}$, $\sigma_2\sqrt{E}$, $\sigma_3\sqrt{E}$. Then the triangle partition constellation symbols are $\sigma_x\sqrt{E}$. For a given $K$, the minimum distance of the resulting triangle partition constellation can then be obtained in general as:

$$d^2_{\min} = \frac{\min\{\|\sigma_1-\sigma_2\|^2, \|\sigma_1-\sigma_3\|^2, \|\sigma_2-\sigma_3\|^2\}E}{K^2}, \tag{4.3}$$

$$\leq \frac{2E}{K^2}, \tag{4.4}$$

which for a triangle with orthogonal vertices (and also equilateral in this case) results in $d^2_{\min} = 2E/K^2$. The average energy per symbol of the constellation is obtained as:

$$\bar{E} = \frac{E}{6K}\left[(K+1)\sum_{i=1}^{3}\sigma_i^T\sigma_i + (K-1)\sum_{i=1}^{2}\sum_{j=i+1}^{3}\sigma_i^T\sigma_j\right], \tag{4.5}$$

which for an intensity triangle plane with orthogonal vertices (which implies an equilateral triangle) becomes $\bar{E} = (K+1)E/2K$. Letting $\bar{E}_b$ be the average energy per information bit we have $\bar{E} = \bar{E}_b \log_2(N)$. Using this and replacing (4.5) in (4.3), the normalized minimum distance of TP constellations can be expressed as:

$$\frac{d^2_{\min}}{\bar{E}_b} = \left[\frac{3}{2}.\frac{\delta^2_{\min}}{1+\frac{K-1}{K+1}\delta_c^2}\right]\left[\frac{4\log_2(N)}{K(K+1)}\right], \tag{4.6}$$

where

$$\delta^2_{\min} = \frac{\min\{\|\sigma_1-\sigma_2\|^2, \|\sigma_1-\sigma_3\|^2, \|\sigma_2-\sigma_3\|^2\}}{\|\sigma_1\|^2+\|\sigma_2\|^2+\|\sigma_3\|^2} \leq \frac{2}{3}, \tag{4.7}$$

$$\delta_c^2 = \frac{\sigma_1^T\sigma_2+\sigma_1^T\sigma_3+\sigma_2^T\sigma_3}{\|\sigma_1\|^2+\|\sigma_2\|^2+\|\sigma_3\|^2} \geq 0, \tag{4.8}$$

where equality in equations (4.7) and (4.8) is iff $\sigma_1,\ \sigma_2,\ \sigma_3$ are orthogonal, in which case the triangle intensity plane is an equilateral triangle. Notice that $\delta^2_{\min}$, and $\delta_c^2$ depend on the selection of the triangle vertices.

In analyzing (4.6) for different values of the $T_c$, we redifine the left-hand side bracket of the

mentioned expression as

$$\theta = \frac{3}{2}.\frac{\delta_{\min}^2}{1+\frac{K-1}{K+1}\delta_c^2} \leq 1 \tag{4.9}$$

where the upper bound above is in view of the bounds in (4.7) and (4.8), with equality again iff the vertices are orthogonal. In that (equilateral triangle) case, the expression in (4.6) becomes

$$\frac{d_{\min}^2}{\bar{E}_b} = \frac{4\log_2(N)}{K(K+1)}. \tag{4.10}$$

Fig. 4.3 presents the normalized minimum squared distance for an intensity triangle plane with vertices $\sigma_1 = \left[\alpha \; \frac{1-\alpha}{2} \; \frac{1-\alpha}{2}\right]^T$, $\sigma_2 = [0\,1\,0]^T$, $\sigma_3 = [0\,0\,1]^T$, and $T_c = [\frac{\alpha}{3} \; \frac{3-\alpha}{6} \; \frac{3-\alpha}{6}]^T$ for $1/3 \leq \alpha \leq 1$ and $1 \leq K \leq 10$. As expected, $\theta$ increases monotonically with $\alpha$ and is maximum when $\alpha = 1$, corresponding to orthogonal vertices and an equilateral triangle.

For orthogonal vertices $\sigma_1 = [1\,0\,0]^T$, $\sigma_2 = [0\,1\,0]^T$, $\sigma_3 = [0\,0\,1]^T$, Fig. 4.4 compares TP constellations with the powers of two constellations proposed in [6] and [28]. The superior performance of TP constellations for all rates studied is clear from the figure. We include in the comparison the optimal/conjectured equidistant distribution of points in an equilateral triangle (no color constraint) presented in [35] and the optimized constellations presented in [36], thus confirming that ideal TP constellations (or triangular number constellations) is best for providing maximum minimum distance for their achieved rates.

On the other hand, performance is worse when $\theta \neq 1$ (and thus $T_c \neq [\frac{1}{3} \; \frac{1}{3} \; \frac{1}{3}]^T$) and constellations designed with algorithms like billiards and interior points could provide better results for symbol-by-symbol decoding. However, TP is the key for designing CSK-FSM and CSK-TCM codes because the symmetry in the symbol allocation is important to control the desired $T_c$. We will show next that codes using TP constellations provide good coding gains while preserving the balance around $T_c$.

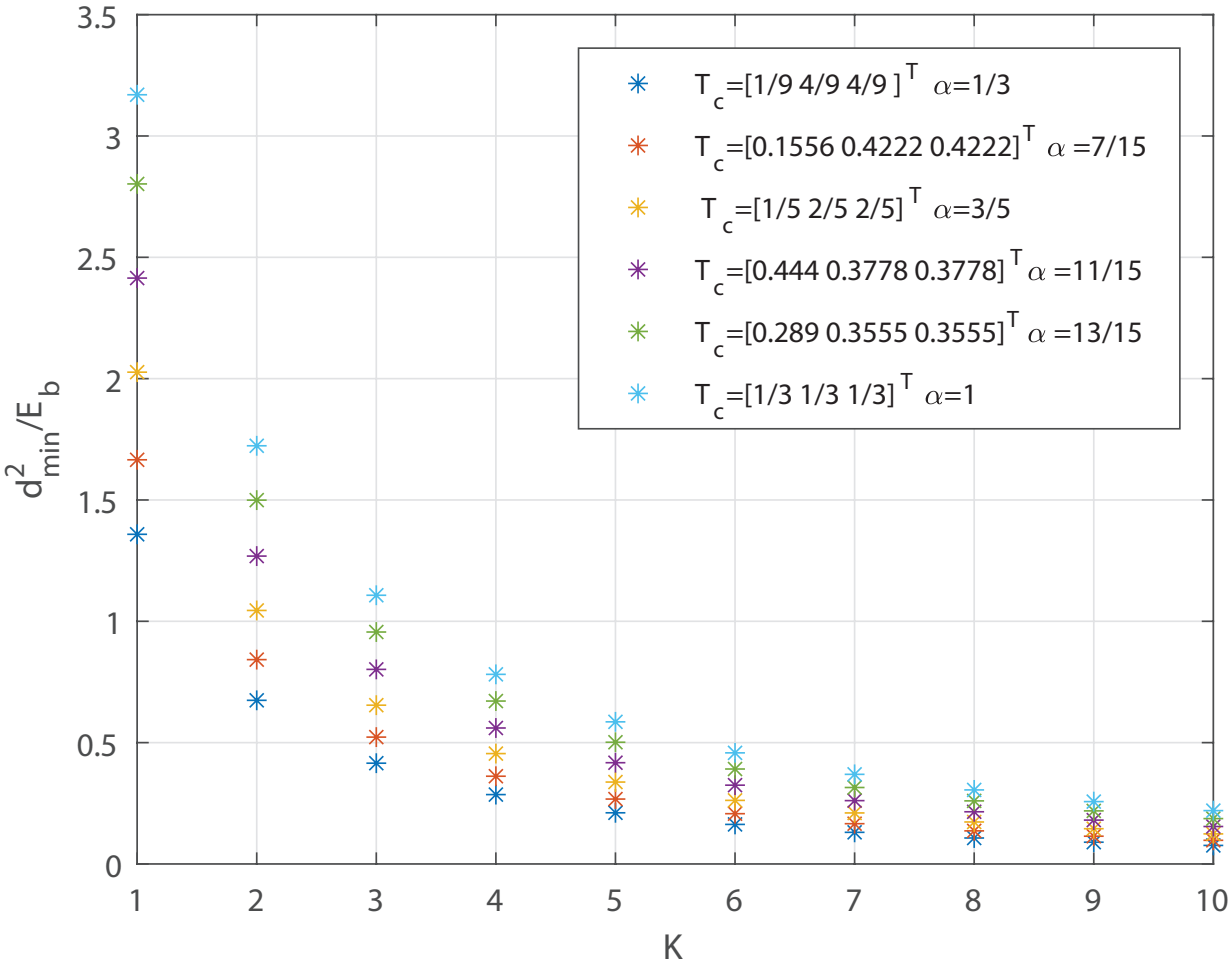


Figure 4.3: Normalized minimum squared distance as a function of $\alpha$ and $K$.

## 4.2 Code Design Using CSK-FSM

### 4.2.1 Illumination Constraints in CSK-FSM

Based on expression (2.15) and the analytical analysis of the previous subsections, the intensity symbols have a direct relation with the desired perceived chromaticity. Thus, we continue our study in the intensity domain at the receiver side to facilitate the analysis for comparing the proposed codes. The desired perceived chromaticity in the time domain is equal to

$$\Omega_n = \mathcal{P}\mathcal{I}T_c, \tag{4.11}$$

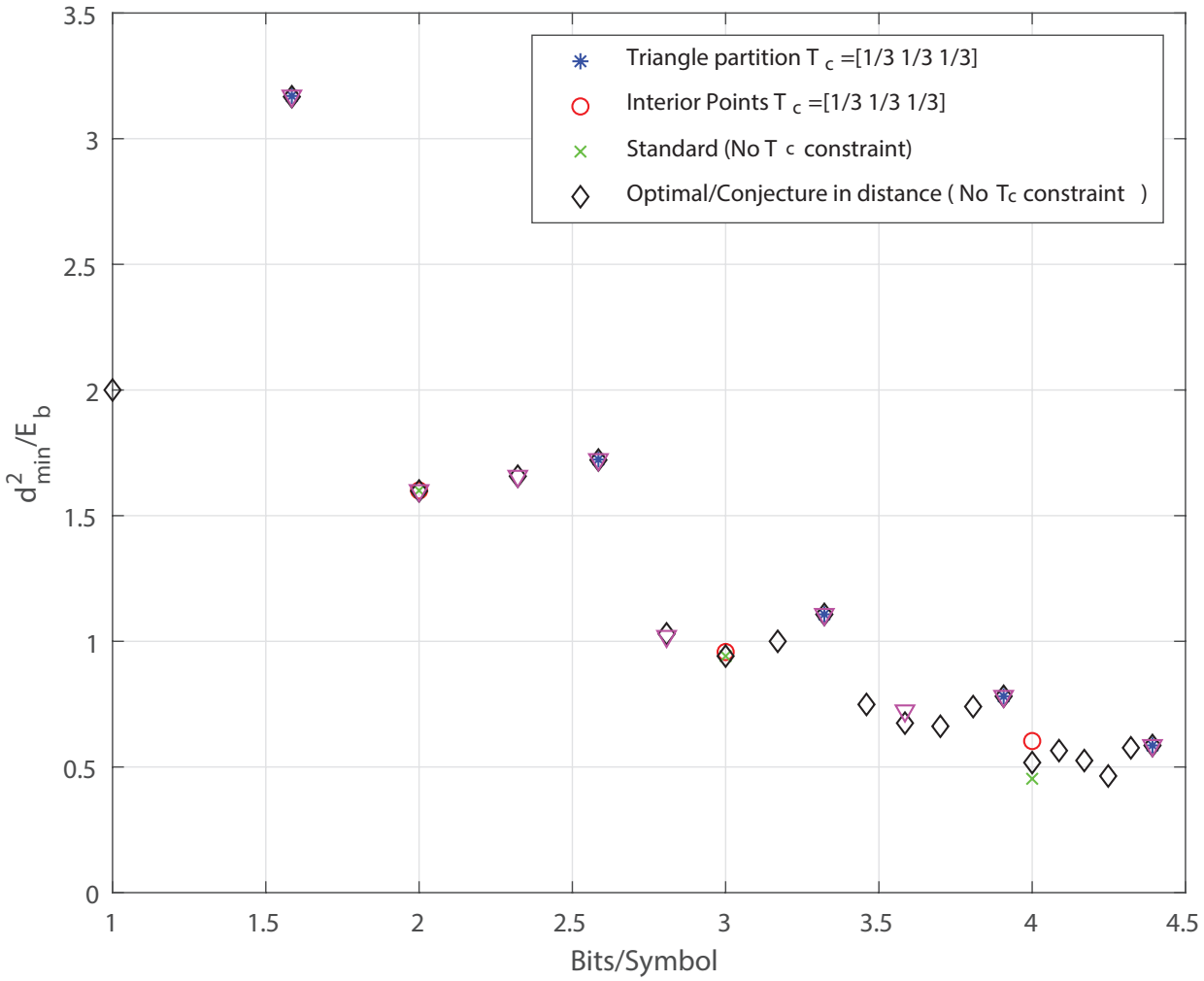


Figure 4.4: Normalized minimum squared distance versus rate for TP constellations with $\theta = 1$.

where $T_c$ represents the *relative intensity symbol corresponding to the target color*.

In the CSK-FSM methodology, the finite state machine is designed to make sure sequences produced by it average to the $T_c$ within a small number of symbols. In particular, under this methodology, the designed FSM guarantees that the color perception is proportional to $T_c$ every time the sequence returns to the state the sequence begins at, which the FSM guarantees will happen after a small number of transitions.

### 4.2.2 3-CSK-FSM and 10-CSK-FSM Properties

The FSMs presented in this paper are composed of a number of states and edges that represent the transmitted color derived from one of the previously introduced constellations. In this paper, the FSMs are represented with enumerated circles and arrows denoting the states and the transmitted relative intensity symbol, respectively.

Figures 4.5(a) and 4.5(b) show the FSMs designed for the 3-CSK and 10-CSK constellations presented in Section 4.1. The sequences of colors are constrained such that $T_c$ is achieved every time the transmitted sequence returns to its original state. For example, in Fig. 4.5(a) if any state is chosen to begin the sequence, every time the sequence returns to that state the average relative intensity is $T_c$. We refer to the FSMs in Figures 4.5(a) and 4.5(b) as “cells" because larger FSMs with similar color perception properties are constructed by concatenating them. An example of a 3-CSK-FSM composed of four cells with the constituent cell in Fig. 4.5(a), $N_{cell} = 4$, is presented in Fig. 4.6.

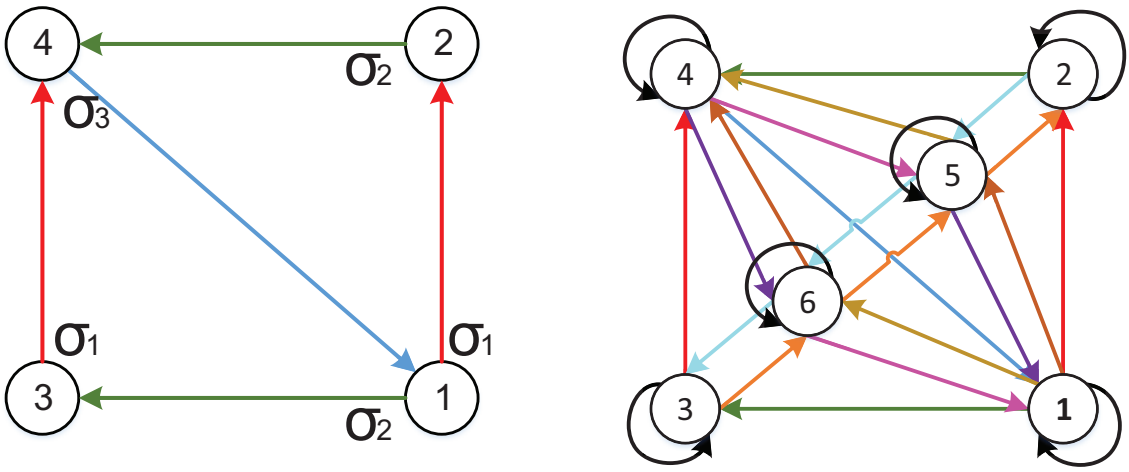


(a) 3CSK-FSM $N_{cell} = 1$.

(b) 10-CSK-FSM $N_{cell} = 1$.

Figure 4.5: 3-CSK-FSM and 10-CSK-FSM cells.

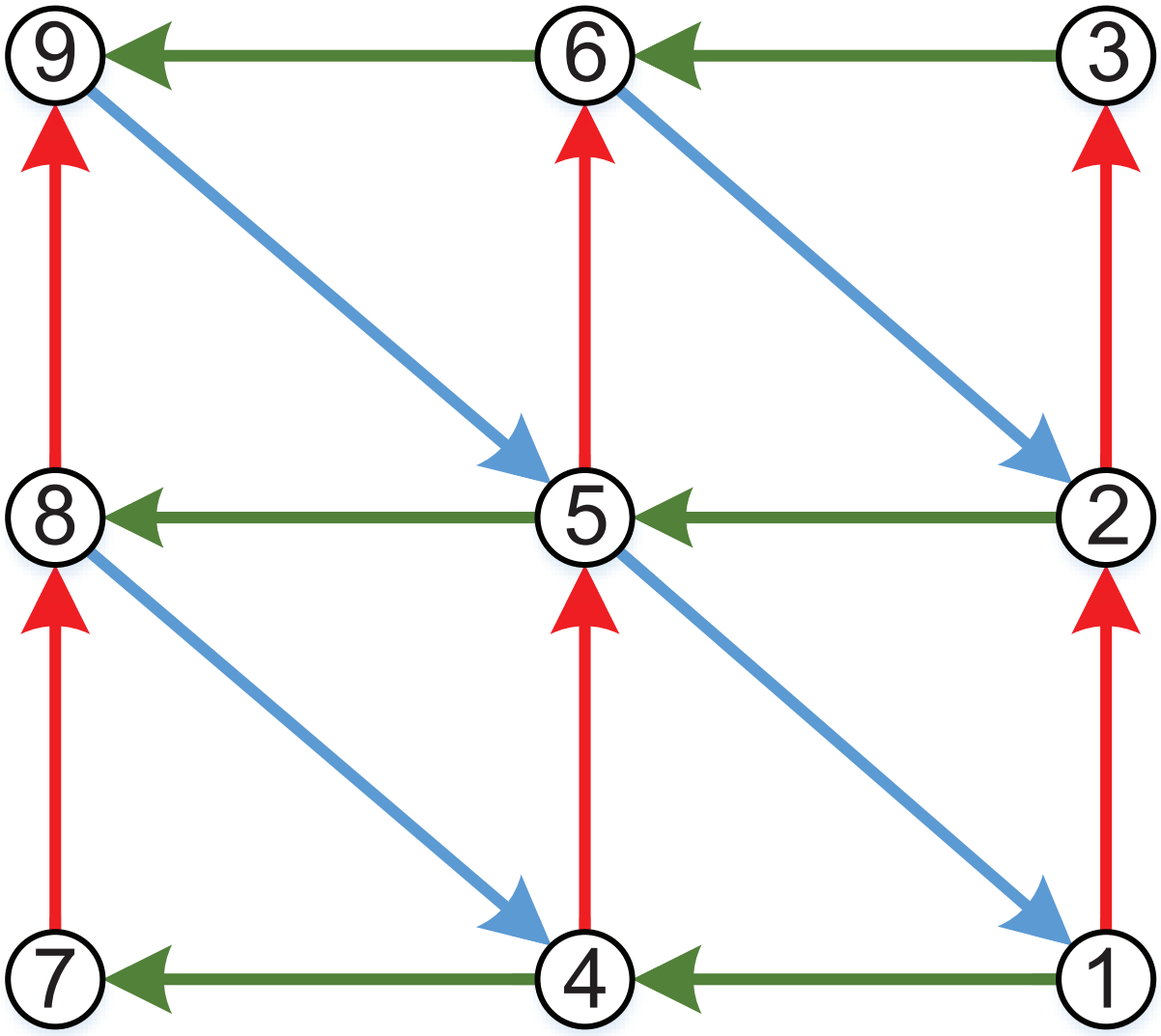


Figure 4.6: 3-CSK-FSM constructed for $N_{cell} = 4$ ($N_r = 2$, $N_c = 2$) [Reprinted with permission from "Code design in visible light communications using color-shift-keying constellations" by Mejia CE, Georghiades CN, Al-Badarneh YH, 2016. *Global Communications Conference (GLOBECOM)*, IEEE 2016 Dec 4 (pp. 1-7), Copyright © 2011 IEEE].

By concatenating groups of cells, the number of transitions per state grows, obtaining FSMs with higher capacity. Denoting $N_{cells} = N_r N_c$ where $N_c$ and $N_r$ are respectively the number of cells per vertical and horizontal direction, the total number of states for 3-CSK-FSMs and 10-CSK-FSMs is equal to

$$N_{3CSK} = (N_r + 1)(N_c + 1) \tag{4.12}$$

and

$$N_{10CSK} = (N_r + 1)(N_c + 1) + 2N_r N_c. \tag{4.13}$$

The adjacency matrices for the concatenated "cells" such that $N_c = N_r$ can be obtained through the algorithms presented in Appendix C. Also, Fig. 4.7 shows that the capacity of 3-CSK-FSMs and 10-CSK-FSMs grows asymptotically to $\log_2(3)$ and $\log_2(10)$, respectively, as the number of cells, $N_{cells}$, increase.

Finally, for both the 3-CSK-FSMs and 10-CSK-FSMs the minimum Euclidean distance achieved by the codes is $d^2_{\min,c} = 2d^2_{\min}$, where $d^2_{\min}$ is the minimum distance of the constellation. This indicates a 3dB coding gain, while at the same time satisfying color shift constraints, but it does not account for the rate loss.

As mentioned in Section 4.1, TP are not the best constellations for maximizing the minimum pairwise distance when $\theta < 1$ compared to constellations obtained using the interior points and billiards algorithms. However, the code design and symbol selection using TP together naturally control the average relative intensity corresponding to the desired perceived color during the transmission without depending on the probability distribution of the information bits.

We denote the designed codes as $\left(R, d^2_{\min,c}, N_{cells}, N\right)$ where $R$ denotes the code rate, $d^2_{\min,c}$ is the minimum Euclidean distance of the code for $\bar{E} = 1$ and $\theta = 1$, $N_{cells}$ is the number of cells, and $N$ is the size of the constellation.

### 4.2.3 Basic Code Design Example.

CSK-FSMs with sequence estimation can provide substantial coding gains compared to uncoded symbol-by-symbol decoding while avoiding color shift.

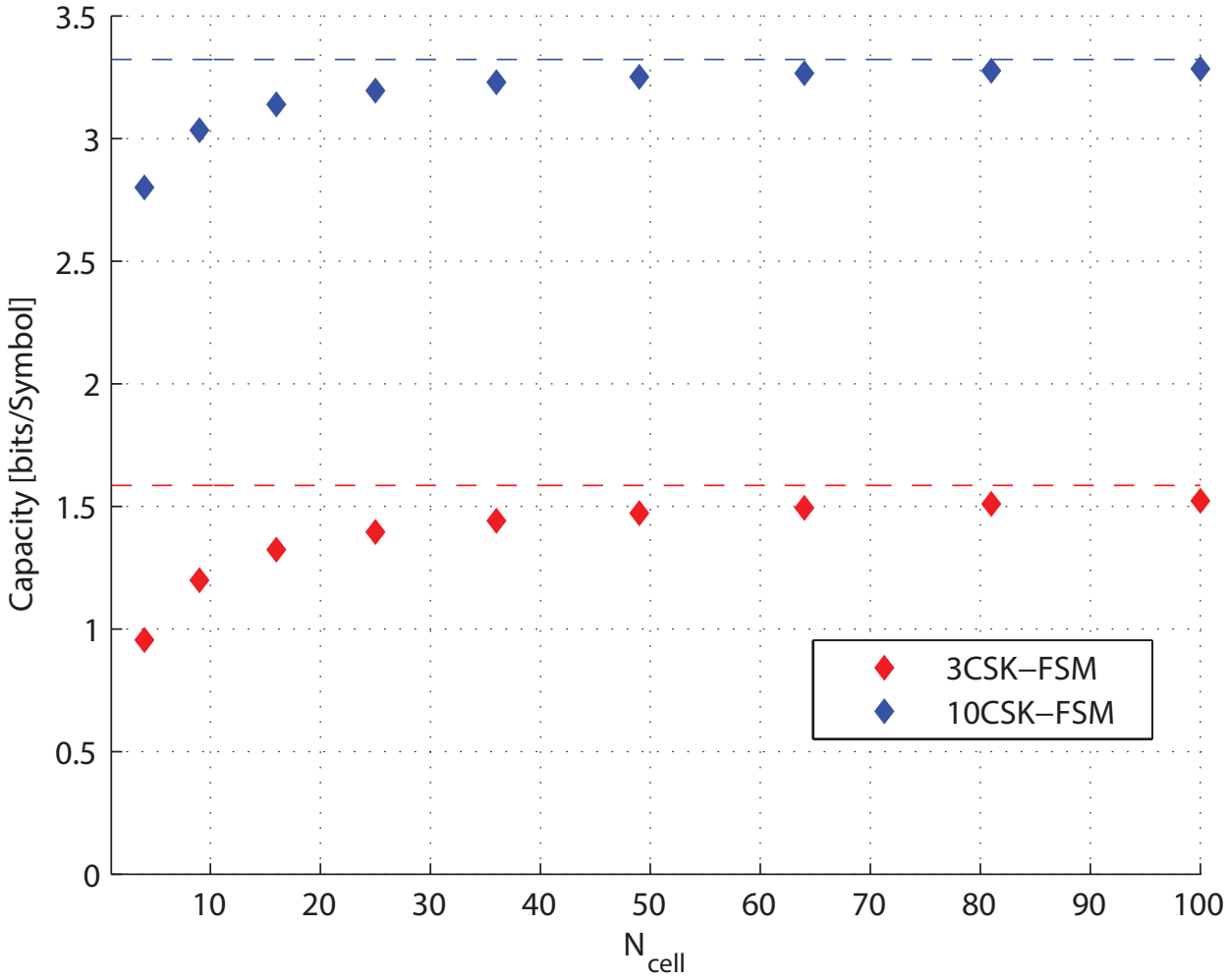


Figure 4.7: Asymptotic capacity 3-CSK-FSM and 10-CSK-FSM [Reprinted with permission from "Code design in visible light communications using color-shift-keying constellations" by Mejia CE, Georghiades CN, Al-Badarneh YH, 2016. *Global Communications Conference (GLOBECOM)*, IEEE 2016 Dec 4 (pp. 1-7), Copyright © 2011 IEEE.]

The adjacency matrix of the FSM with $N_r = N_c = 1$ presented in Fig. 4.5(a) is

$$D = \begin{bmatrix} 0 & 1 & 1 & 0 \\ 0 & 0 & 0 & 1 \\ 0 & 0 & 0 & 1 \\ 1 & 0 & 0 & 0 \end{bmatrix}. \tag{4.14}$$

Calculating the eigenvalues of the matrix using (2.26), the capacity of the FSM is equal to $1/3$

bits/symbol. For $q = 3$, $D^3$ is equal to

$$D^3 = \begin{bmatrix} 2 & 0 & 0 & 0 \\ 0 & 1 & 1 & 0 \\ 0 & 1 & 1 & 0 \\ 0 & 0 & 0 & 2 \end{bmatrix}. \tag{4.15}$$

The previous matrix presents three independent FSMs where each state has 2 codewords as shown in Fig. 4.8(a). Each FSM has equal capacity and their states meet the condition to be the reference state. Choosing the FSM composed of states 2 and 3 for $p = 1$, a single bit is assigned to each codeword obtaining the FSM presented in Figure 4.8(b). In this particular case, codeword elimination at each state is not necessary to obtain a number of codewords in powers of two. Finally, the parameters of this code are: rate = $1/3$, $d^2_{\mathrm{min,c}} = 2d^2_{min}$, $N_{cells} = 1$, and constellation 3-CSK, so this code is named (1/3, 4 , 1 , 3) code.

### 4.2.4 Minimum distance increase by codeword set partitioning and state splitting

CSK-FSMs with sequence estimation can provide substantial coding gains compared to uncoded symbol-by-symbol decoding while avoiding color shift. In general, the minimum square Euclidean distance of codes designed by FSMs is calculated as

$$d^2_{\mathrm{min,c}} = \min\{d^2_{\mathrm{mcw}}, d^2_{\mathrm{scw}}\}, \tag{4.16}$$

where $d^2_{\mathrm{mcw}}$ and $d^2_{\mathrm{scw}}$ are the minimum squared Euclidean distances among parallel codeword transitions and paths longer than one codeword transition in length, respectively. In order to increase the minimum distance of the code, we manipulate the FSM by partitioning codewords and splitting/eliminating states in order to obtain a code with $d^2_{\mathrm{min,c}} > 2d^2_{\mathrm{min}}$.

The general steps for designing codes based on CSK-FSM are the following:

1. Obtain an adjacency matrix, $D$, concatenating CSK-FSM cells and obtain $D^q$

2. Select a subset of states of the CSK-FSM such that the sum of each row of the $D^q$ matrix is

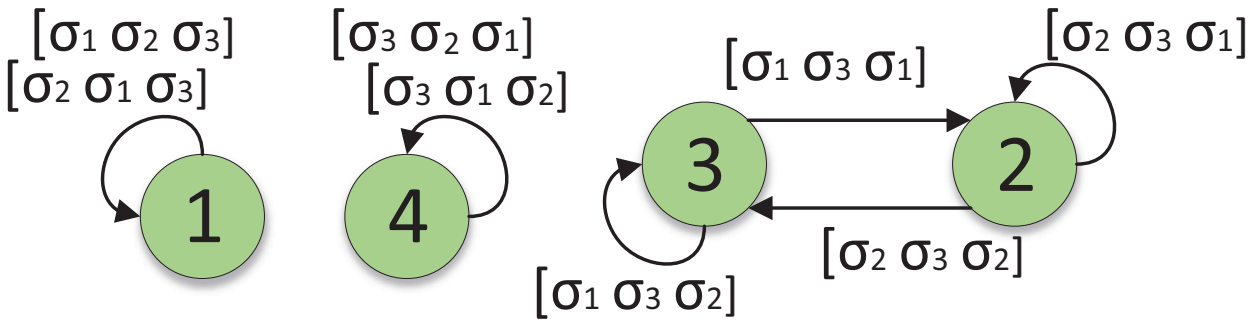


(a) 3CSK-FSM for $q = 3$.

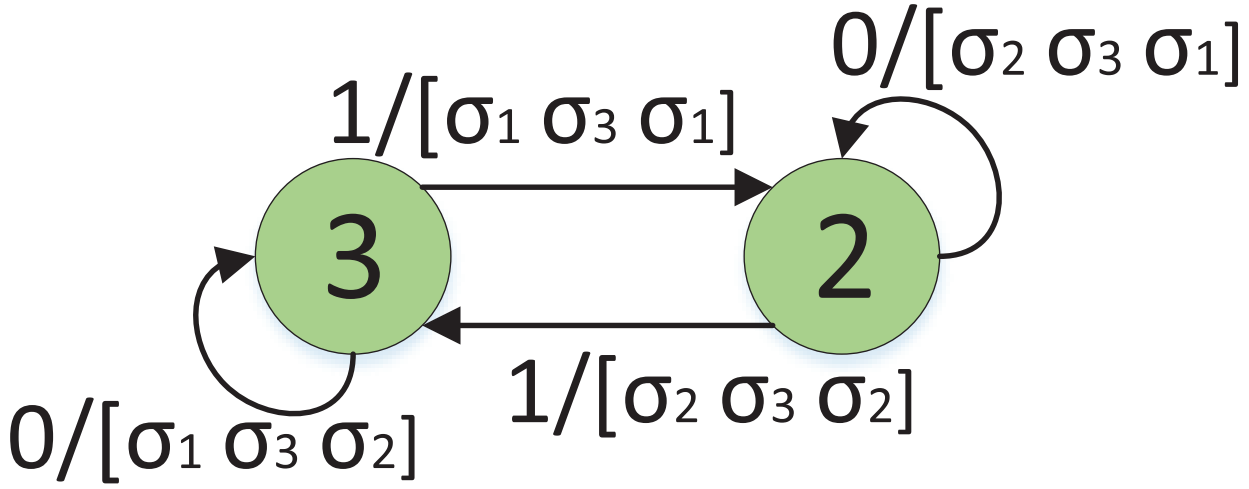


(b) (1/3, 4, 1, 3) Code.

Figure 4.8: Example Code Design Using 3CSK-FSM.

greater than $2^p$

3. Partitioned the codeword set of each state in subgroups of codewords for obtaining $d^2_{\text{mcw}} > 2d^2_{\min}$

4. Split, connect, and eliminate states/transitions such that $d^2_{\text{scw}} > 2d^2_{\min}$ and the number of transitions at each state is greater or equal to $2^p$

5. Eliminate codewords and mapping the codewords once $d^2_{\min,\text{c}} = \min\{d^2_{\text{mcw}}, d^2_{\text{scw}}\} > 2d^2_{\min}$ until obtain a desired code rate, $R = \frac{p}{q}$

6. Map the codewords at each state with $p$ information bits.

In our notation, $CW_{x,y}$ is the set of all possible sequences (codewords) of length $q$ allowed by the FSM in transitioning from State $x$ to State $y$. Each codeword in the set is represented by the $q$-tuple $[s_1 s_2 ... s_q]$ where $s_i$ is the symbol located in the $i^{th}$ position of the codeword in strict time order. In the mapping tables, each codeword is identified only by the symbol subindex according to its sequence; for instance, codeword $[\sigma_1\sigma_2\sigma_3]$ is represented by $[123]$.

In the next example, we explain how the $(7/3, 1, 9, 10)$ code is designed using a 10-CSK-FSM composed of nine cells. This code is a more powerful code than the one presented in [37], the $(7/3, 1, 9, 10)$ code.

*Example:* $(7/3, 1, 9, 10)$ *code design.*

Using the algorithm presented in Appendix C.2 to design 10-CSK-FSMs, we select $N_r = N_c = 3$ obtaining an FSM with an adjacency matrix of 34 states. The capacity of this 34 state FSM is 3.03 bits/symbol. For $q = 3$, we observe from the $D^3$ matrix a large number of codewords concentrated in six middle states: 6, 7, 10, 11, 21, and 30. The adjacency matrix corresponding to this subset of

six states is:

$$A = \begin{bmatrix} 55 & 33 & 33 & 30 & 45 & 45 \\ 30 & 55 & 10 & 33 & 45 & 27 \\ 30 & 10 & 55 & 33 & 27 & 45 \\ 33 & 30 & 30 & 55 & 45 & 45 \\ 45 & 45 & 27 & 45 & 55 & 45 \\ 45 & 27 & 45 & 45 & 45 & 55 \end{bmatrix}, \tag{4.17}$$

whose elements present the number of codewords from state to state, where states 6, 7, 10, 11, 21, and 30 are represented by columns/rows 1-6, respectively. For example $A(2,3) = 10$ means that the set $CW_{7,10}$ is composed of 10 codewords. The capacity per symbol (i.e. one third of the log based two of the largest positive eigenvalue of $A$) of this truncated FSM is 2.63 bits/symbol whereas the capacity of the 34-state 9 cell 10-CSK-FSM is 3.03 bits/symbol, indicating some potential loss in code rate but at a significant complexity (number of states) reduction. At this point, any high rate designed code using this 6-state FSM has a $d^2_{\text{min,c}} = 2d^2_{\text{min}}$, but with appropriate state and codeword manipulation it is possible to design codes with a higher $d^2_{\text{min,c}}$.

To increase $d^2_{\text{mcw}}$, each codeword set produced by the FSM is partitioned in subsets such that the pairwise minimum squared Euclidean distance between codewords is higher. To explain this step, we introduce a general codeword set partition using a 10-CSK constellation, motivated by the multidimensional TCM for a 8-PSK constellation presented in [29, Section 18]; we will apply this process to the $(7/3, 1, 9, 10)$ code design.

For a 10-CSK constellation, the symbols are partitioned in three sub-constellations $SS_0 = \{\sigma_1\sigma_2\sigma_3\sigma_{10}\}$, $SS_1 = \{\sigma_4\sigma_6\sigma_9\}$, and $SS_2 = \{\sigma_5\sigma_7\sigma_8\}$, as presented in Fig. 4.9, whose minimum squared Euclidean distance among symbols at each sub-constellation is $\tilde{d}^2_{\text{min}} = 3d^2_{\text{min}}$.

Without considering any constraint imposed by the FSM for now, we obtain $3^q$ codeword subsets whose elements have a $d^2_{\text{mcw}} = 3d^2_{\text{min}}$ as a result of the Cartesian product of $q$ possible combinations of the three sub-constellations. Then, the codeword subsets are reduced by grouping them such that their elements satisfy $d^2_{\text{mcw}} = 3d^2_{\text{min}}$.

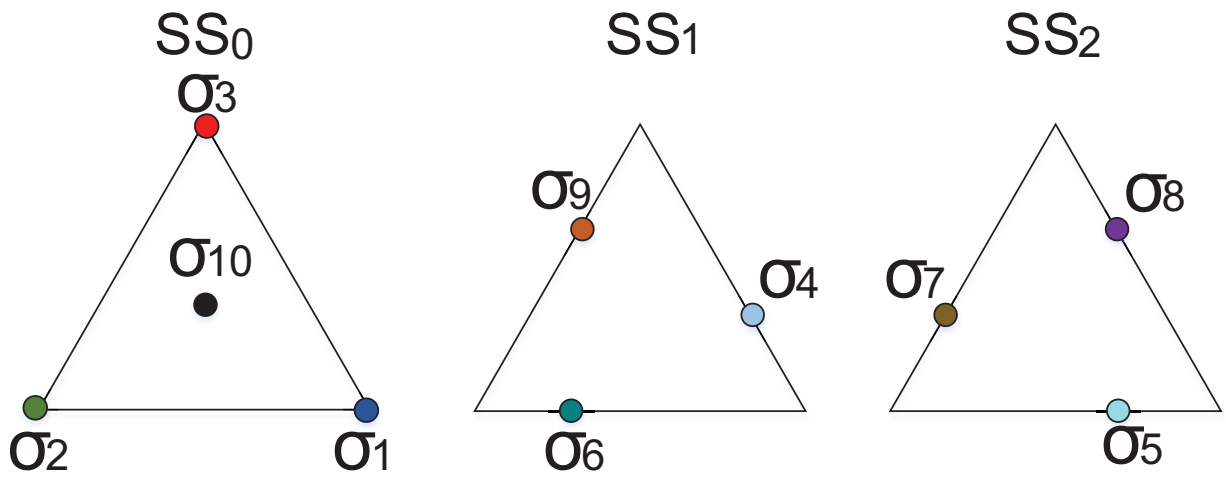


Figure 4.9: 10-CSK partition subsets with $\tilde{d}^2_{\min} = 3d^2_{\min}$.

For $q = 3$, the set that contains all possible codeword combinations, $B$, is partitioned in nine subsets whose elements have a $d^2_{\text{mcw}} = 3d^2_{\min}$ as follows

$$B = \{b_{(0,0)}, b_{(0,1)}, b_{(0,2)}, b_{(1,0)}, b_{(1,1)}, b_{(1,2)}, b_{(2,0)}, b_{(2,1)}, b_{(2,2)}\}, \tag{4.18}$$

where

$$b_{(j,k)} = \bigcup_{i=0}^{2} SS_i \times SS_{(i+j)_3} \times SS_{(i+k)_3} \tag{4.19}$$

and $(\cdot)_3$ represents the modulo-3 addition.

The above subsets are unconstrained; imposing the FSM constraint means taking the intersection between the unconstrained subsets and those allowable by the FSM in transitioning from State $x$ to State $y$:

$$b_{(j,k,x,y)} = b_{(j,k)} \cap CW_{x,y}. \tag{4.20}$$

As a result, some of these subsets are empty due to the FSM color constraint. As an example, the set $CW_{7,10} = \{[\sigma_2\sigma_2\sigma_3], [\sigma_2\sigma_3\sigma_2], [\sigma_3\sigma_2\sigma_2], [\sigma_7\sigma_7\sigma_7], [\sigma_7\sigma_2\sigma_9], [\sigma_9\sigma_7\sigma_2], [\sigma_2\sigma_9\sigma_7], [\sigma_9\sigma_2\sigma_7], [\sigma_7\sigma_9\sigma_2], [\sigma_2\sigma_7\sigma_9]\}$ produces the following subsets: $b_{(0,0,7,10)} = \{[\sigma_2\sigma_2\sigma_3], [\sigma_2\sigma_3\sigma_2], [\sigma_3\sigma_2\sigma_2], [\sigma_7\sigma_7\sigma_7]\}$, $b_{(1,2,7,10)} = \{[\sigma_7\sigma_2\sigma_9], [\sigma_9\sigma_7\sigma_2], [\sigma_2\sigma_9\sigma_7]\}$, and $b_{(2,1,7,10)} = \{[\sigma_9\sigma_2\sigma_7], [\sigma_7\sigma_9\sigma_2], [\sigma_2\sigma_7\sigma_9]\}$, and the

other six subsets are empty. Each codeword subset has a $d^2_{\text{mcw}} = 3d^2_{\min}$.

In order to increase $d^2_{\text{scw}}$, we split each state according to the number of subsets generated from the codeword set $CW_{x,x}$ corresponding to the codeword transition loops at each state. For instance, State $6$ is split in three states, $6.1$, $6.2$, and $6.3$, because $CW_{6,6}$ was partitioned in three codeword subsets $b_{(0,0,6,6)}$, $b_{(1,2,6,6)}$, and $b_{(2,1,6,6)}$. The split states are connected with the codeword subsets to obtain a $d^2_{\text{scw}} > 2d^2_{\min}$. Fig. 4.10 presents a trellis diagram of how the codewords sets $W_1$, $W_2$, and $W_3$ whose elements are contained in subsets $b_{(0,0,6,6)}$, $b_{(1,2,6,6)}$, and $b_{(2,1,6,6)}$, respectively, are connected among the split states $6.1$, $6.2$, and $6.3$, obtaining a $d^2_{\text{scw}} = 4d^2_{\min}$ calculated by the paths of two codeword sequences long.

For the trellis diagram notation, each codeword set $W_x$ from left to right corresponds to the parallel transitions among states from top to bottom in strict order. For example, $W_3$, $W_1$, and $W_2$ correspond to parallel transitions from State $6.2$ to States $6.1$, $6.2$, and $6.3$, respectively. Because in this particular case all states have the same codeword set in the transition loop, each state is split in three states where $W_1 = b_{(0,0,i,i)}$, $W_2 = b_{(1,2,i,i)}$, and $W_3 = b_{(2,1,i,i)}$ for $i = 6, 7, 10, 11, 21$, and $30$.

After connecting the split states with the transition loop codeword subsets, we connect the states with the other codeword subsets such that $d^2_{\text{scw}} > 2d^2_{\min}$. During this process, we notice that States $21$ and $30$ reduce the $d^2_{\text{scw}}$ to $2d^2_{\min}$. Hence, the set of split States $21$ and $30$ are eliminated reducing the FSM capacity to 2.37 bits/symbol, but obtaining a $d^2_{\text{scw}} = 3d^2_{\min}$ (which is equal to $d^2_{\text{mcw}}$ obtained in Step 2) after the states are properly connected according to the color transition. Fig. D.2 in Appendix D.2 presents the trellis transition diagram of the $(7/3, 1, 9, 10)$ code composed of twelve states with a $d^2_{\min,\text{c}} = \min\{d^2_{\text{scw}}, d^2_{\text{mcw}}\} = 3d^2_{\min}$. Each codeword set $W_x$ represents a parallel transition between states while hyphens (- - - -) denote an absence of transition.

For a code rate of $7/3$ bits/symbol, the excess codewords are eliminated at the split states $6$ and $11$ until obtaining $128$ codewords at each. States $7$ and $10$ have exactly 128 codewords (after the removal of States 21 and 30) and thus no need for elimination. Once the states are connected, we assign a unique binary label to each codeword.

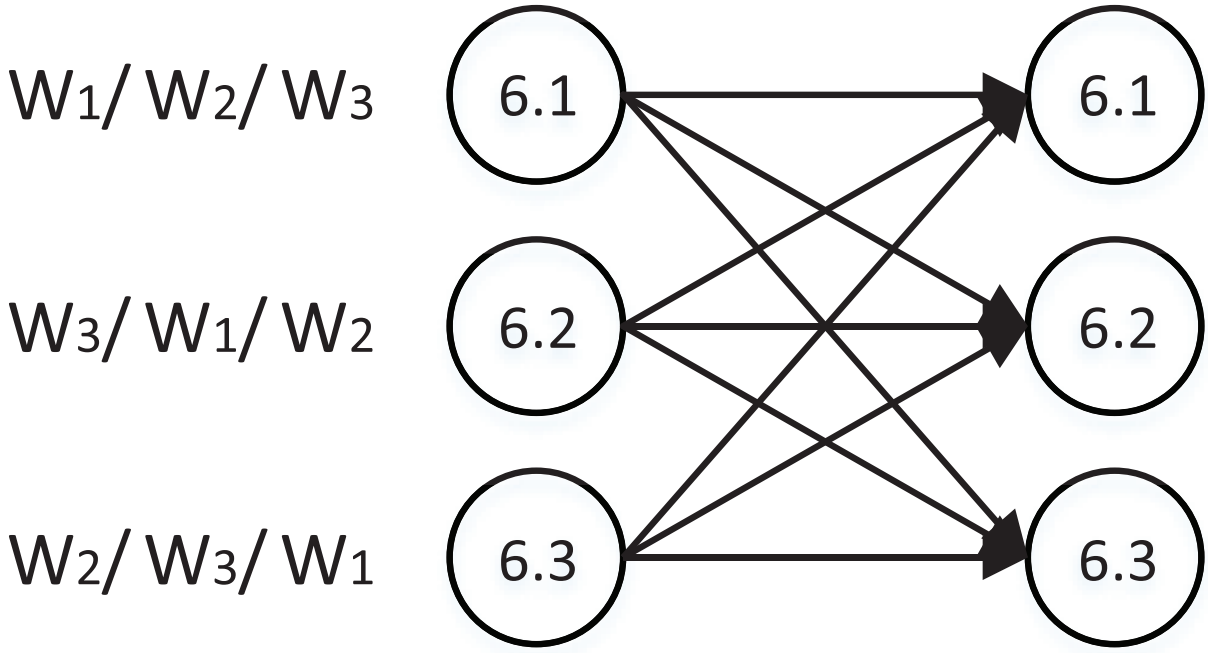


Figure 4.10: Example of splitting State $6$ and codeword subset connections for $d^2_{\text{scw}} = 4d^2_{\min}$.

The mapping of this code is presented in Table D.2 in Appendix D.2 where the codeword mapping is in strict order. For example, the input bits $0 = 0000000_2$ are mapped to the codeword $[\sigma_1\sigma_2\sigma_3]$ for all twelve states, and the input bits $55 = 0110111_2$ corresponds to codewords $[\sigma_1\sigma_{10}\sigma_{10}]$ at States $6.1$, $6.2$, $6.3$, $10.1$, $10.2$ and $10.3$, and $[\sigma_2\sigma_3\sigma_{10}]$ at States $7.1$, $7.2$, $7.3$, $11.1$, $11.2$ and $11.3$.

## 4.3 Code Design Using CSK-TCM

### 4.3.1 Illumination Constraints in CSK-TCM

For CSK-TCM, the color constraint is expressed as

$$\mathbb{E}\left[\Omega_n\right] = \mathcal{P}\mathcal{I}T_c. \tag{4.21}$$

Under this methodology, we propose a steady-state illumination model (S2IM) which depends on the trellis transition probabilities, the input information bit probabilities, and the constellation

coordinates to guarantee that the average perceived color is equal to the $T_c$. Compared to the CSK-FSM methodology, which by design guarantees the balance of colors through imposed constraints, CSK-TCM depends on the constellation and its partition, which on *average* result in a balance of colors around $T_c$.

### 4.3.2 The Steady-State Illumination Model (S2IM)

From (2.15) and (4.21), the $T_c$ as a function of the transmitted symbols for long enough sequences is

$$\mathbb{E}[\Omega_n] = \mathcal{P}\mathcal{I}T_c = \frac{\mathcal{P}\mathcal{I}}{n}\sum_{l=0}^{n-1}\mathbb{E}\left[\chi_l\right]. \tag{4.22}$$

where $\chi_l$ is a symbol chosen from a constellation $S$. Focusing on the symbol randomness at time $l$, $\mathbb{E}\left[\chi_l\right]$ can be expanded as

$$\mathbb{E}\left[\chi_l\right] = \Sigma\Upsilon_l \tag{4.23}$$

where $\Upsilon_l$ is a (column) vector of dimension $N$ ($N$ is the number of constellation symbols) that represents the probability of transmitting each symbol at time $l$ and $\Sigma$ is a matrix of dimension $3 \times N$ in which each column represents the relative intensity symbol coordinates in the intensity plane.

Decomposing $\Upsilon_l$ in Bayesian probability in matrix form, we obtain

$$\Upsilon_l = \Lambda\pi_l, \tag{4.24}$$

where $\Lambda$ is an $N \times L$ matrix (where $L$ is the number of trellis states) with elements $\Lambda(x, y)$ representing the probability that a symbol $\sigma_x$ was transmitted given the current state is $v_y$ and $\pi_l$ is the discrete probability vector where each element corresponds to the state probability at time $l$.

If the trellis diagram evolves as a Markov chain, $\pi_l$ can be written as

$$\pi_l = Q\pi_{l-1}, \tag{4.25}$$

where $Q$ is the transition probability matrix and $\pi = \pi_l = \pi_{l-1}$ is the steady-state probability for each state.

Substituting (4.23), (4.24), and (4.25) into (4.22), the expression for S2IM at steady-state is

$$T_c = \Sigma \Lambda \pi. \tag{4.26}$$

which shows that a desired $T_c$ in trellis diagrams depends on the relative intensity symbol constellation coordinates, the prior probabilities of information bits and the trellis transition design.

The expression presented in (4.26) shows that there are multiple alternatives to design trellis codes to attain the average relative intensity coordinates $T_c$.

### 4.3.3 CSK-TCM Code Design for Balanced $T_c$

Similar to CSK-FSMs, the objective of the designed codes is to increase the minimum Euclidean distance of the code $d^2_{\text{min,c}}$ calculated in trellis diagrams as

$$d^2_{\text{min,c}} = \min\{d^2_{\text{mcw}}, d^2_{\text{scw}}\}, \tag{4.27}$$

where $d^2_{\text{mcw}}$ and $d^2_{\text{scw}}$ are the minimum squared Euclidean distances among parallel symbol transitions and paths longer than one symbol transition in length, respectively. To design these code, we manipulate the trellis structure and partition the symbols in subsets, while keeping in mind the average relative intensity, $T_c$.

In the proposed design CSK-TCM code design, we assume that the information bit probability is independent and equiprobable and the desired $T_c$ is equal to the coordinates at the centroid of the intensity plane. The steps for designing CSK-TCM codes are the following:

1. Choose a TP constellation size, $N$, where $N > 2^p$ where $p$ is the length of the information bits.

2. Partition the symbols in $L$ subsets $\{SS_0, SS_1, \ldots, SS_L\}$ where $d^2_{\text{mcw}} \geq 2d^2_{\text{min}}$

3. Design a full connected trellis diagram where the number of states is equal to the number of subsets. This guarantees that all elements of the vector probability $\pi$ are equal to $1/L$

4. Group symbols in $m$ subsets $\{M_0, M_1, \ldots, M_m\}$ such that $\mathbb{E}[M_i] = T_c$ and organize consecutively in the symbol matrix $\Sigma$

5. Design the symbol probability vector $\Upsilon$ such that the each symbol of the subset $M_i$ is transmitted with equal probability. $\Upsilon$ is obtained from the matrix probability $\Lambda$ (whose elements are $0$ or $1/2^p$ to guarantee that the $d^2_{\text{scw}} \geq 2d^2_{\min}$) and the probability vector $\pi$.

6. Map the each symbol with the $p$ information bits at each state

In the following example, we present the 6-CSK-TCM code design for a code rate of $2$ bits/symbol for $T_c = [\frac{1}{3}\ \frac{1}{3}\ \frac{1}{3}]^T$ and $\sigma_1 = [1\,0\,0]^T$, $\sigma_2 = [0\,1\,0]^T$, and $\sigma_3 = [0\,0\,1]^T$ assuming that the information bits are independent and equiprobable.

*Example: 6-CSK-TCM Code Design.*

For a code rate of $2$ bits/symbol and selecting a 6-CSK constellation in Fig. 4.2(b), we partition the symbols in subsets $SS_0 = \{\sigma_1, \sigma_4\}$ and $SS_1 = \{\sigma_2, \sigma_5\}$, and $SS_2\{\sigma_3, \sigma_6\}$ obtaining a trellis diagram of three states. For this full connected trellis diagram, the steady-state probability is equal to

$$\pi = \begin{bmatrix} \frac{1}{3} & \frac{1}{3} & \frac{1}{3} \end{bmatrix}^T. \tag{4.28}$$

Grouping the 6-CSK symbol in subsets $M_0 = \{\sigma_1, \sigma_2, \sigma_3\}$ and $M_1 = \{\sigma_4, \sigma_5, \sigma_6\}$ because $\mathbb{E}[M_0] = \mathbb{E}[M_1] = [1/3\,1/3\,1/3]^T$, we organize the symbol in the matrix $\Sigma$ as follows:

$$\Sigma = [\sigma_1\,\sigma_2\,\sigma_3\,\sigma_4\,\sigma_5\,\sigma_6]. \tag{4.29}$$

According to the symbol organization of $\Sigma$, we would like $\Upsilon(1) = \Upsilon(2) = \Upsilon(3)$ and $\Upsilon(4) = \Upsilon(5) = \Upsilon(6)$. Also, for minimizing the average energy per symbol of the code, we need $\Upsilon(i) \leq \Upsilon(j)$ for $i = 1, 2, 3$ and $j = 4, 5, 6$ because the symbol energy of the symbols in $M_0$ are larger than

the symbol energy of the symbols in $M_1$. Since $\Upsilon(x) = \Lambda(x,1)\pi(1) + \Lambda(x,2)\pi(2) + \Lambda(x,3)\pi(3)$ for $x = [1, 2, ...6]$, $\pi(1) = \pi(2) = \pi(3) = 1/3$, and the elements of $\Lambda$ are either $0$ or $1/4$, we obtain for $\Lambda$ and $\Upsilon$

$$\Lambda = \begin{bmatrix} \frac{1}{4} & 0 & 0 & \frac{1}{4} & \frac{1}{4} & \frac{1}{4} \\ 0 & \frac{1}{4} & 0 & \frac{1}{4} & \frac{1}{4} & \frac{1}{4} \\ 0 & 0 & \frac{1}{4} & \frac{1}{4} & \frac{1}{4} & \frac{1}{4} \end{bmatrix}^T \tag{4.30}$$

and

$$\Upsilon = \begin{bmatrix} \frac{1}{12} & \frac{1}{12} & \frac{1}{12} & \frac{1}{4} & \frac{1}{4} & \frac{1}{4}, \end{bmatrix}^T \tag{4.31}$$

respectively. Notice that $\bar{E} = 5E_c/8$ which is less than the $\bar{E}$ for equiprobable symbol transmission ($\bar{E} = 2E_c/3$). Finally, we map the information bits and the symbols obtaining the trellis code presented in Fig. 4.11.

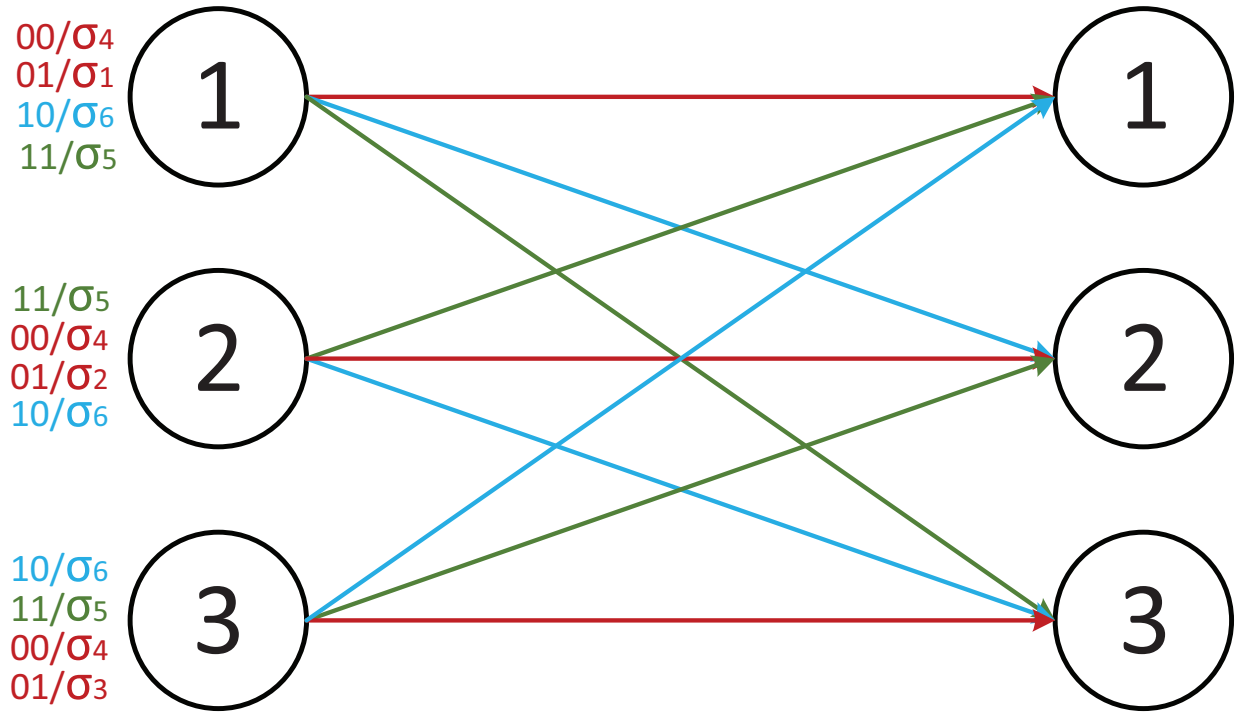


Figure 4.11: 6-CSK-TCM code.

Using the constellation presented in Fig. 4.2(c), the 10-CSK-TCM code is designed following the same code design process as for 6-CSK-TCM. The final code is in Fig. 4.12. Related to the code parameters, the 10-CSK-TCM code has a rate 3 bits/symbol and $d^2_{\min,c} = 16\bar{E}/21$ for $T_c = [\frac{1}{3}\ \frac{1}{3}\ \frac{1}{3}]^T$ and $\sigma_1 = [1\,0\,0]^T$, $\sigma_2 = [0\,1\,0]^T$, and $\sigma_3 = [0\,0\,1]^T$.

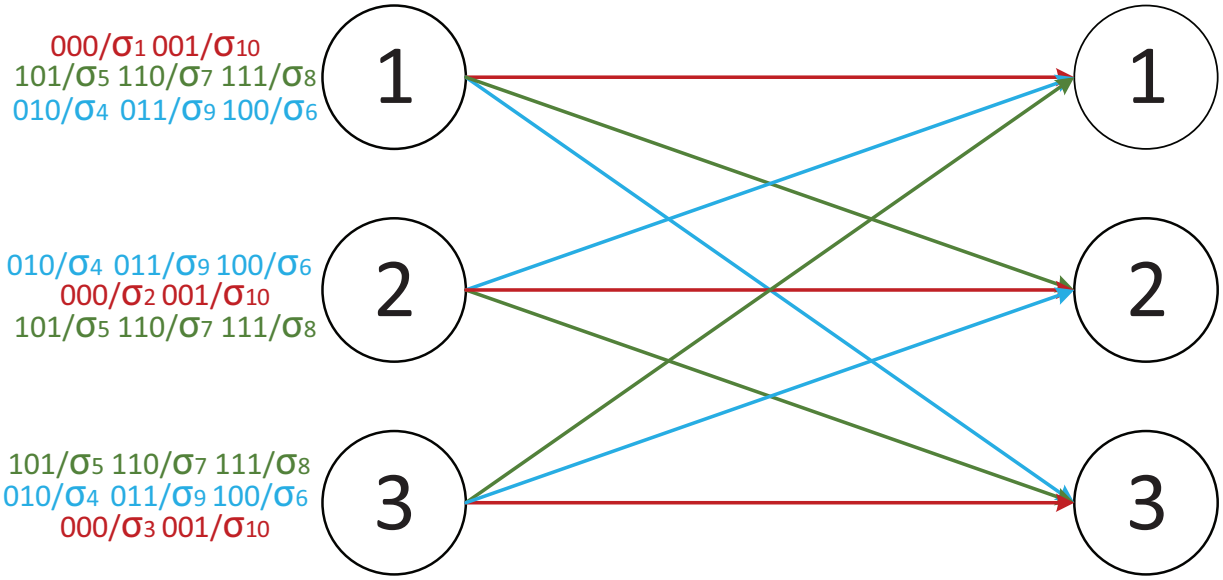


Figure 4.12: 10-CSK-TCM code.

## 4.4 Simulations and Results

### 4.4.1 System Model and Simulation Parameters

The tri-chromaticity system model is described in Subsection 2.1.1. In the simulations, the intensity plane vertices are $\sigma_1 = [1\,0\,0]^T$, $\sigma_2 = [0\,1\,0]^T$, and $\sigma_3 = [0\,0\,1]^T$ for $T_c = \left[\frac{1}{3}\ \frac{1}{3}\ \frac{1}{3}\right]^T$. The developed codes are soft-decision decoded using the Viterbi algorithm, while 4-CSK and 8-CSK presented in [28] are decoded by brute-force soft-decision decoding. For the developed codes, the receiver knows the state where the transmitter begins to encode. The simulated codes in this paper are the (1, 4, 9, 3) code, the (7/3, 1, 9, 10) code presented in Appendix D, and the 6-CSK-TCM and 10-CSK-TCM codes designed in Subsection 4.3.3.

Table 4.1 presents the parameters for the theoretical approximate codeword error rate (CER) performance of the various codes, where $R$ is the code rate, $K_s$ is the approximate average number of neighbor symbol sequences, and $\bar{E}$, the average energy per symbol. Fig. 4.13 shows the simulated and theoretical CER performances as a function of the SNR per information bit and Fig. 4.14 presents the minimum distance of the codes normalized by the average energy per information bit as a function of achieved rate.

Table 4.1: Parameters for the various codes and uncoded 4-CSK and 8-CSK.

| Code | Parameters | | |
|---|---|---|---|
| | $R$ | $K_s$ | $\frac{d^2_{\min,c}}{\bar{E}}$ |
| 4-CSK | $2$ | $3/2$ | $4/5$ |
| 8-CSK | $3$ | $5/2$ | $8/25$ |
| (1, 4, 9, 3) | $1$ | $18.75$ | $4$ |
| (7/3, 1, 9, 10) | $7/3$ | $35.95$ | $1$ |
| 6-CSK-TCM | $2$ | $20.4$ | $8/5$ |
| 10-CSK-TCM | $3$ | $75.10$ | $16/21$ |

### 4.4.2 Discussion

Based on the results presented in Fig. 4.13 we observe the following:

- The (1,4,9,3) code has the best CER performance among all codes in view of its large $d_{\min,c}$, but has the lowest rate of $1$ bit/symbol. It may be of interest in low SNR situations.
- The 6-CSK-TCM code is approximately $2$dB better in coding gain at $10^{-6}$ and asymptotically $3$dB better than uncoded 4-CSK for the same code rate of 2 bits/symbol.
- The (7/3, 1, 9, 10) code is approximately $0.6$dB better than uncoded 4-CSK for the same SNR per information bit and $1.64$dB better asymptotically for high SNR. Also, the code is able to transmit $0.33$ bits/symbol more than 4-CSK.

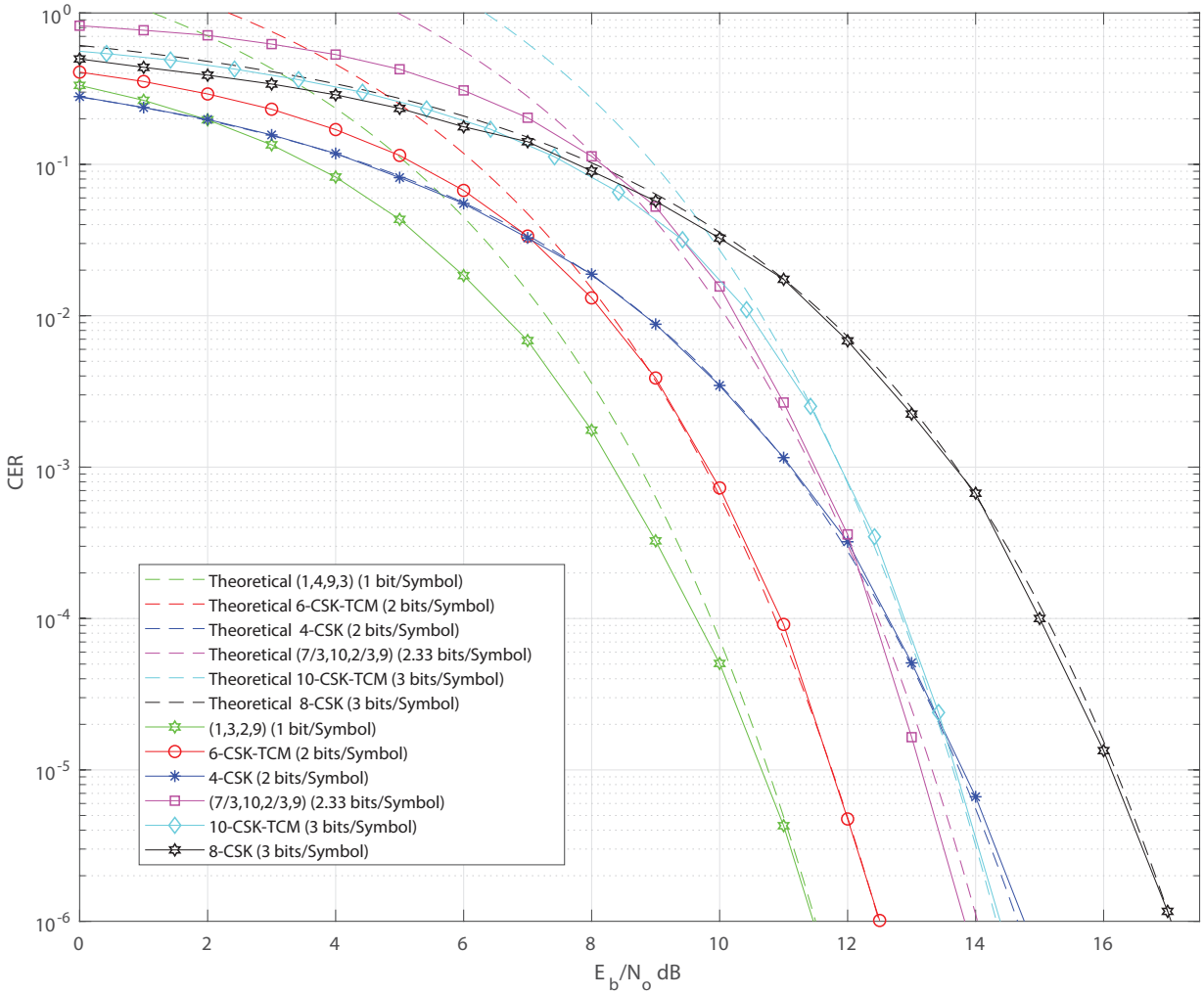


Figure 4.13: Theoretical and simulated CER.

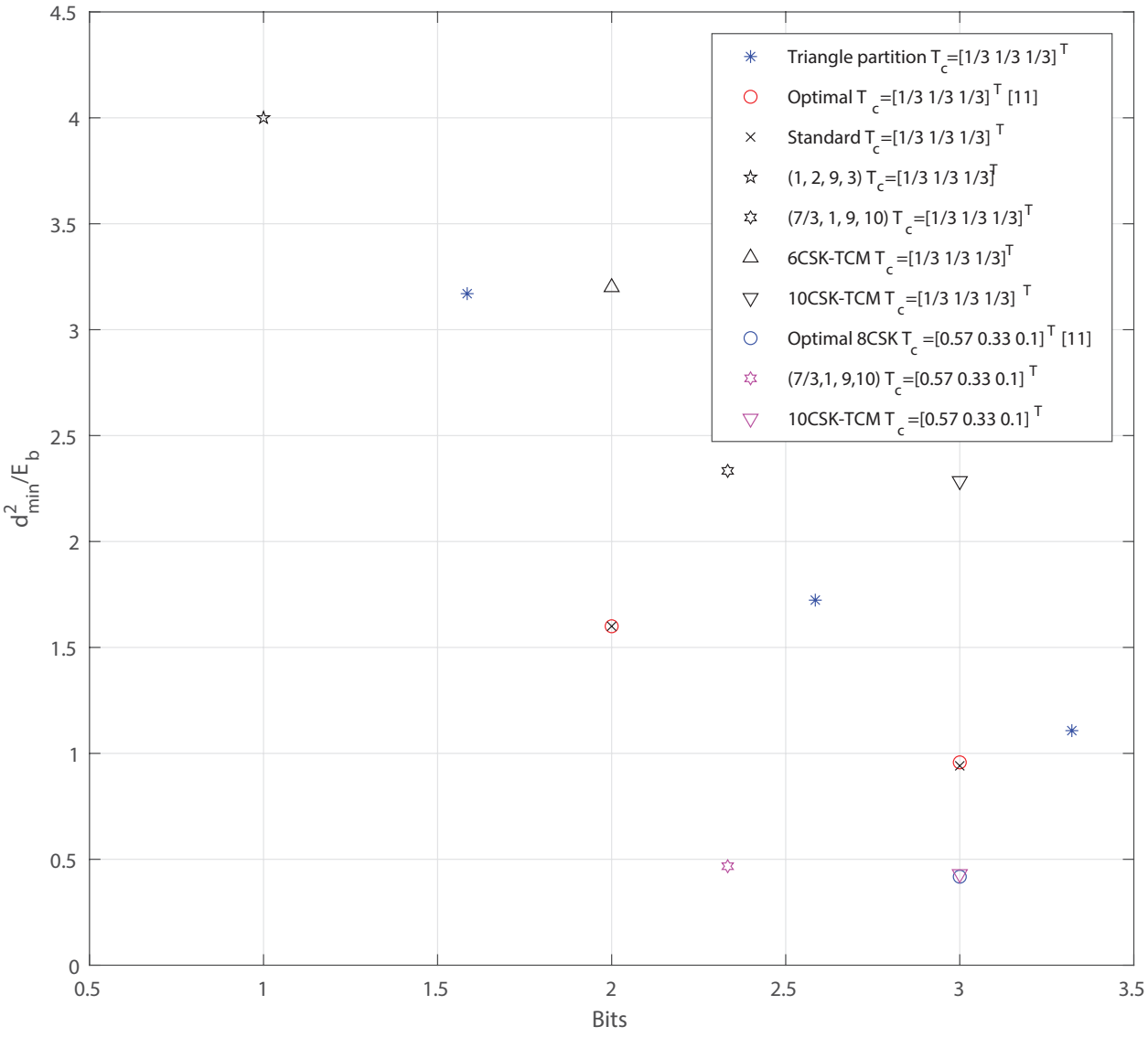


Figure 4.14: Normalized minimum code distance vs achieved code rate for the various codes and constellations.

Table 4.2: Asymptotic gain of codes in dB.

| | 4-CSK | 8-CSK | (1, 4, 9, 3) | (7/3, 1, 9, 10) | 6-CSK-TCM | 10-CSK-TCM |
|---|---|---|---|---|---|---|
| 4-CSK | 0 | 2.22 | -3.98 | -1.64 | -3.01 | -1.55 |
| 8-CSK | -2.22 | 0 | -6.2 | -3.86 | -5.23 | -3.77 |
| (1, 4, 9, 3) | 3.98 | 6.2 | 0 | 2.34 | 0.97 | 2.43 |
| (7/3, 1, 9, 10) | 1.64 | 3.86 | -2.34 | 0 | -1.37 | 0.1 |
| 6-CSK-TCM | 3.01 | 5.23 | -0.97 | 1.37 | 0 | 1.46 |
| 10-CSK-TCM | 1.55 | 3.77 | -2.43 | -0.1 | -1.46 | 0 |

- The 10-CSK-TCM is approximately 3dB better at $10^{-6}$ and asymptotically 3.77dB better than uncoded 8-CSK at the same rate of 3 bits/symbol.

Table 4.2 summarizes the asymptotic coding gains in dB between the various codes and uncoded 4-CSK and 8-CSK.

Fig. 4.14 compares the various codes and uncoded constellations in terms of their normalized minimum distance versus their achieved code rate. The figure includes results for the (7/3, 1, 9, 10), 10-CSK-TCM, and the 8-CSK constellation for $T_c = [0.57\,0.33\,0.1]$. The first two codes use 10-CSK constellations designed using TP with vertices $\sigma_1 = [1\,0\,0]^T$, $\sigma_2 = [0.09\,0.91\,0]^T$, and $\sigma_3 = [0.62\,0.08\,0.3]^T$ and the symbol coordinates of 8-CSK are designed using the billiards algorithm [22]. Comparing this case and the case when $T_c = [\frac{1}{3}\ \frac{1}{3}\ \frac{1}{3}]$, we observe that the performance of the first two codes decreases approximately by 7dB, while 8-CSK with optimal distance symbol decreases around 3dB in performance. As expected in Section 4.1, there is a higher loss in performance using TP compared with the optimal distance constellation designs.

The codes designed with CSK-FSMs have an advantage in the control of the perceived color due to the hard constraint that reduces color shifts during transmission compared with other schemes.

Another advantage is that color perception is independent of the input bit probabilities. A way to improve their code rate is by increasing together $N_{cell}$ and $q$, but this comes at the cost of complexity in the large number of states involved.

Compared with CSK-FSM, CSK-TCM codes have a lower code design complexity to obtain high code rates and increase $d_{\min}$. The constraint relaxation provides a larger number of combinations among symbols that increase the code rate. In addition, this methodology provides more degrees of freedom in the code design because S2IM depends on the prior information bit probabilities, the constellation coordinates, and the trellis transition probabilities.

# 5. CODE DESIGN WITH VARIABLE WEIGHT MULTIPULSE PULSE-POSITION SYMBOLS FOR DIMMING CONTROL

Multipulse pulse-position modulation (MPPM) is an alternative for obtaining a constant perceived dimming level in visible light communications (VLC) by transmitting symbols of fix weight (number of active chips per symbol). Through the selection of $n$-dimensional MPPM symbols of diverse weight and the relaxation of the perceived intensity level constraint in VLC, this chapter introduces variable-weight multipulse pulse-position modulation (VW-MPPM) as an alternative to MPPM which increases the spectral efficiency. The higher spectral efficiency of VW-MPPM compared with MPPM comes with the cost of worse error-rate performance. Thus, a methodology to design VW-MPPM-TCM codes based on Huffman codes and trellis coded modulation (TCM) together is proposed for improving the spectral efficiency and coding gain.

## 5.1 Codes for Dimming Control

In the literature, there are several methods for dimming control. This section describes the most common codes in terms of dimming level and code rate.

### 5.1.1 Variable On-Off Keying (VOOK)

OOK is a modulation that encodes ones and zeros by turning the LED on and off with equal time period, $T_b$. In VOOK, the symbol period is divided in an active slot with duration $\tau_d$ which carries the information bit, and an inactive slot with duration $T_b - \tau_d$ which do not carry any information but compensate the optical signal according to the dimming level. For example, Fig. 5.1 presents a VOOK symbol sequence for $\tau = 0.7T_b$. In this modulation, the brightness is controlled by varying the duty cycle of the signal, $\delta_d = \tau_d/T_b$, while the complemented pulse presence or absence during the inactive period depends if $\gamma > 0.5$ or $\gamma \leq 0.5$, respectively. Therefore, the

dimming level in VOOK for equiprobable zeros and ones is equal to

$$\gamma = \begin{cases} \frac{1}{2}\delta_d & \text{for } \gamma \leq 0.5 \\ 1 - \frac{1}{2}\delta_d & \text{for } \gamma > 0.5 \end{cases} \tag{5.1}$$

whose capacity, defined as the maximum number of bits per symbol per Hz, is equal to

$$R_v = \begin{cases} 2\gamma & \text{for } \gamma \leq 0.5 \\ 2 - 2\gamma & \text{for } \gamma > 0.5 \end{cases} \tag{5.2}$$

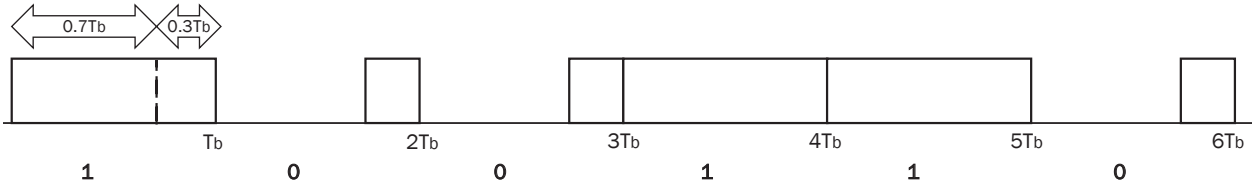


Figure 5.1: Example VOOK symbol sequence 100110 for $\gamma = 0.65$.

### 5.1.2 Inverse Source Coding (ISC)

Source coding is a data compression scheme where non-equiprobable information bits are coded in equiprobable ones and zeros for maximizing the source entropy. In contrast, Inverse Source Coding (ISC) is an operation where equiprobable information bits encode ones and zeros with probability $\gamma$ and $1 - \gamma$, respectively. Hence, the variable length ISC symbols achieve a dimming level $\gamma$ during transmission whose capacity is

$$R_i = -\gamma \log_2(\gamma) - (1 - \gamma) \log_2(1 - \gamma). \tag{5.3}$$

### 5.1.3 Multipulse Pulse-Position Modulation (MPPM)

In multipulse pulse-position modulation (MPPM), each symbol period is divided into $n$ slots where a fix number of slots $\omega \in \{1, 2, ..., n-1\}$ are active depending on the dimming level. Because MPPM symbols have equal weight, the MPPM dimming level is equal to

$$\gamma = \frac{\omega}{n}. \tag{5.4}$$

Due to the maximum number of possible MPPM symbols being equal to the number of possible combinations of $\omega$ active pulses in $n$ slots per symbol, $\binom{n}{\omega}$, the MPPM capacity is given by

$$R_m = \frac{\log_2 \binom{n}{\omega}}{n}, \tag{5.5}$$

where MPPM codes achieve the ISC capacity as $n \to \infty$.

### 5.1.4 Unary-codes

A unary-code is a variable length code where a symbol of length $i$ is composed of $i-1$ consecutive zeros followed by a one for $\gamma < 0.5$, and $i-1$ consecutive ones followed by a zero for $\gamma > 0.5$. For encoding $k \geq 2$ equiprobable data bits, the dimming level is equal to

$$\gamma = \begin{cases} 1 - \frac{2^k - 1}{2^k + 1} & \text{for } \gamma < 0.5 \\ \frac{2^k - 1}{2^k + 1} & \text{for } \gamma > 0.5 \end{cases} \tag{5.6}$$

and the code rate is

$$R_u = \frac{2k}{2^k + 1}. \tag{5.7}$$

The referred modulations are compared with the VW-MPPM modulation introduced in Chapter 5 in terms of spectral efficiency. Further characteristics of these modulations are described in [11, 15, 18].

## 5.2 Variable-Weight Multipulse Pulse-Position Modulation

Variable-weight multipulse pulse-position modulation (VW-MPPM) is simply MPPM symbols of length, $n$, but not restricted to a fix weight. For a desired dimming level, the VW-MPPM symbol set, $S$, is composed of MPPM symbol subsets, $S_\nu$, of weight $\nu \in \{0, 1, ..., \omega, ..., n\}$ chosen according to the desired average weight per symbol, $\omega'$, and the symbol transmission probability. Hence, the dimming level is expressed as

$$\gamma = \frac{\omega'}{n} = \frac{1}{n} \sum_{\nu=1}^{n} \sum_{s_j \in S_\nu} \nu p(s_j) \text{ for } j \in \{1, 2, ..., |S_\nu|\}, \tag{5.8}$$

where $s_j$ is a MPPM symbol of weight $\nu$, $p(\cdot)$ denotes the symbol transmission probability, and $|\cdot|$ is the subset cardinality.

For $\omega' = \omega$ and assuming each VW-MPPM symbol is transmitted with equal probability, the maximum data throughput is obtained when the number of selected symbols of weight $\omega$ is equal to $\binom{n}{\omega}$, and the number of selected symbols with weight $\omega - i$ and $\omega + i$ are equal to $\min\left\{\binom{n}{\omega-i}, \binom{n}{\omega+i}\right\}$ for balancing the average symbol weight around $\omega$. Therefore, the number of symbols for each MPPM subset is

$$|S_\omega| = \binom{n}{\omega} \text{ for all } \gamma, \tag{5.9}$$

$$|S_{\omega-i}| = |S_{\omega+i}| = \binom{n}{\omega-i} \quad \text{for} \begin{cases} 0 < i \leq \frac{n}{2} \text{ when } \gamma = 0.5 \\ 0 < i \leq \omega \text{ when } \gamma < 0.5 \\ \omega - n \leq i < 0 \text{ when } \gamma > 0.5 \end{cases}, \tag{5.10}$$

and

$$|S_i| = 0 \quad \text{for} \begin{cases} 2\omega < i \leq n \text{ when } \gamma < 0.5 \\ \\ 0 \leq i < 2\omega - n \text{ when } \gamma > 0.5 \end{cases} . \tag{5.11}$$

Thus, the VW-MPPM symbol set is composed of

$$|S| = \begin{cases} 2^n & \text{for } \gamma = 0.5 \\ \binom{n}{\omega} + 2\sum_{i=1}^{\omega} \binom{n}{\omega - i} & \text{when } \gamma < 0.5 \\ \binom{n}{\omega} + 2\sum_{i=1}^{n-\omega} \binom{n}{\omega + i} & \text{when } \gamma > 0.5 \end{cases}, \tag{5.12}$$

symbols, and capacity

$$R_w = \frac{\log_2 |S|}{n}. \tag{5.13}$$

Fig. 5.2 compares the spectral efficiency between VW-MPPM, ISC, VOOK, and MPPM as a function of $\gamma$. The figure shows that VW-MPPM spectral efficiency is greater than MPPM and VOOK for all dimming levels and superior than unary-code for middle $\gamma$ levels. Similar to MPPM for large $n$, VW-MPPM asymptotically reach the ISC capacity.

In order to achieve a code rate close to the VW-MPPM capacity, in this work, variable length Huffman codes are developed as the source code where the shorter input bits are mapped to the symbols of weight $\omega$ for reducing the dimming level shifts and increasing the average code rate. Recalling, the average code rate is calculated as

$$\overline{R}_w = \frac{\sum_{l_i} 2^{-l_i} l_i}{n \sum_{l_i} 2^{-l_i}} \leq R_w, \tag{5.14}$$

where $l_i$ denotes the input bits length of symbol $i$.

Even VW-MPPM has a spectral efficiency larger than MPPM, the odd and even weight VW-MPPM symbols together reduce the minimum Euclidean distance $d_{\min}$ deceasing the error-rate

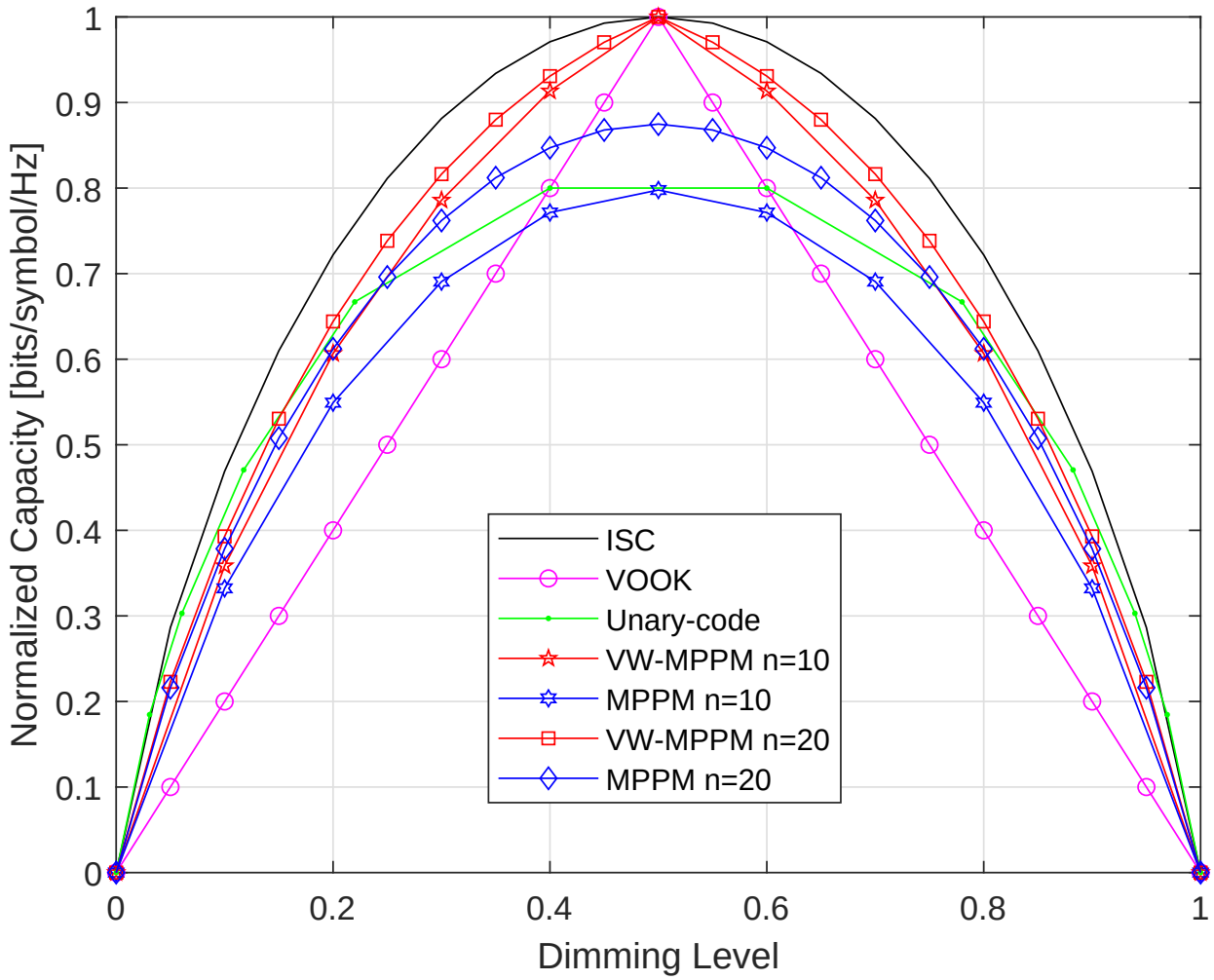


Figure 5.2: Spectral Efficiency Comparison

performance by 3 dB (not counting for code gain) compared with MPPM ($d^2_{\min} = 2E$ where $E$ is the energy per slot).

### 5.2.1 Uncoded VW-MPPM Design Example

For $n = 3$, the MPPM symbol sets with weights 0, 1, 2, and 3 are $\{000\}$, $\{001, 010, 100\}$, $\{011, 110, 101\}$, and $\{111\}$, respectively. For $\omega' = 2$ and equiprobable symbol transmission, a possible set of VW-MPPM symbols is $S = \{S_1, S_2, S_3\} = \{100, 011, 101, 110, 111\}$. Notice that the symbol of weight 0 (000) and the two symbols of weight 1 (001 and 010) are not selected to keep the average weight per symbol. Finally, the input bits are mapping for each symbol by

encoding the information bits using Huffman code for the input bits assuming ones and zeros in the information bits are equiprobable.

The resultant code is presented in Table E.1 presented in Appendix E where shorter information bits are assigned to symbols of weight 2 and obtaining $\overline{R}_w = 0.75$ bits/symbol which is close to the capacity ($R_w = 0.774$).

Table 5.1: Example code $\overline{R}_w = 0.75$ bits/symbol and $\gamma = \frac{2}{3}$

| Input Bits | Symbols |
|---|---|
| 11 | 110 |
| 10 | 101 |
| 01 | 011 |
| 001 | 100 |
| 000 | 111 |

### 5.3 VW-MPPM-TCM codes

To increase the error rate performance of VW-MPPM, VW-MPPM-TCM is designed based on VW-MPPM symbols, Huffman encoding in the information bits to reach the VW-MPPM capacity, and trellis-coded modulation (TCM) codes to improve the distance between symbols [32].

In order to design the VW-MPPM-TCM codes for a desired $\omega' = \omega$, this section proposes the following steps:

1. Based on the process described in Section 5.2, partition the VW-MPPM symbols into two symbol sets composed of even weight symbols $CW(E, 1)$ and odd weight symbols $CW(O, 1)$

2. Due to

$$\binom{n}{\omega + i} > \binom{n}{\omega - i} \quad \text{for } \gamma < 0.5 \tag{5.15}$$

and

$$\binom{n}{\omega - i} > \binom{n}{\omega + i} \quad \text{for } \gamma > 0.5, \tag{5.16}$$

create another couple of sets $CW(E, 2)$ and $CW(O, 2)$ based on $CW(E, 1)$ and $CW(O, 1)$ and replace some of the unchosen symbols in step 1 with symbols of equal weight

3. Depict the trellis diagram as presented in Fig. 5.3 where each branch represents a parallel transition of the symbols in the set

4. Assign a one-to-one mapping to each symbol in both states by using Huffman code as described in Section 5.2.

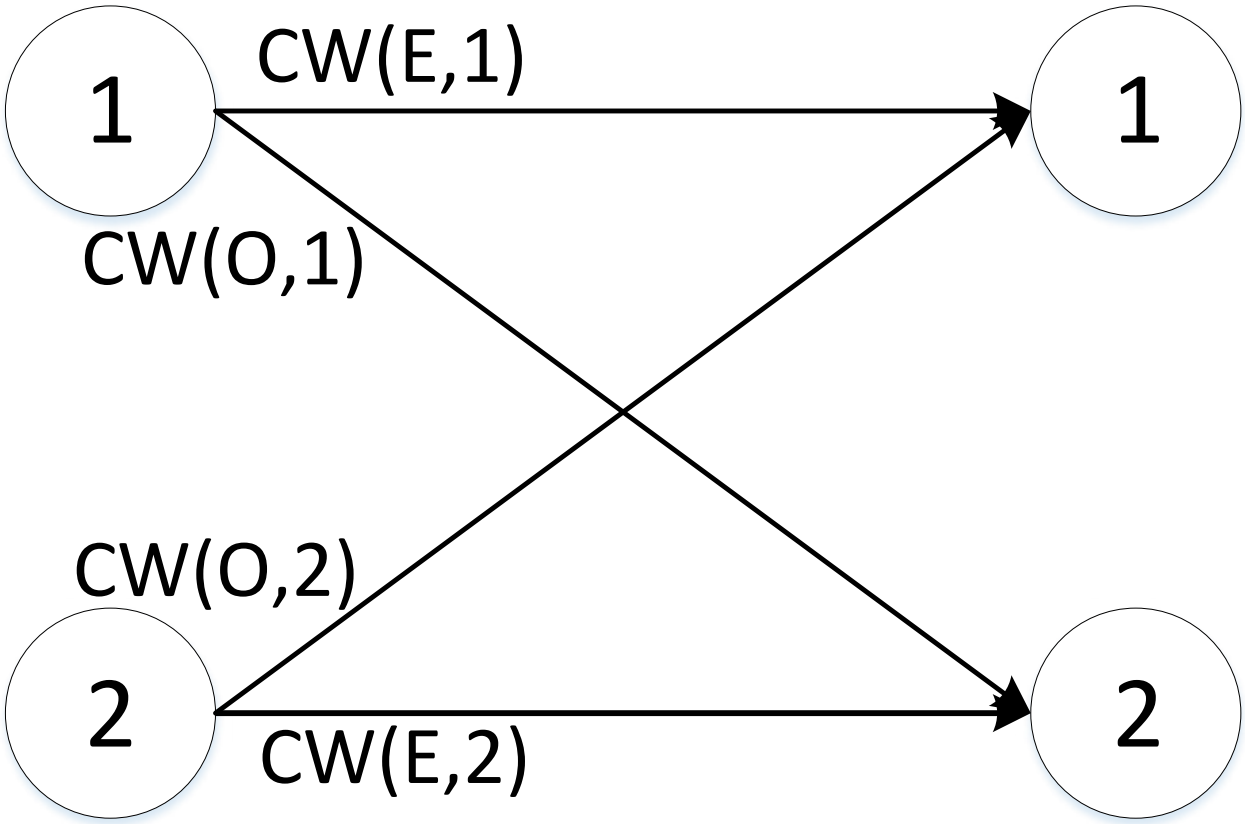


Figure 5.3: Trellis Diagram for VW-MPPM-TCM

The previous steps are able to design VW-MPPM-TCM codes with a $d^2_{\min} = 2E_c$ without sacrificing the average code rate of uncoded VW-MPPM. The designed codes are named according to their characteristics as ($\overline{R}_w$, $\omega'$, $n$)

### 5.3.1 VW-MPPM-TCM Code Design Example

Based on the example presented in Section 5.2, $CW(E,1) = \{110, 101, 011\}$ and $CW(O,1) = \{100, 111\}$, $CW(O,2) = \{001, 111\}$ is formed by replacing the symbol of weight one $100 \in CW(O,1)$ with the symbol $001$ which is one of the two unchosen symbols. In this particular case, sets $CW(E,2)$ and $CW(E,1)$ are equal due to absence of extra symbols of even weight.

Applying Huffman coding to the information bits, the designed code is presented in Table 5.2 where $\overline{R}_w = 0.75$ bits/symbol, $\omega' = 2$, and $n = 3$. In this case, the designed code is named as $(0.75, 2, 3)$ code.

Table 5.2: Mapping Table $(0.75, 2, 3)$ code

| Input Bits | CW(E,1) | CW(E,2) |
|---|---|---|
| 11 | 110 | 110 |
| 10 | 101 | 101 |
| 01 | 011 | 011 |
| | CW(O,1) | CW(O,2) |
| 001 | 100 | 001 |
| 000 | 111 | 111 |

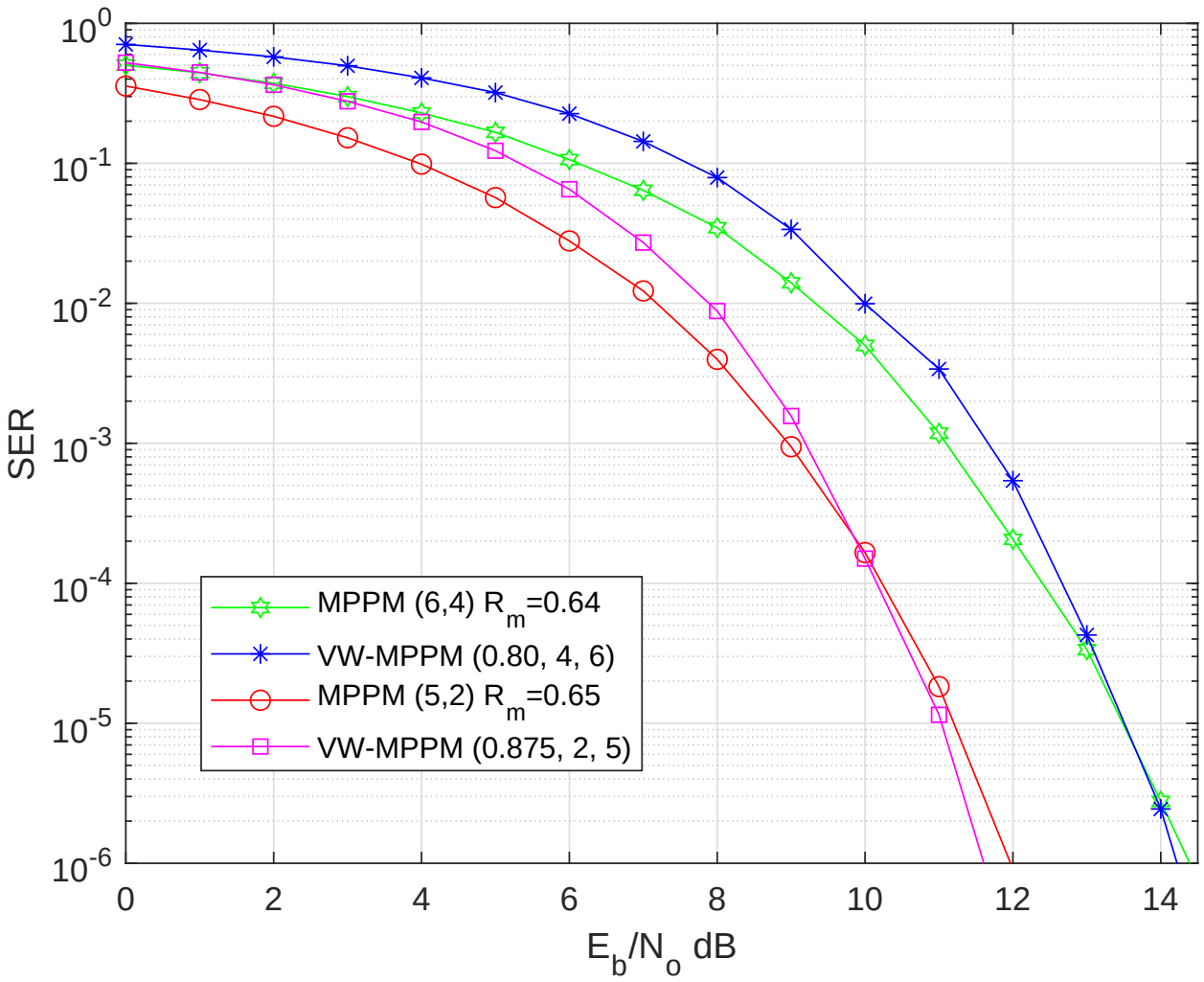


Figure 5.4: SER of MPPM and VW-MPPM-TCM codes for $\gamma = \frac{2}{5}$ and $n = 5$, and $\gamma = \frac{2}{3}$ and $n = 6$ .

### 5.4 Simulations and Results

In this case, the information bits, which are equally and identically distributed, are mapped into input bits using Huffman codes to be encoded in optical symbols according to the tables VM-MPPM-TCM and MPPM encoded tables presented in Appendix E. The (0.875, 2, 5) code and (5,2) code are designed for a dimming level of $\gamma = 2/5$ and the (0.80, 4, 6) code, and the (6,4) code are designed ($n$,$\omega$) MPPM codes are designed for a dimming level of $\gamma = 2/3$.

Fig. 5.4 presents the simulation results corresponding to the symbol-error rate (SER) of the

codes. Comparing the codes for equal dimming level doing the folowing observations:

- The error rate performance of (0.875, 2, 5) code is better than (5,2) code for an SNR higher than $10$ dB. Asymptotically, the designed code is $1.29$ dB better than the MPPM code due to its higher rate.

- Similar to the previous case, the error rate performance of (0.8, 4, 6) code is superior than (6,4) code for an SNR larger than $13$ dB, implying an asymptotic improvement in coding gain of $0.94$ dB due to its higher rate.

Given VW-MPPM-TCM has a larger code rate and equal $d^2_{\mathrm{min,c}}$ compared with MPPM, VW-MPPM-TCM presents a better asymptotically coding gain, which depends the code rate for equal $\gamma$ and $n$. However, this coding gain difference decreases as $n$ becomes larger.

# 6. CONCLUSIONS*

This dissertation proposes code design methodologies based on FSM and TCM concepts for three modulation schemes under illumination constraints and also compares the trade-offs with coding schemes proposed in the literature.

In Chapter 3, the design of codes using FSMs constraining the runs of zeros or ones for VLC has potential for both perceived flicker mitigation and coding gain. In general, better flicker mitigation is achieved by a smaller number of states in the FSM at the cost of capacity and, thus, in the resulting code rate. Rates closer to the FSM capacity can be achieved by considering encoding longer sequences, while both potential performance and rate can be better achieved by considering FSMs with larger number of states (at the cost of flicker mitigation). The FSM-based code design methods presented above provide a way to trade-off between flicker mitigation and performance. Several codes were designed with these algorithms. In particular, the $(8, 10, 11)$ code has over 4dB in coding gain at a CER rate of $10^{-5}$ compared to the 8B10B standard code for the same code rate. In addition to code design, this thesis proposes a mathematical definition of perceived flicker to quantify the flicker performance in addition to the bit-error rate performance of the designed codes.

In Chapter 4, signal constellation design and coding based on CSK under luminous flux and color constraints are studied as a solution for mitigating color shifts around the desired color. The constant intensity constrains the constellation points to be on a triangle and mitigating target color flicker imposes some constellation symmetry constraints as well as a constraint on the transmitted sequences of CSK symbols through appropriate coding. This study shows that triangle partition constellations perform best in the minimum distance versus rate plane and uses them to construct codes based on two methodologies, CSK-FSM and CSK-TCM. CSK-FSM relies on a finite state machine which imposes hard constraints to mitigate the color-shifts around the desired color and

*Parts of this chapter are reprinted with permission from "Code design for flicker mitigation in visible light communications using finite state machines" by Mejia CE, Georghiades CN, Abdallah MM, Al-Badarneh YH, 2017. *IEEE Transactions on Communications*, 65(5) pp.2091-2100, Copyright © 2011 IEEE

CSK-TCM is based on the concept of trellis-coded modulation with set partitioning and relies on appropriate design to probabilistically (on average) meet the color shift constraint. The design codes using 6-CSK and 10-CSK constellations span several rates. In particular, the 10-CSK-TCM code has an asymptotic high SNR coding gain of 3.77dB compared to uncoded 8-CSK and for the same rate of 3 bits/symbol, the CSK-TCM code has a 3dB asymptotic coding gain compared to 4-CSK at 2 bits/symbol and the (7/3, 1, 9, 10) CSK-FSM code has a 1.64 dB gain over uncoded 4-CSK while also achieving 1/3 bits/symbol higher rate than uncoded 4-CSK.

In Chapter 5, variable-weight multipulse pulse-position modulation (VW-MPPM) is presented as a solution to increase the spectral efficiency by relaxing the perceived dimming level constraint and using variable weight MPPM symbols. Because the use of odd and even weight symbols decreases the $d_{\min}$, a trellis code design methodology composed of two states improves the coding gain compared with uncoded VW-MPPM. As a result, two codes are developed for $\gamma = 0.667$ and $\gamma = 0.4$ showing an asymptotic coding gain of $1.29$ dB and $0.94$ dB better compared with MPPM codes for symbols with similar characteristics.

The codes designed with FSM and TCM present a loss in the code rate with respect the uncoded symbols. However, the designed codes could achieve higher asymptotically coding gains by the adequate manipulation of the trellis structure. Compared with FSM codes, the TCM codes have a lower complexity to increase the $d_{\min,\mathrm{c}}$. The relaxation of the illumination constraints generates a large number of possible combinations improving the data rate. However, the TCM codes depend on the information bit probability, while the FSMs codes transmission is more deterministic for fulfilling the illumination constraints. The choice between one code design or the other depends on the allowed illumination tolerance which in part relies on the OCR and the designed code.

## 6.1 Challenges and Further Work

Some challenges in our research and some of the future extensions that account for more practical considerations are:

In Chapter 3, the comparisons of the relative values of PFI for various codes show the sacrifice in flicker perception. Of course, the natural question is what value of PFI is acceptable to the

human eye. There is a need for a study to assess what values of PFI are acceptable to humans and this can only be done through experiments involving human perceptions. Also, the analytic measure could change in real experiments because the PFI do not consider other flicker sources that appear in the physics of the LED. It would seem however that flicker will be less and less of an issue as data rates in VLC increase. In any case, the higher OCRs required in the introduced codes are still substantially less than 100MHz, which is easily manageable. There remains the question of associating the introduced objective measure of PFI to how it is perceived by the human eye; i.e., how small of a PFI value is small enough. This is something only further experiments with human subjects can achieve, which is outside the scope of this dissertation.

In Chapter 4, this study assumes that the power spectral density of each color of the LED scales linearly over the current range to achieve the perceived chromaticity. The non-linearities could change the intensity plane shape, therefore requiring adjustments in the symbol allocation balance to achieve the desired color. However, this assumption is done in the optimal constellation design proposed by different authors. Even though the crosstalk between the red, green, and blue channel is small, the independent channel model assumption could change the coding gain between uncoded and coded modulation.

In Chapter 5, the flicker problem is not considered because of the fast changes in the intensity during the symbol time. However, this assumption depends on the LED physical properties for modulating the transmitted symbol that is not considered in this study.

In general, the designed codes were designed "by hand". In the future partitioning of the codewords by using computational tool could design codes with higher rates and code gains, but at the cost of increasing the number of states.

REFERENCES


[1] J. Thompson, X. Ge, H. Wu, and R. Irmer, "5G Wireless Communication Systems: Prospects and Challenges," *2015 IEEE 2015 Int. Conf. Comput. Commun. Control Technol. (I4CT 2015)*, no. February, pp. 62–64, 2014.

[2] S. Wu, H. Wang, and C.-H. Youn, "Visible light communications for 5G wireless networking systems: from fixed to mobile communications," *IEEE Netw.*, vol. 28, no. 6, pp. 41–45, 2014.

[3] D. A. Steigerwald, J. C. Bhat, D. Collins, R. M. Fletcher, M. O. Holcomb, M. J. Ludowise, P. S. Martin, and S. L. Rudaz, "Illumination with solid state lighting technology," *IEEE J. Sel. Top. Quantum Electron.*, vol. 8, no. 2, pp. 310–320, 2002.

[4] T. Komine and M. Nakagawa, "Fundamental analysis for visible-light communication system using LED lights," *IEEE Trans. Consum. Electron.*, vol. 50, no. 1, pp. 100–107, 2004.

[5] A. Wilkins, J. Veitch, and B. Lehman, "LED lighting flicker and potential health concerns: Ieee standard par1789 update," in *Energy Conversion Congress and Exposition (ECCE), 2010 IEEE*, pp. 171–178, 2010.

[6] IEEE STANDARD ASSOCIATION, "802.15.7-2011 - IEEE Standard for Local and Metropolitan Area Networks–Part 15.7: Short-Range Wireless Optical Communication Using Visible Light," Tech. Rep. September, 2011.

[7] S. Rajagopal, R. D. Roberts, and S. K. Lim, "IEEE 802.15.7 visible light communication: Modulation schemes and dimming support," *IEEE Commun. Mag.*, vol. 50, no. 3, pp. 72–82, 2012.

[8] A. X. Widmer and P. A. Franaszek, "A DC-Balanced, Partitioned-Block, 8B/10B Transmission Code," *IBM J. Res. Dev.*, vol. 27, no. 5, pp. 440–451, 1983.

[9] E. Sarbazi and M. Uysal, "PHY layer performance evaluation of the IEEE 802.15.7 visible light communication standard," *Opt. Wirel. Commun. (IWOW), 2013 2nd Int. Work.*, no. JAN-

UARY, pp. 35–39, 2013.

[10] B. Bai, Z. Xu, and Y. Fan, "Joint LED dimming and high capacity visible light communication by overlapping PPM," in *WOCC2010 Tech. Progr. - 19th Annu. Wirel. Opt. Commun. Conf. Converging Commun. Around Pacific*, 2010.

[11] K. Lee and H. Park, "Modulations for visible light communications with dimming control," *IEEE Photonics Technol. Lett.*, vol. 23, no. 16, pp. 1136–1138, 2011.

[12] M. Oh, "A flicker mitigation modulation scheme for visible light communications," *Adv. Commun. Technol. (ICACT), 2013 15th Int. Conf.*, pp. 933–936, 2013.

[13] S. He, G. Ren, Z. Zhong, and Y. Zhao, "M-ary variable period modulation for indoor visible light communication system," *IEEE Commun. Lett.*, vol. 17, no. 7, pp. 1325–1328, 2013.

[14] A. M. Cailean, B. Cagneau, L. Chassagne, M. Dimian, and V. Popa, "Miller code usage in visible light communications under the PHY I layer of the IEEE 802.15.7 standard," in *IEEE Int. Conf. Commun.*, 2014.

[15] J. K. Kwon, "Inverse source coding for dimming in visible light communications using NRZ-OOK on reliable links," *IEEE Photonics Technol. Lett.*, vol. 22, no. 19, pp. 1455–1457, 2010.

[16] S. Kim and S. Y. Jung, "Novel FEC coding scheme for dimmable visible light communication based on the modified Reed-Muller codes," *IEEE Photonics Technol. Lett.*, vol. 23, no. 20, pp. 1514–1516, 2011.

[17] S. H. Lee and J. K. Kwon, "Turbo code-based error correction scheme for dimmable visible light communication systems," *IEEE Photonics Technol. Lett.*, vol. 24, no. 17, pp. 1463–1465, 2012.

[18] Z. Babar, M. A. M. Izhar, H. V. Nguyen, P. Botsinis, D. Alanis, D. Chandra, S. X. Ng, R. G. Maunder, and L. Hanzo, "Unary-coded dimming control improves on-off keying visible light communication," *IEEE Transactions on Communications*, vol. 66, pp. 255–264, Jan 2018.

[19] A. B. Siddique and M. Tahir, "Bandwidth efficient multi-level mppm encoding decoding algorithms for joint brightness-rate control in vlc systems," in *2014 IEEE Global Communications Conference*, pp. 2143–2147, Dec 2014.

[20] E. N. Mambou and T. G. Swart, "Construction of q -ary Constant Weight Sequences using a Knuth-like Approach," no. June, pp. 2028–2032, 2017.

[21] R. Singh, T. O'Farrell, and J. P. R. David, "Performance evaluation of IEEE 802.15.7 CSK physical layer," in *2013 IEEE Globecom Work. GC Wkshps 2013*, pp. 1064–1069, 2013.

[22] R. J. Drost and B. M. Sadler, "Constellation design for color-shift keying using billiards algorithms," in *2010 IEEE Globecom Work. GC'10*, pp. 980–984, 2010.

[23] E. Monteiro and S. Hranilovic, "Constellation design for color-shift keying using interior point methods," in *2012 IEEE Globecom Work. GC Wkshps 2012*, pp. 1224–1228, 2012.

[24] R. J. Drost and B. M. Sadler, "Constellation design for channel precompensation in multi-wavelength visible light communications," *IEEE Trans. Commun.*, vol. 62, no. 6, pp. 1995–2005, 2014.

[25] R. Singh, T. O'Farrell, and J. P. R. David, "An enhanced color shift keying modulation scheme for high-speed wireless visible light communications," *J. Light. Technol.*, vol. 32, no. 14, pp. 2582–2592, 2014.

[26] R. Singh, T. O'Farrell, and J. P. R. David, "Analysis of forward error correction schemes for colour shift keying modulation," *IEEE Int. Symp. Pers. Indoor Mob. Radio Commun. PIMRC*, vol. 2015-Decem, pp. 575–579, 2015.

[27] K. Immink, *Codes for mass data storage systems*. 2004.

[28] E. Monteiro and S. Hranilovic, "Design and Implementation of Color-Shift Keying for Visible Light Communications," *J. Light. Technol.*, vol. 32, no. 10, pp. 2053–2060, 2014.

[29] S. Lin and C. Daniel, *Error control coding fundamental and applications*. Prentice Hall UK, 2004.

[30] C. E. Shannon, “A mathematical theory of communication,” *Bell Syst. Tech. J.*, vol. 27, no. July 1928, pp. 379–423, 1948.

[31] B. H. Marcus, P. H. Siegel, and J. K. Wolf, “Finite-State Modulation Codes for Data Storage,” 1992.

[32] G. Ungerboeck, “Channel Coding with Multilevel/Phase Signals,” *IEEE Trans. Inf. Theory*, vol. 28, no. 1, pp. 55–67, 1982.

[33] B. Lehman, A. Wilkins, S. Berman, M. Poplawski, and N. Johnson Miller, “Proposing measures of flicker in the low frequencies for lighting applications,” *IEEE Energy Convers. Congr. Expo. Energy Convers. Innov. a Clean Energy Futur. ECCE 2011, Proc.*, pp. 2865–2872, 2011.

[34] T.-M. Chien, “Upper Bound on the Efficiency of dc-Constrained Codes,” *Bell Syst. Tech. J.*, vol. 49, no. 9, pp. 2267–2287, 1970.

[35] H. J. B. M. Melissen, “Densest packings of congruent circles in an equilateral triangle,” *The American Mathematical Monthly*, vol. 100, no. 10, pp. 916–925, 1993.

[36] A. E. Aziz, K. T. Wong, and J.-C. Chen, “Color-shift keyingâĂŤhow its largest obtainable minimum distance depends on its preset operating chromaticity and constellation size,” *Journal of Lightwave Technology*, vol. 35, no. 13, pp. 2724–2733, 2017.

[37] C. E. Mejia, C. N. Georghiades, and Y. H. Al-Badarneh, “Code Design in Visible Light Communications Using Color-Shift-Keying Constellations,” *2016 IEEE Glob. Commun. Conf.*, no. 3, pp. 1–7, 2016.

APPENDIX A

DEFINITION OF POWER SPECTRAL DENSITY AND ENERGY SPECTRUM*

## A.1 Power Spectral Density

Based on [27], $P(\omega)$ is defined as

$$\begin{aligned} P(\omega) &= \sum_{k=-\infty}^{\infty} R_x(k) e^{-jk\omega} \\ &= R_x(0) + 2\sum_{k=1}^{\infty} R_x(k)\cos(k\omega), \end{aligned} \tag{A.1}$$

where $R_x(k)$ is the *autocorrelation coefficients* and $\omega$ is the normalized angular frequency.

## A.2 The Energy Spectrum of OOK and 2PPM

Let the transmitted signal be:

$$y(t) = \sum_{k=-\infty}^{\infty} x_k s_{x_k}(t - kT_b), \tag{A.2}$$

where $x_k$ represents the data at time $k$, $s_{x_k}(t)$ is the pulse-shape associate to $x_k$, and $T_b$ is the bit period.

According to [27], the total power spectral density of a stationary process is equal to the product of the power spectral density $P(\omega)$ (which corresponds to the intrinsic randomness of the code) and the *energy spectrum*, $Q(\omega)$. $Q(\omega)$ is defined as

$$Q(\omega) = \sum_{x_i}\sum_{x_j}\int_{-\infty}^{\infty} r_s(t, x_i, x_j) p(x_i, x_j) e^{-j\omega t} dt, \tag{A.3}$$

where $r_s(\tau, x_i, x_j) = \frac{1}{T_b}\int_{-\infty}^{\infty} s_{x_i}(t) s_{x_j}(t+\tau) dt$. Using the fact codes are DC-balanced, $p(x_i, x_j) =$

*Reprinted with permission from "Code design for flicker mitigation in visible light communications using finite state machines" by Mejia CE, Georghiades CN, Abdallah MM, Al-Badarneh YH, 2017. *IEEE Transactions on Communications*, 65(5) pp.2091-2100, Copyright © 2011 IEEE

$1/4$ for all $i, j$. To differentiate the flicker effect due to the randomness of the code and its modulation, 2PPM and OOK symbols are represented as

$$s^{2ppm}(t) = \begin{cases} \Pi(\frac{2t}{T_b} - \frac{1}{2}) & \text{if } x = 1 \\ -\Pi(\frac{2t}{T_b} - \frac{3}{2}) & \text{if } x = -1 \end{cases} \tag{A.4}$$

and

$$s^{ook}(t) = \begin{cases} \Pi(\frac{t}{T_b} - \frac{1}{2}) & \text{if } x = 1 \\ 0 & \text{if } x = -1. \end{cases} \tag{A.5}$$

Using (A.3), the energy spectrum for 2PPM signal is

$$Q^{2ppm}(\omega) = \frac{1}{2}\left[1 - \cos\left(\frac{\omega}{2}\right)\right] \operatorname{sinc}^2\left(\frac{\omega}{4}\right). \tag{A.6}$$

Similarly, the energy spectrum for OOK signals is

$$\begin{aligned} Q^{ook}(\omega) &= \frac{1}{4}\operatorname{sinc}^2\left(\frac{\omega}{2}\right) \\ &= \frac{1}{8}\left[1 + \cos\left(\frac{\omega}{2}\right)\right] \operatorname{sinc}^2\left(\frac{\omega}{4}\right). \end{aligned} \tag{A.7}$$

### A.3 Perceived Flicker Energy for Uncoded

To calculate $E_u(\omega_0)$ we use $P(\omega) = 1$ and $Q(\omega)$ as in (A.7). Applying (3.2), an expression for $E_u(\omega_0)$ is

$$E_u(\omega_0) = \frac{[\omega_0 \operatorname{Si}(\omega_0) + \cos(\omega_0) - 1]}{2\pi\omega_0}, \tag{A.8}$$

where $\operatorname{Si}(z) = \int_0^z \frac{\sin(t)}{t} dt$.

# APPENDIX B

# DESIGNED CODES CHAPTER 3*

## B.1 Preliminaries

In the trellis diagram, the current and next states, from left to right, are connected by an arrow. The arrow represents all the transitions given a codeword subset. The codeword subsets and the arrows are mapped in strict order. Because of the complexity in making a graphical representation of the trellis diagrams, some of the codes are replaced by encoder/decoder tables below.

The mapping tables present the mapping between information bits and codeword bits. The information bits and the codeword subset are strictly assigned one-to-one at each state. Both the information bits and the codeword subsets are in decimal notation.

*Reprinted with permission from "Code design for flicker mitigation in visible light communications using finite state machines" by Mejia CE, Georghiades CN, Abdallah MM, Al-Badarneh YH, 2017. *IEEE Transactions on Communications*, 65(5) pp.2091-2100, Copyright © 2011 IEEE

## B.2 Mapping Table, Trellis Diagram and Decoder Table for the (4,6,3) Code

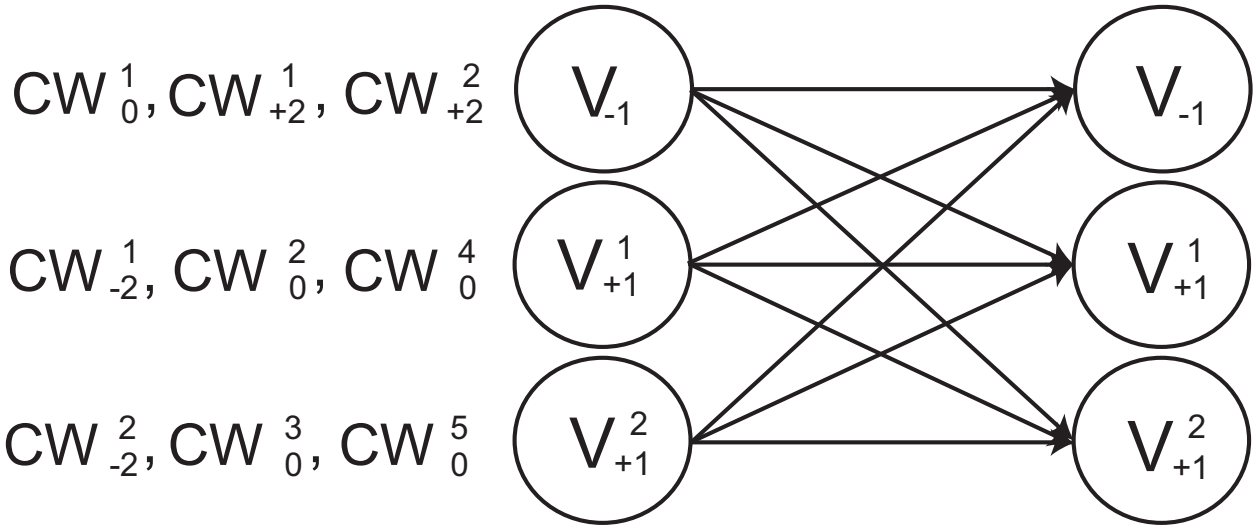


Figure B.1: The trellis diagram of the (4,6,3) code [Reprinted with permission from "Code design for flicker mitigation in visible light communications using finite state machines" by Mejia CE, Georghiades CN, Abdallah MM, Al-Badarneh YH, 2017. *IEEE Transactions on Communications*, 65(5) pp.2091-2100, Copyright © 2011 IEEE].

Table B.1: Mapping Table (4,6,3) code [ Reprinted with permission from "Code design for flicker mitigation in visible light communications using finite state machines" by Mejia CE, Georghiades CN, Abdallah MM, Al-Badarneh YH, 2017. *IEEE Transactions on Communications*, 65(5) pp.2091-2100, Copyright © 2011 IEEE].

| Information Bits | Codeword Set | | |
|---|---|---|---|
| | $V_{-1}$ | $V_{-1}^{1}$ | $V_{-1}^{2}$ |
| 0-3 | $CW_{0}^{1}$ = {11,13,19,7} | $CW_{-2}^{1}$ = { 5,6,9,10} | $CW_{-2}^{2}$ = {12,17,18,20} |
| 4-9 | $CW_{+2}^{1}$ = {27,29,43,45,51,53} | $CW_{0}^{2}$ = {21,22,25,26,37} | $CW_{0}^{3}$ = {41,42,44,49,50,52} |
| 10-15 | $CW_{+2}^{2}$ = {27,29,43,45,51,53} | $CW_{0}^{4}$ = {21,22,25,26,37} | $CW_{0}^{5}$ = {41,42,44,49,50,52} |

Table B.2: Decoder Decision Table (4,6,3) code [Reprinted with permission from "Code design for flicker mitigation in visible light communications using finite state machines" by Mejia CE, Georghiades CN, Abdallah MM, Al-Badarneh YH, 2017. *IEEE Transactions on Communications*, 65(5) pp.2091-2100, Copyright © 2011 IEEE].

| Decoded Codeword set $W(1)$ | Next Codeword Set (NCS) | Decoded Information bits | |
|---|---|---|---|
| | | $M(2) \in NCS$ | $M(2) \notin NCS$ |
| $CW_0^1$ | - | 0-3 | |
| $CW_{-2}^1$ | - | 0-3 | |
| $CW_{-2}^2$ | - | 0-3 | |
| $CW_0^2$ | $CW_0^2$/$CW_0^4$, $CW_{-2}^1$ | 4-9 | 10-15 |
| $CW_0^3$ | $CW_0^2$/$CW_0^4$, $CW_{-2}^1$ | | |
| $CW_{+2}^1$ | $CW_0^2$/$CW_0^4$, $CW_{-2}^1$ | | |

## B.3 Mapping Table, Encoder/Decoder Table for the (3,4,4) Code

Table B.3: Encoder/Decoder Table (3,4,4) Code Based on Trellis Diagram [Reprinted with permission from "Code design for flicker mitigation in visible light communications using finite state machines" by Mejia CE, Georghiades CN, Abdallah MM, Al-Badarneh YH, 2017. *IEEE Transactions on Communications*, 65(5) pp.2091-2100, Copyright © 2011 IEEE].

| | | Next State | |
|---|---|---|---|
| | | $V_{-1}$ | $V_{+1}$ |
| Current State | $V_{-1}$ | $CW_0^1$ | $CW_{+2}^1$ |
| | $V_{+1}$ | $CW_{-2}^1$ | $CW_0^2$ |

Table B.4: Mapping Table (3,4,4) code [Reprinted with permission from "Code design for flicker mitigation in visible light communications using finite state machines" by Mejia CE, Georghiades CN, Abdallah MM, Al-Badarneh YH, 2017. *IEEE Transactions on Communications*, 65(5) pp.2091-2100, Copyright © 2011 IEEE].

| Information Bits | Codeword Set | |
|---|---|---|
| | $V_{-1}$ | $V_{+1}$ |
| 0-3 | $CW_0^1$ = {10,5,3,9} | $CW_0^2$ = {10,5,6,12} |
| 4-7 | $CW_{+2}^1$ = {14,13,11,7} | $CW_{-2}^1$ = {1,2,4,8} |

## B.4 Mapping Table, Encoder/Decoder Table (4,6,7) Code

Table B.5: Encoder/Decoder Table of the (4,6,7) Code Based on Trellis Diagram [Reprinted with permission from "Code design for flicker mitigation in visible light communications using finite state machines" by Mejia CE, Georghiades CN, Abdallah MM, Al-Badarneh YH, 2017. *IEEE Transactions on Communications*, 65(5) pp.2091-2100, Copyright © 2011 IEEE].

| | | Next State | | | | | | | |
|---|---|---|---|---|---|---|---|---|---|
| | | $V_{-2}^1$ | $V_{-2}^2$ | $V_{-2}^3$ | $V_{-2}^4$ | $V_{+2}^1$ | $V_{+2}^2$ | $V_{+2}^3$ | $V_{+2}^4$ |
| Current State | $V_{-2}^1$ | $CW_0^2$ | $CW_0^4$ | $CW_0^5$ | $CW_0^3$ | $CW_{+4}^1$ | $CW_{+4}^6$ | $CW_{+4}^5$ | $CW_{+4}^2$ |
| | $V_{-2}^2$ | $CW_0^3$ | $CW_0^2$ | $CW_0^4$ | $CW_0^1$ | $CW_{+4}^2$ | $CW_{+4}^1$ | $CW_{+4}^4$ | $CW_{+4}^3$ |
| | $V_{-2}^3$ | $CW_0^5$ | $CW_0^3$ | $CW_0^2$ | $CW_0^6$ | $CW_{+4}^3$ | $CW_{+4}^2$ | $CW_{+4}^1$ | $CW_{+4}^6$ |
| | $V_{-2}^4$ | $CW_0^6$ | $CW_0^1$ | $CW_0^3$ | $CW_0^2$ | $CW_{+4}^4$ | $CW_{+4}^5$ | $CW_{+4}^2$ | $CW_{+4}^1$ |
| | $V_{+2}^1$ | $CW_{-4}^1$ | $CW_{-4}^6$ | $CW_{-4}^5$ | $CW_{-4}^2$ | $CW_0^2$ | $CW_0^4$ | $CW_0^5$ | $CW_0^3$ |
| | $V_{+2}^2$ | $CW_{-4}^2$ | $CW_{-4}^1$ | $CW_{-4}^4$ | $CW_{-4}^3$ | $CW_0^3$ | $CW_0^2$ | $CW_0^4$ | $CW_0^1$ |
| | $V_{+2}^3$ | $CW_{-4}^3$ | $CW_{-4}^2$ | $CW_{-4}^1$ | $CW_{-4}^6$ | $CW_0^5$ | $CW_0^3$ | $CW_0^2$ | $CW_0^6$ |
| | $V_{+2}^4$ | $CW_{-4}^4$ | $CW_{-4}^5$ | $CW_{-4}^2$ | $CW_{-4}^1$ | $CW_0^6$ | $CW_0^1$ | $CW_0^3$ | $CW_0^2$ |

Table B.6: Mapping Table (4,6,7) code Reprinted with permission from "Code design for flicker mitigation in visible light communications using finite state machines" by Mejia CE, Georghiades CN, Abdallah MM, Al-Badarneh YH, 2017. *IEEE Transactions on Communications*, 65(5) pp.2091-2100, Copyright © 2011 IEEE].

| Information Bits Set | Codeword Set | |
|---|---|---|
| | $V_{-2}^{x}$ | $V_{+2}^{x}$ |
| 0-2 | $CW_0^2$={19,13,38} | $CW_0^2$={19,13,38} |
| 3-5 | $CW_0^4$={28,42,49} | $CW_0^4$={28,42,49} |
| | $CW_0^6$={52,26,41} | $CW_0^6$={52,26,41} |
| 6-8 | $CW_0^1$={35,21,14} | $CW_0^1$={35,21,14} |
| | $CW_0^5$={44,50,25} | $CW_0^5$={44,50,25} |
| 9-11 | $CW_0^3$={11,37,22} | $CW_0^3$={11,37,22} |
| 12 | $CW_{+4}^1$={31} | $CW_{-4}^1$={32} |
| 13 | $CW_{+4}^4$={59} | $CW_{-4}^4$={4} |
| | $CW_{+4}^6$={62} | $CW_{-4}^6$={1} |
| 14 | $CW_{+4}^3$={55} | $CW_{-4}^3$={8} |
| | $CW_{+4}^5$={61} | $CW_{-4}^5$={2} |
| 15 | $CW_{+4}^2$={47} | $CW_{-4}^2$={16} |

## B.5 Mapping Table, Encoder/Decoder Table (6,8,9) Code.

Table B.7: Encoder/Decoder Table (6,8,9) Code Based on Trellis Diagram [Reprinted with permission from "Code design for flicker mitigation in visible light communications using finite state machines" by Mejia CE, Georghiades CN, Abdallah MM, Al-Badarneh YH, 2017. *IEEE Transactions on Communications*, 65(5) pp.2091-2100, Copyright © 2011 IEEE].

| | | Next State | | | | | | | | | |
|---|---|---|---|---|---|---|---|---|---|---|---|
| | | $V_{-2}^1$ | $V_{-2}^2$ | $V_{-2}^3$ | $V_{-2}^4$ | $V_{-2}^5$ | $V_{+2}^1$ | $V_{+2}^2$ | $V_{+2}^3$ | $V_{+2}^4$ | $V_{+2}^5$ |
| Current State | $V_{-2}^1$ | $CW_0^1$ | $CW_0^2$ | $CW_0^3$ | $CW_0^4$ | $CW_0^6$ | $CW_{+4}^1$ | $CW_{+4}^2$ | $CW_{+4}^3$ | $CW_{+4}^4$ | $CW_{+4}^5$ |
| | $V_{-2}^2$ | $CW_0^5$ | $CW_0^1$ | $CW_0^2$ | $CW_0^3$ | $CW_0^4$ | $CW_{+4}^7$ | $CW_{+4}^1$ | $CW_{+4}^2$ | $CW_{+4}^3$ | $CW_{+4}^6$ |
| | $V_{-2}^3$ | $CW_0^4$ | $CW_0^6$ | $CW_0^1$ | $CW_0^2$ | $CW_0^3$ | $CW_{+4}^4$ | $CW_{+4}^7$ | $CW_{+4}^1$ | $CW_{+4}^2$ | $CW_{+4}^3$ |
| | $V_{-2}^4$ | $CW_0^3$ | $CW_0^4$ | $CW_0^7$ | $CW_0^1$ | $CW_0^2$ | $CW_{+4}^3$ | $CW_{+4}^6$ | $CW_{+4}^5$ | $CW_{+4}^1$ | $CW_{+4}^2$ |
| | $V_{-2}^5$ | $CW_0^2$ | $CW_0^3$ | $CW_0^4$ | $CW_0^5$ | $CW_0^1$ | $CW_{+4}^2$ | $CW_{+4}^3$ | $CW_{+4}^4$ | $CW_{+4}^5$ | $CW_{+4}^1$ |
| | $V_{+2}^1$ | $CW_{-4}^1$ | $CW_{-4}^2$ | $CW_{-4}^3$ | $CW_{-4}^4$ | $CW_{-4}^5$ | $CW_0^1$ | $CW_0^2$ | $CW_0^3$ | $CW_0^4$ | $CW_0^7$ |
| | $V_{+2}^2$ | $CW_{-4}^7$ | $CW_{-4}^1$ | $CW_{-4}^2$ | $CW_{-4}^3$ | $CW_{-4}^6$ | $CW_0^5$ | $CW_0^1$ | $CW_0^2$ | $CW_0^3$ | $CW_0^4$ |
| | $V_{+2}^3$ | $CW_{-4}^4$ | $CW_{-4}^7$ | $CW_{-4}^1$ | $CW_{-4}^2$ | $CW_{-4}^3$ | $CW_0^4$ | $CW_0^6$ | $CW_0^1$ | $CW_0^2$ | $CW_0^3$ |
| | $V_{+2}^4$ | $CW_{-4}^3$ | $CW_{-4}^6$ | $CW_{-4}^5$ | $CW_{-4}^1$ | $CW_{-4}^2$ | $CW_0^3$ | $CW_0^4$ | $CW_0^7$ | $CW_0^1$ | $CW_0^2$ |
| | $V_{+2}^5$ | $CW_{-4}^2$ | $CW_{-4}^3$ | $CW_{-4}^4$ | $CW_{-4}^5$ | $CW_{-4}^1$ | $CW_0^2$ | $CW_0^3$ | $CW_0^4$ | $CW_0^5$ | $CW_0^1$ |

Table B.8: Mapping Table (6,8,9) code [Reprinted with permission from "Code design for flicker mitigation in visible light communications using finite state machines" by Mejia CE, Georghiades CN, Abdallah MM, Al-Badarneh YH, 2017. *IEEE Transactions on Communications*, 65(5) pp.2091-2100, Copyright © 2011 IEEE].

| Information Bits | Codeword Set | |
|---|---|---|
| | $V_{-2}^{x}$ | $V_{+2}^{x}$ |
| 0-7 | $CW_0^1$={135,120,75,180,45,210,30,225} | $CW_0^1$={135,120,75,180,45,210,30,225} |
| 8-15 | $CW_0^2$={71,184,43,212,29,226,142,113} | $CW_0^2$={71,184,43,212,29,226,142,113} |
| 16-23 | $CW_0^3$={39,216,27,228,141,114,78,177} | $CW_0^3$={39,216,27,228,141,114,78,177} |
| 24-31 | $CW_0^4$={23,232,139,116,77,178,46,209} | $CW_0^4$={23,232,139,116,77,178,46,209} |
| 32-43 | $CW_0^5$={85,170,165,90,153,102,105,150 ,51,204,195,60} | $CW_0^5$={85,170,165,90,153,102,105,150 ,51,204,195,60} |
| | $CW_0^6$={149,106,101,154,57,198,201,54 ,83,172,163,92} | $CW_0^6$={149,106,101,154,57,198,201,54 ,83,172,163,92} |
| | $CW_0^7$={53,202,197,58,89,166,169,86, ,147,108,99,156} | $CW_0^7$={53,202,197,58,89,166,169,86 ,147,108,99,156} |
| 44-47 | $CW_{+4}^1$={63,207,243,252} | $CW_{-4}^1$={192,48,12,3} |
| 48-51 | $CW_{+4}^2$={159,111,249,246} | $CW_{-4}^2$={96,14,6,9} |
| 52-55 | $CW_{+4}^3$={95,175,245,250} | $CW_{-4}^3$={160,80,10,5} |
| 56-59 | $CW_{+4}^4$={119,187,221,238 | $CW_{-4}^4$={136,68,34,17} |
| | $CW_{+4}^6$={215,235,125,190} | $CW_{-4}^6$={40,20,130,65} |
| 60-63 | $CW_{+4}^5$={183,219,237,126} | $CW_{-4}^5$={72,36,18,129} |

## B.6 Mapping Table, Encoder/Decoder Table (8,10,11) Code

Table B.9: Encoder/Decoder Table (8,10,11) Code Based on Trellis Diagram [Reprinted with permission from "Code design for flicker mitigation in visible light communications using finite state machines" by Mejia CE, Georghiades CN, Abdallah MM, Al-Badarneh YH, 2017. *IEEE Transactions on Communications*, 65(5) pp.2091-2100, Copyright © 2011 IEEE].

| | | Next State (CW) | | | | | | | | | | | | | | | |
|---|---|---|---|---|---|---|---|---|---|---|---|---|---|---|---|---|---|
| | | $V_{-2}^{1}$ | $V_{-2}^{2}$ | $V_{-2}^{3}$ | $V_{-2}^{4}$ | $V_{-2}^{5}$ | $V_{-2}^{6}$ | $V_{-2}^{7}$ | $V_{-2}^{8}$ | $V_{+2}^{1}$ | $V_{+2}^{2}$ | $V_{+2}^{3}$ | $V_{+2}^{4}$ | $V_{+2}^{5}$ | $V_{+2}^{6}$ | $V_{+2}^{7}$ | $V_{+2}^{8}$ |
| Current State | $V_{-2}^{1}$ | $CW_0^1$ | $CW_0^2$ | $CW_0^3$ | $CW_0^4$ | $CW_0^5$ | $CW_0^6$ | $CW_0^7$ | $CW_0^8$ | $CW_{+4}^{1}$ | $CW_{+4}^{2}$ | $CW_{+4}^{3}$ | $CW_{+4}^{4}$ | $CW_{+4}^{5}$ | $CW_{+4}^{11}$ | $CW_{+4}^{12}$ | $CW_{+4}^{13}$ |
| | $V_{-2}^{2}$ | $CW_0^9$ | $CW_0^1$ | $CW_0^2$ | $CW_0^3$ | $CW_0^4$ | $CW_0^5$ | $CW_0^6$ | $CW_0^7$ | $CW_{+4}^{14}$ | $CW_{+4}^{1}$ | $CW_{+4}^{2}$ | $CW_{+4}^{3}$ | $CW_{+4}^{4}$ | $CW_{+4}^{5}$ | $CW_{+4}^{11}$ | $CW_{+4}^{12}$ |
| | $V_{-2}^{3}$ | $CW_0^9$ | $CW_0^8$ | $CW_0^1$ | $CW_0^2$ | $CW_0^3$ | $CW_0^4$ | $CW_0^5$ | $CW_0^6$ | $CW_{+4}^{12}$ | $CW_{+4}^{15}$ | $CW_{+4}^{1}$ | $CW_{+4}^{2}$ | $CW_{+4}^{3}$ | $CW_{+4}^{4}$ | $CW_{+4}^{5}$ | $CW_{+4}^{11}$ |
| | $V_{-2}^{4}$ | $CW_0^6$ | $CW_0^9$ | $CW_0^9$ | $CW_0^1$ | $CW_0^2$ | $CW_0^3$ | $CW_0^4$ | $CW_0^5$ | $CW_{+4}^{11}$ | $CW_{+4}^{12}$ | $CW_{+4}^{18}$ | $CW_{+4}^{1}$ | $CW_{+4}^{2}$ | $CW_{+4}^{3}$ | $CW_{+4}^{4}$ | $CW_{+4}^{5}$ |
| | $V_{-2}^{5}$ | $CW_0^5$ | $CW_0^6$ | $CW_0^7$ | $CW_0^8$ | $CW_0^1$ | $CW_0^2$ | $CW_0^3$ | $CW_0^4$ | $CW_{+4}^{6}$ | $CW_{+4}^{7}$ | $CW_{+4}^{8}$ | $CW_{+4}^{9}$ | $CW_{+4}^{10}$ | $CW_{+4}^{16}$ | $CW_{+4}^{17}$ | $CW_{+4}^{19}$ |
| | $V_{-2}^{6}$ | $CW_0^4$ | $CW_0^5$ | $CW_0^6$ | $CW_0^7$ | $CW_0^9$ | $CW_0^1$ | $CW_0^2$ | $CW_0^3$ | $CW_{+4}^{20}$ | $CW_{+4}^{6}$ | $CW_{+4}^{7}$ | $CW_{+4}^{8}$ | $CW_{+4}^{9}$ | $CW_{+4}^{10}$ | $CW_{+4}^{16}$ | $CW_{+4}^{17}$ |
| | $V_{-2}^{7}$ | $CW_0^3$ | $CW_0^4$ | $CW_0^5$ | $CW_0^6$ | $CW_0^9$ | $CW_0^8$ | $CW_0^1$ | $CW_0^2$ | $CW_{+4}^{17}$ | $CW_{+4}^{13}$ | $CW_{+4}^{6}$ | $CW_{+4}^{7}$ | $CW_{+4}^{8}$ | $CW_{+4}^{9}$ | $CW_{+4}^{10}$ | $CW_{+4}^{16}$ |
| | $V_{-2}^{8}$ | $CW_0^2$ | $CW_0^3$ | $CW_0^4$ | $CW_0^5$ | $CW_0^6$ | $CW_0^9$ | $CW_0^9$ | $CW_0^1$ | $CW_{+4}^{16}$ | $CW_{+4}^{17}$ | $CW_{+4}^{14}$ | $CW_{+4}^{6}$ | $CW_{+4}^{7}$ | $CW_{+4}^{8}$ | $CW_{+4}^{9}$ | $CW_{+4}^{10}$ |
| | $V_{+2}^{1}$ | $CW_{-4}^{1}$ | $CW_{-4}^{2}$ | $CW_{-4}^{3}$ | $CW_{-4}^{4}$ | $CW_{-4}^{5}$ | $CW_{-4}^{11}$ | $CW_{-4}^{12}$ | $CW_{-4}^{13}$ | $CW_0^1$ | $CW_0^2$ | $CW_0^3$ | $CW_0^4$ | $CW_0^5$ | $CW_0^6$ | $CW_0^7$ | $CW_0^8$ |
| | $V_{+2}^{2}$ | $CW_{-4}^{14}$ | $CW_{-4}^{1}$ | $CW_{-4}^{2}$ | $CW_{-4}^{3}$ | $CW_{-4}^{4}$ | $CW_{-4}^{5}$ | $CW_{-4}^{11}$ | $CW_{-4}^{12}$ | $CW_0^9$ | $CW_0^1$ | $CW_0^2$ | $CW_0^3$ | $CW_0^4$ | $CW_0^5$ | $CW_0^6$ | $CW_0^7$ |
| | $V_{+2}^{3}$ | $CW_{-4}^{12}$ | $CW_{-4}^{15}$ | $CW_{-4}^{1}$ | $CW_{-4}^{2}$ | $CW_{-4}^{3}$ | $CW_{-4}^{4}$ | $CW_{-4}^{5}$ | $CW_{-4}^{11}$ | $CW_0^9$ | $CW_0^8$ | $CW_0^1$ | $CW_0^2$ | $CW_0^3$ | $CW_0^4$ | $CW_0^5$ | $CW_0^5$ |
| | $V_{+2}^{4}$ | $CW_{-4}^{11}$ | $CW_{-4}^{12}$ | $CW_{-4}^{18}$ | $CW_{-4}^{1}$ | $CW_{-4}^{2}$ | $CW_{-4}^{3}$ | $CW_{-4}^{4}$ | $CW_{-4}^{5}$ | $CW_0^6$ | $CW_0^9$ | $CW_0^9$ | $CW_0^1$ | $CW_0^2$ | $CW_0^3$ | $CW_0^4$ | $CW_0^5$ |
| | $V_{+2}^{5}$ | $CW_{-4}^{6}$ | $CW_{-4}^{7}$ | $CW_{-4}^{8}$ | $CW_{-4}^{9}$ | $CW_{-4}^{10}$ | $CW_{-4}^{16}$ | $CW_{-4}^{17}$ | $CW_{-4}^{19}$ | $CW_0^5$ | $CW_0^6$ | $CW_0^7$ | $CW_0^8$ | $CW_0^1$ | $CW_0^2$ | $CW_0^3$ | $CW_0^4$ |
| | $V_{+2}^{6}$ | $CW_{-4}^{20}$ | $CW_{-4}^{6}$ | $CW_{-4}^{7}$ | $CW_{-4}^{8}$ | $CW_{-4}^{9}$ | $CW_{-4}^{10}$ | $CW_{-4}^{16}$ | $CW_{-4}^{17}$ | $CW_0^4$ | $CW_0^5$ | $CW_0^6$ | $CW_0^7$ | $CW_0^9$ | $CW_0^1$ | $CW_0^2$ | $CW_0^3$ |
| | $V_{+2}^{7}$ | $CW_{-4}^{17}$ | 3.13 | $CW_{-4}^{6}$ | $CW_{-4}^{7}$ | $CW_{-4}^{8}$ | $CW_{-4}^{9}$ | $CW_{-4}^{10}$ | $CW_{-4}^{16}$ | $CW_0^3$ | $CW_0^4$ | $CW_0^5$ | $CW_0^6$ | $CW_0^9$ | $CW_0^8$ | $CW_0^1$ | $CW_0^2$ |
| | $V_{+2}^{8}$ | $CW_{-4}^{16}$ | $CW_{-4}^{17}$ | $CW_{-4}^{14}$ | $CW_{-4}^{6}$ | $CW_{-4}^{7}$ | $CW_{-4}^{8}$ | $CW_{-4}^{9}$ | $CW_{-4}^{10}$ | $CW_0^2$ | $CW_0^3$ | $CW_0^4$ | $CW_0^5$ | $CW_0^6$ | $CW_0^9$ | $CW_0^9$ | $CW_0^1$ |

Table B.10: Mapping Table (8,10,11) code [Reprinted with permission from "Code design for flicker mitigation in visible light communications using finite state machines" by Mejia CE, Georghiades CN, Abdallah MM, Al-Badarneh YH, 2017. *IEEE Transactions on Communications*, 65(5) pp.2091-2100, Copyright © 2011 IEEE].

| Information Bits | Codeword Set | |
|---|---|---|
| | $V_{-2}^{x}$ | $V_{+2}^{x}$ |
| 0-24 | $CW_0^1$ = {124,103,796,775,341,331,661,651,217,214,313,310, 403,398,563,558,589,602,173,186,496,744,868,930,961} | $CW_0^1$ = {124,103,796,775,341,331,661,651,217,214,313,310, 403,398,563,558,589,602,173,186,496,744,868,930,961} |
| 25-49 | $CW_0^2$ = {348,327,668,647,213,203,309,299,409,406,569,566, 595,590,179,174,109,122,781,794,752,872,932,962,481} | $CW_0^2$ = {348,327,668,647,213,203,309,299,409,406,569,566, 595,590,179,174,109,122,781,794,752,872,932,962,481} |
| 50-74 | $CW_0^3$ = {220,199,316,295,405,395,565,555,601,598,185,182, 115,110,787,782,333,346,653,666,880,936,964,482,737} | $CW_0^3$ = {220,199,316,295,405,395,565,555,601,598,185,182, 115,110,787,782,333,346,653,666,880,936,964,482,737} |
| 75-99 | $CW_0^4$ = {412,391,572,551,597,587,181,171,121,118,793,790, 339,334,659,654,205,218,301,314,944,968,484,738,865} | $CW_0^4$ = {412,391,572,551,597,587,181,171,121,118,793,790, 339,334,659,654,205,218,301,314,944,968,484,738,865} |
| 100-124 | $CW_0^5$ = {604,583,188,167,117,107,789,779,345,342,665,662, 211,206,307,302,397,410,557,570,976,488,740,866,929} | $CW_0^5$ = {604,583,188,167,117,107,789,779,345,342,665,662, 211,206,307,302,397,410,557,570,976,488,740,866,929} |
| 125-149 | $CW_0^6$ = {899,227,920,248,682,362,692,372,806,710,809,713, 620,460,625,465,434,850,421,837,527,279,155,93,62 } | $CW_0^6$ = {899,227,920,248,682,362,692,372,806,710,809,713, 620,460,625,465,434,850,421,837,527,279,155,93,62 } |
| 150-174 | $CW_0^7$={ 675,355,696,376,810,714,820,724,614,454,617,457, 428,844,433,849,914,242,901,229,271,151,91,61,542 } | $CW_0^9$={ 611,451,632,472,426,842,436,852,902 ,230,905, 233,684,364,689,369,818,722,805,709,79,55,539,285,158 } |
| 175-199 | $CW_0^8$={ 803,707,824,728,618,458,628,468,422,838,425,841, 908,236,913,241,690,370,677,357,143,87,59,541,286 } | $CW_0^{10}$={ 419,835,440,856,906,234,916,244,678,358,681,361, 812,716,817,721,626,466,613,453,47,535,283,157,94 } |
| 200-209 | $CW_{+4}^1$={911,239,695,375,827,731,637,477,446,862 } | $CW_{-4}^1$={ 112,784,328,648,196,292,386,546,577,161} |
| | $CW_{+4}^6$={508,487,757,747,889,886,947,942,973,986 } | $CW_{-4}^6$={ 515,536,266,276,134,137,76,81,50,37 } |
| 210-219 | $CW_{+4}^2$={815,719,631,471,443,859,925,253,702,382 } | $CW_{-4}^2$={ 208,304,392,552,580,164,98,770,321,641} |
| | $CW_{+4}^7$={892,871,949,939,985,982,499,494,749,762 } | $CW_{-4}^7$={ 131,152,74,84,38,41,524,529,274,261 } |
| 220-229 | $CW_{+4}^3$={431,847,919,247,699,379,829,733,638,478 } | $CW_{-4}^3$={ 592,176,104,776,324,644,194,290,385,545} |
| | $CW_{+4}^8$={892,871,949,939,985,982,499,494,749,762 } | $CW_{-4}^8$={ 35,56,522,532,262,265,140,145,82,69 } |
| 230-239 | $CW_{+4}^4$={687,367,823,727,635,475,445,861,926,254 } | $CW_{-4}^4$={ 336,656,200,296,388,548,578,162,97,769} |
| | $CW_{+4}^9$={764,743,885,875,953,950,979 ,974,493,506 } | $CW_{-4}^9$={ 259,280,138,148,70,73,44,49,530,517 } |
| 240-249 | $CW_{+4}^5$={623,463,439,855,923,251,701,381,830,734 } | $CW_{-4}^5$={ 400,560,584,168,100,772,322,642,193,289} |
| | $CW_{+4}^{10}$={956,935,981,971,505,502,755,750,877,890 } | $CW_{-4}^{10}$={ 67,88,42,52,518,521,268,273,146,133 } |
| 250-251 | $CW_{+4}^{11}$={995,1016} | $CW_{-4}^{11}$={28,7} |
| | $CW_{+4}^{16}$={127,799} | $CW_{-4}^{16}$={ 896,241} |
| 252-253 | $CW_{+4}^{12}$={1002,1012} | $CW_{-4}^{12}$={21,11} |
| | $CW_{+4}^{17}$={351,671} | $CW_{-4}^{17}$={672,352} |
| 254-255 | $CW_{+4}^{13}$={998,1001} | $CW_{-4}^{13}$={25,22} |
| | $CW_{+4}^{14}$={1004,1009} | $CW_{-4}^{14}$={19,14} |
| | $CW_{+4}^{15}$={1010,997} | $CW_{-4}^{15}$={13,26} |
| | $CW_{+4}^{18}$={223,319} | $CW_{-4}^{18}$={800,704} |
| | $CW_{+4}^{19}$={415,575} | $CW_{-4}^{19}$={608,448} |
| | $CW_{+4}^{20}$={607,191} | $CW_{-4}^{20}$={416,832} |

APPENDIX C

RECURSIVE ALGORITHMS TO DESIGN ADJACENCY MATRIX OF CSK-FSM *

## C.1 Adjacency Matrix 3-CSK-FSM

**Algorithm 3** Algorithm to generate adjacency matrix of 3CSK-FSM.

1: $D = \text{MATRIXV1}(\sqrt{N_{cell}}, 3)$ ▷ $V_1, V_2$, and $V_3$

## C.2 Adjacency Matrix 10-CSK-FSM

**Algorithm 4** Algorithm to generate adjacency matrix of 10CSK-FSM

1: $D_{11} = \text{MATRIXV1}(\sqrt{N_{cell}}, 4)$ ▷ $V_1, V_2, V_3$ and $V_{10}$
2: $D_{22} = \text{MATRIXV1}(\sqrt{N_{cell}} - 1, 4)$ ▷ $V_1, V_2, V_3$ and $V_{10}$
3: $D_{33} = \text{MATRIXV1}(\sqrt{N_{cell}} - 1, 4)$ ▷ $V_1, V_2, V_3$ and $V_{10}$
4: $D_{12} = \text{MATRIXV2}(\sqrt{N_{cell}}, 0)$ ▷ $V_5, V_7$ and $V_8$
5: $D_{13} = \text{MATRIXV2}(\sqrt{N_{cell}}, 1)$ ▷ $V_9, V_4$ and $V_6$
6: $D_{31} = D_{13}^T$ ▷ $V_5, V_7$ and $V_8$
7: $D_{21} = D_{12}^T$ ▷ $V_9, V_4$ and $V_6$
8: $D_{23} = \text{MATRIXV3}(\sqrt{N_{cell}})$ ▷ $V_7, V_8$ and $V_5$
9: $D_{32} = D_{23}^T$ ▷ $V_4, V_6$ and $V_9$
10: $D = \begin{bmatrix} D_{11} & D_{12} & D_{13} \\ D_{21} & D_{22} & D_{23} \\ D_{31} & D_{32} & D_{33} \end{bmatrix}$

*Reprinted with permission from "Code design in visible light communications using color-shift-keying constellations" by Mejia CE, Georghiades CN, Al-Badarneh YH, 2016. *Global Communications Conference (GLOBECOM)*, IEEE 2016 Dec 4 (pp. 1-7), Copyright © 2011 IEEE.

## C.3 Functions for Algorithms

1: **function** MATRIXV1($M$,$k$)
▷ $k = 3$ for 3-CSK; $k = 4$ for 10-CSK
2: $N = (M + 1)^2$
3: $D = zeros(N, N)$
4: $X = [1 : N]$ ▷ $X$ = Current State
5: $Y = [1 : N]$ ▷ $Y$ = Next State
6: **for all** $[(Y = X + 1) \wedge (mod(X, M + 1) \neq 0)]$ **or**
$[Y = X + (M + 1)]$ **or**
$[(Y = X - (M + 2)) \wedge (mod(Y, M + 1) \neq 0)]$
**do** ▷ $V_1$, $V_2$ ,and $V_3$ respectively
7: $D(X, Y) = 1$
8: **end for**
9: **if** $k = 4$ **then**
10: **for all** $X = Y$ **do**
11: $D(X, Y) = 1$ ▷ $V_{10}$
12: **end for**
13: **end if**
14: **return** $D$ ▷ $V_1, V_2, V_3$, and $V_{10}$
15: **end function**

```
1: function MATRIXV3(M)
2:     N = M^2
3:     D = zeros(N, N)
4:     X = [1 : N]                                          ▷ X = Current State
5:     Y = [1 : N]                                          ▷ Y = Next State
6:     for all [Y = X] or [Y = X − M] or
       [(Y = X + 1) ∧ (mod(X, M) ≠ 0)]
       do                                                   ▷ V_i, V_j, and V_k respectively
7:         D(X, Y) = 1
8:     end for
9:  return D                                                ▷ V_i, V_j and V_k
10: end function
```

```
1: function MATRIXV2(M,k)
2:     N_1 = (M + 1)^2
3:     N_2 = M^2
4:     D = zeros(N_1, N_2)
5:     i = 0
6:     for Y = 1 : N_2 do
7:         if mod(Y, M + 1) ≠ 0 then
8:             D(Y + i, Y) = 1                              ▷ V_i
9:             D(Y + (i + M + 2), Y) = 1                    ▷ V_k
10:            if k = 0 then
11:                D(Y + (i + 1), Y) = 1                    ▷ V_j
12:            else
13:                D(Y + (i + M + 1), Y) = 1                ▷ V_j
14:            end if
15:        else
16:            i = i + 1
17:        end if
18:    end for
19: return D                                                ▷ V_i, V_j and V_k
20: end function
```

APPENDIX D

DESIGNED CODES CHAPTER 4

## D.1 Trellis diagram and mapping table (1, 4, 9, 3) code

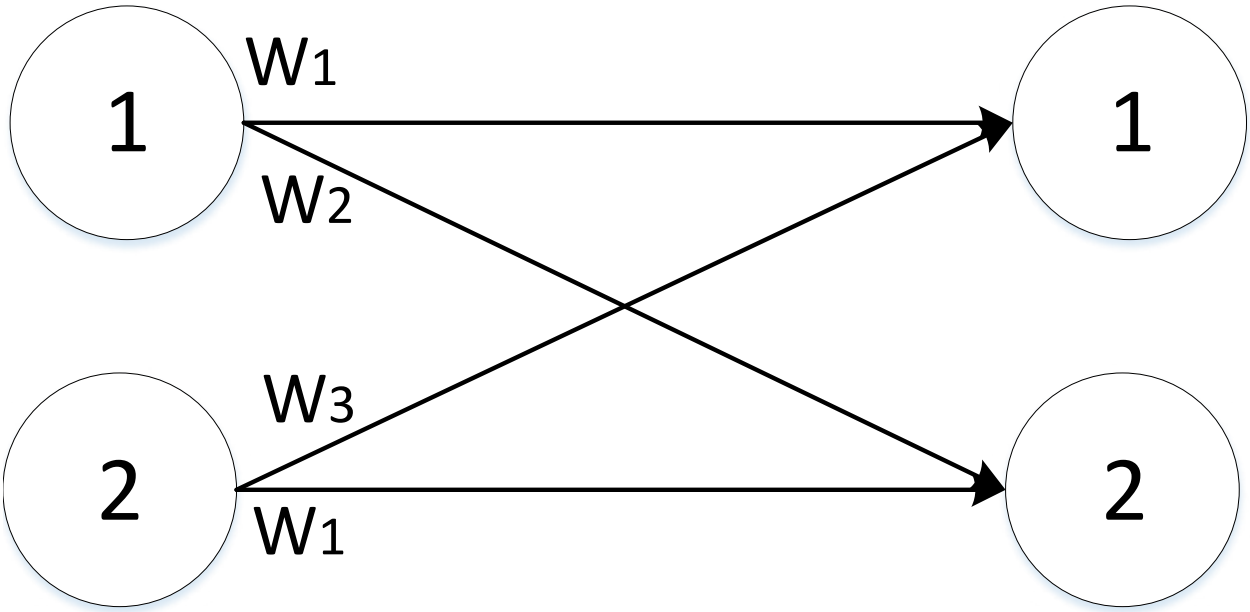


Figure D.1: Trellis Diagram (1, 4, 9, 3) code.

Table D.1: Mapping table for the (1, 4, 9, 3) code.

| Input Bits | Codeword set | Codewords |
|---|---|---|
| $0-5$ | $W_1$ | [123][132][213][231][312][321] |
| $6-7$ | $W_2$ | [232][322] |
| | $W_3$ | [131][311] |

## D.2 Trellis diagram and mapping table (7/3, 1, 9,10) code

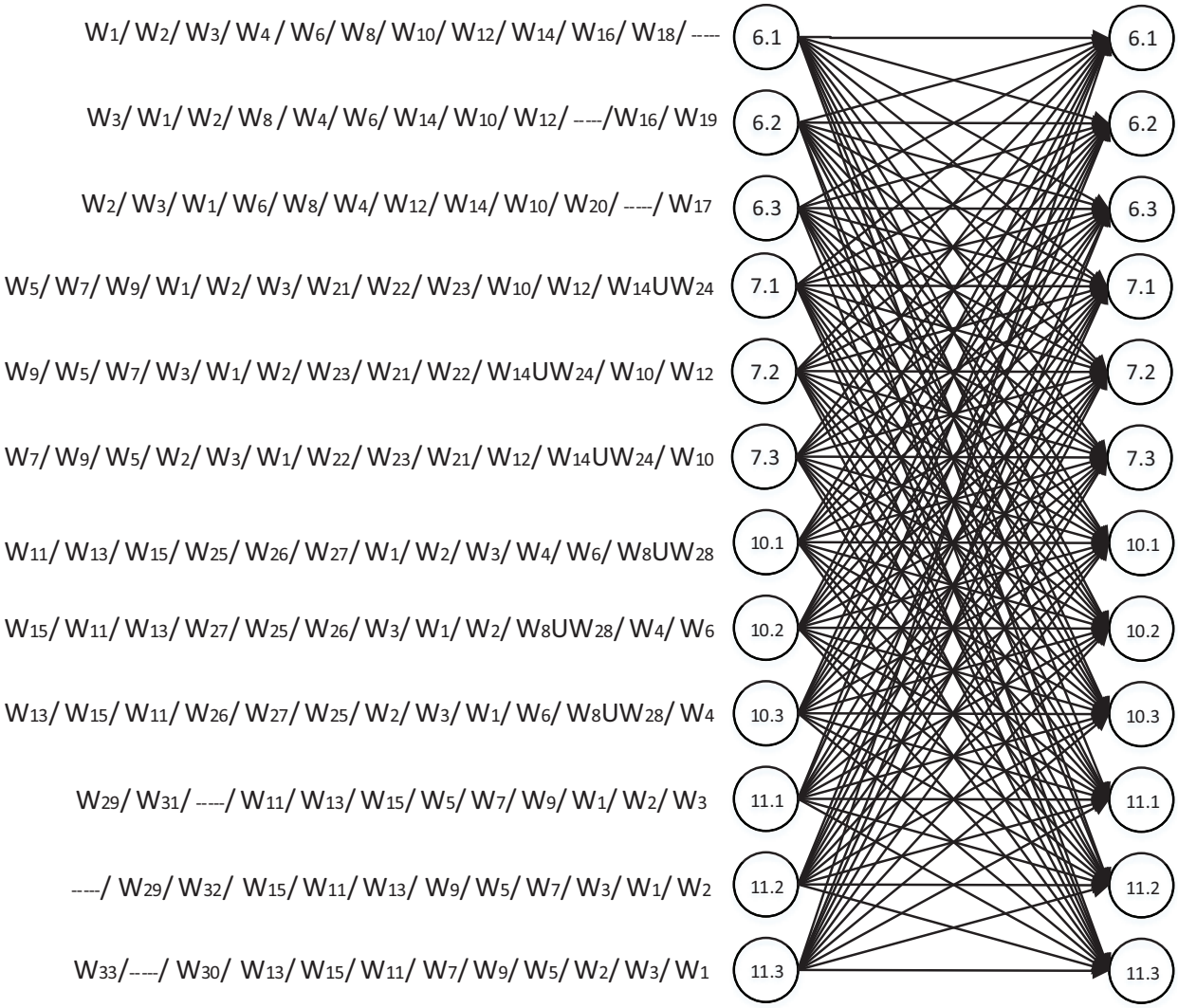


Figure D.2: Trellis Diagram (7/3, 1, 9,10) code.

Table D.2: Mapping table for the (7/3, 1, 9,10) code.

| Input Bits | Codeword Set | Codewords |
|---|---|---|
| $0-18$ | $W_1$ | [123], [132], [213], [231], [312], [321], [469], [496], [578], [587], [649], [694], [758], [785], [857], [875], [946], [964], [101010] |
| $19-36$ | $W_2$ | [197], [248], [365], [4710], [482], [536], [5109], [653], [6810], [719], [7104], [824], [8106], [9510], [971], [1047], [1068], [1095] |
| $37-54$ | $W_3$ | [179], [284], [356], [428], [4107], [563], [5910], [635], [6108], [7410], [791], [842], [8610], [917], [9105], [1059], [1074], [1086] |
| $55-63$ | $W_4$ | [11010], [446], [464], [558], [585], [644], [855], [10110], [10101] |
| $55-66$ | $W_5$ | [2310], [2103], [3210], [3102], [699], [778], [787], [877], [969], [996], [1023], [1032] |
| $64-75$ | $W_6$ | [147], [168], [195], [4510], [471], [519], [5104], [681], [714], [816], [951], [1045] |
| $67-75$ | $W_7$ | [298], [367], [673], [736], [7109][829], [9710], [982], [1097] |
| $76-84$ | $W_8$ | [159], [174], [186], [417], [4105][5410], [591], [618], [741] |
| | $W_9$ | [289], [376], [637], [763], [7910][892], [928], [9107], [1079] |
| $85-93$ | $W_{10}$ | [21010], [577], [669], [696], [757], [775], [966], [10210], [10102] |
| $85-96$ | $W_{11}$ | [1310], [1103], [3110], [3101], [449], [494], [588], [858], [885], 944], [1013], [1031] |
| $94-105$ | $W_{12}$ | [247], [268], [295], [472], [529], [6710], [682], [724], [7106], [826], [952], [1067] |
| $97-105$ | $W_{13}$ | [198], [345], [453], [4810], [534], [819], [8104], [981], [1048] |
| $106-114$ | $W_{14}$ | [259], [274], [286], [427], [592], [628], [6107], [742], [7610] |
| | $W_{15}$ | [189], [354], [435], [4108], [543], [8410], [891], [918], [1084] |
| $115-123$ | $W_{16}$ | [167], [245], [452], [524], [5106], [6510], [671], [716], [1065] |
| | $W_{17}$ | [176], [254], [425], [542], [5610], [617], [6105], [761], [1056 |
| $124-127$ | $W_{18}$ | [1210], [1102], [2110], [2101] |
| | $W_{19}$ | [466], [557], [575], [646] |
| | $W_{20}$ | [664], [755], [1012], [1021] |
| $115-124$ | $W_{21}$ | [223], [232], [322], [777] |
| | $W_{22}$ | [729], [972], [297] |
| | $W_{23}$ | [927], [792], [279] |
| $125-127$ | $W_{24}$ | [285], [592], [1076] |
| $115-124$ | $W_{25}$ | [113], [131], [311], [444] |
| | $W_{26}$ | [148], [481], [814] |
| | $W_{27}$ | [184], [418], [841] |
| $125-127$ | $W_{28}$ | [861], [915], [1054] |
| $115-123$ | $W_{29}$ | [31010], [499], [788], [878], [887], [949], 994], [10310], [10103] |
| | $W_{30}$ | [347], [368], [395], [473], [539], [683], [734], [836], [8109] |
| $124-127$ | $W_{31}$ | [374], [386], [437], [359] |
| | $W_{32}$ | [593], [638], [743], [863] |
| | $W_{33}$ | [8910], [935], [9108], [1089] |

APPENDIX E

DESIGNED CODES CHAPTER 5

## E.1 Mapping Table MPPM (5,2) code

Table E.1: Mapping Table MPPM (5, 2) code

| Input Bits | Symbols |
|---|---|
| 011 | 00011 |
| 010 | 10010 |
| 101 | 01010 |
| 100 | 00110 |
| 111 | 10001 |
| 110 | 01001 |
| 0001 | 00101 |
| 0000 | 11000 |
| 0011 | 10100 |
| 0010 | 01100 |

## E.2 Mapping Table MPPM (6,4) code

Table E.2: Mapping Table MPPM (6, 4) code

| Input Bits | Symbols |
|---|---|
| 111 | 111100 |
| 1100 | 110011 |
| 1101 | 001111 |
| 0010 | 101011 |
| 0011 | 010111 |
| 0000 | 100111 |
| 0001 | 011011 |
| 0110 | 101110 |
| 0111 | 011110 |
| 0100 | 101101 |
| 0101 | 011101 |
| 1010 | 101011 |
| 1011 | 011011 |
| 1000 | 100111 |
| 1001 | 010111 |

## E.3 Mapping Table VW-MPPM (0.875, 2, 5) code

Table E.3: Mapping Table (0.875, 2, 5) code

| Input Bits | CW(E,1) | CW(E,2) |
|---|---|---|
| 0111 | 00011 | 00011 |
| 0110 | 10010 | 10010 |
| 1101 | 01010 | 01010 |
| 1100 | 00110 | 00110 |
| 1111 | 10001 | 10001 |
| 1110 | 01001 | 01001 |
| 1001 | 00101 | 00101 |
| 1000 | 11000 | 11000 |
| 1011 | 10100 | 10100 |
| 1010 | 01100 | 01100 |
| 01001 | 00000 | 00000 |
| 01000 | 01111 | 11110 |
| | CW(O,1) | CW(O,2) |
| 01011 | 10000 | 10000 |
| 01010 | 01000 | 01000 |
| 00101 | 00100 | 00100 |
| 00100 | 00010 | 00010 |
| 00101 | 00001 | 00001 |
| 00110 | 11100 | 11001 |
| 00001 | 10110 | 01101 |
| 00000 | 11010 | 10011 |
| 00011 | 01110 | 01011 |
| 00010 | 10101 | 00111 |

## E.4 Mapping Table VW-MPPM (0.80, 4, 6) code

Table E.4: Mapping Table (0.80, 4, 6) code

| Input Bits | CW(E,1) | CW(E,2) |
|---|---|---|
| 1111 | 111100 | 111100 |
| 1110 | 110011 | 110011 |
| 00101 | 001111 | 001111 |
| 00100 | 101011 | 101011 |
| 00100 | 010111 | 010111 |
| 00111 | 100111 | 100111 |
| 00110 | 011011 | 011011 |
| 00001 | 101110 | 101110 |
| 00000 | 011110 | 011110 |
| 00011 | 101101 | 101101 |
| 00010 | 011101 | 011101 |
| 01101 | 101011 | 101011 |
| 01100 | 011011 | 011011 |
| 01111 | 100111 | 100111 |
| 01110 | 010111 | 010111 |
| 01001 | 111111 | 111111 |
| 01000 | 000011 | 001100 |
| | CW(O,1) | CW(O,2) |
| 01011 | 011111 | 011111 |
| 01010 | 101111 | 101111 |
| 10101 | 110111 | 110111 |
| 10100 | 111011 | 111011 |
| 10111 | 111101 | 111101 |
| 10110 | 111110 | 111110 |
| 10001 | 000111 | 101010 |
| 10000 | 001011 | 100101 |
| 10011 | 001101 | 100101 |
| 10010 | 110100 | 101001 |
| 11001 | 111000 | 101100 |
| 11000 | 110010 | 100011 |